University of California, Merced

Title

A Rechargeable Aluminum Battery Electrolyte Based on Aluminum Trifluoromethanesulfonate in Propylene Carbonate and Ethyl Methyl Sulfone

Author

Overton, Bilal

Publication Date

Peer reviewed Dissertation

UNIVERSITY OF CALIFORNIA, MERCED

A Rechargeable Aluminum Battery Electrolyte Based on Aluminum Trifluoromethanesulfonate in Propylene Carbonate and Ethyl Methyl Sulfone

A dissertation submitted for the degree of Doctor of Philosophy

in

Chemistry and Chemical Biology

by

Bilal Overton

Dissertation Committee:

Professor Son Nguyen, chair

Professor Abel Chuang

Professor Hrant P. Hratchian

Professor Erik Menke, advisor

2023

The dissertation of Bilal Overton is approved, and it is acceptable in quality and form for publication on microfilm and electronically:

Professor Son Nguyen, Chair

Professor Erik J. Menke, Advisor

Professor Hrant Hratchian

Professor Po-Ya Abel Chuang

University of California, Merced

2023

In the name of Allah (swt), the most beneficent, the most merciful…

The knowledge of anything, since all things have causes, is not acquired or complete unless it is known by its causes – Psikologi Ibn Sina

Table of Contents

Acknowledgments ..... *vi*

Curriculum Vitae ..... *vii*

List of Figures ..... *viii*

List of Schemes ..... *ix*

List of Tables ..... *x*

Abstract ..... *xi*

Chapter 1: Aluminum Battery Literature Review *1*

1.1 Theory and background relevant to battery systems **1**

1.2 Developing aluminum batteries **2**

1.3 Haloaluminate ionic liquids **4**

1.4 Aluminum halide **5**

1.4.1 Active-halide-free 7

1.5 Solvents **8**

1.6 Cathode materials **9**

Chapter 2: Comparing Computational Predictions and *20*

Experimental Results *20*

for Aluminum Triflate in Ethyl Methyl Sulfone *20*

2.1 Introduction **20**

2.2 Materials and Methods **21**

2.2.1 Density Functional Theory. Calculations 21

2.2.2 Experimental Details. 21

2.3 Results and Discussion **22**

2.3.1 Coordination Structures. 22

2.3.2 Determining the ionic association interaction between aluminum and triflate in EMS using infrared spectroscopy 24

2.3.3 Stability Predictions and electrochemical profiling 27

2.4 Conclusion **31**

2.5 References **32**

Chapter 3: Comparing Computational Predictions and Experimental Results for Aluminum Triflate in Propylene Carbonate *42*

3.1 Introduction **42**

3.2 Materials and Methods **43**

3.2.1 Density Functional Theory Calculations 43

3.2.2 Experimental Details 44

3.3 Results and Discussion **45**

3.3.1 Coordination Structures. 46

3.3.2 Ionic association of triflate in PC through infrared spectroscopy 47

3.3.3 Stability Predictions and Electrochemical Profiling 50

3.4 Conclusion **56**
3.5 References **57**
Chapter 4: Outlook and Future Work ***66***
4.1 Introduction **66**
4.2 Incorporating Chloride-Rich Electrolytes **66**
4.3 Hydride-enhanced plating and stripping **68**
4.4 Borohydrides reversibility assistance **69**
4.5 Conclusion **70**
4.5 supporting information **71**
4.6 References **72**

Acknowledgments

The voyage of discovery that is being a graduate student at the University of California, Merced has been a life-altering experience of growth in scientific understanding as well as overall problem-solving. Graduate school has proven to be training in the art of independence; however, the journey would have not been as enjoyable and fruitful without a few individuals. Professor Erik J. Menke has been a pleasure to work with as my advisor and mentor, using his expertise to answer my questions and guide me toward effectively communicating research. His positive style of offering constructive criticism has been essential to my growth as a scientist, including allowing me to freely request his assistance in all areas. Erik's encouraging nature reinforced the belief in the work we are engaged in. I consider myself blessed to have had Erik as my advisor, I could not have had an advisor that better fit my needs as a graduate student. None of the work that is presented here would be possible without his tutelage. I would like to thank my family who has helped me to get to this point, including my mother **Alexandra** for her love, support, and words of wisdom, my father **Muhammad** for being an excellent example and molding me into the man I am today, my brothers Jamal, Hassan, Hussayn, Tariq, Ali for their constant encouragement and belief in me, my sisters Latima and Samirah for their loving helpful nature as well. The friendships that I have established here on campus have been fruitful as well as full of fun times with Zaher Slim, Abdul Zamani, Duy Nguyen, and Ajay Khanna who all played a part in making these 5 years an enjoyable experience. Zaher has played a significant role in my development, answering my endless questions and talks about science and life. Many days of long hours spent in COB and ACS building troubleshooting DFT calculations with Abdul, Ajay, and others were essential in bridging the gap in improving my computational skills. My love for science was greatly increased during my first year taking graduate-level courses. The friendships that I mentioned previously were cultivated by studying late at night on campus or meeting up on the weekend for revisions. As I was applying to graduate programs my father advised me to also apply to UC Merced, he is an educator and had the vision of the potential of attending a new university with great potential such as Merced for my personal growth. I am happy that I took this advice which that lead me to inquire about Erik and his research that aligned with my interest in comparison to the other schools. Duy played an essential role in helping me work through different obstacles with FTIR through her expertise in organic chemistry. I am incredibly blessed to have a knowledgeable and accessible committee. My wholehearted gratitude to Prof. Son Nguyen, Prof. Hrant Hratchian, and Prof. Abel Chuang for their challenging questions and assistance throughout my entire Ph.D. experience here in Merced. I would like to thank Dave Rice for his assistance in training me to use various instruments such as FTIR and NMR. Also, I would like to thank Kennedy Nguyen for training me in SEM, XRD, and XPS instrumentation. I am grateful for the tutelage that I received from Melissa Russel, Donna Jaramilo-Felin, Alyssa Hua, and the other lab staff during my time as a teacher's assistant. Also, I would like to thank Prof. Son Nguyen for allowing me to use the FTIR, as well as other materials in the laboratory. I would like to thank Randy Espinoza, David Morgan, Karnamohit Ranka, Riley Ball, Pin Lyu, and every student here at UC Merced for their friendship and assistance.

Curriculum Vitae

Education

Ph.D., University of California, Merced, (2018 - 2023).
Advisor: Prof. Erik J. Menke
Chemistry

BS, University of La Verne, (2013-2017).
Chemistry

Academic Positions, University of California, Merced. (2018 - 2023)

Teaching Assistant

Preparatory Chemistry (2018)

General Chemistry 1 & 2 (2019 – 2022)

Inorganic Chemistry (2023)

Publications (in preparation)

Overton, B: Aluminum Electrodeposition from Propylene Carbonate Chloride-Free Organic Electrolyte.

Overton, B: Comparing Computational Predictions and Experimental Results for Aluminum Triflate in Ethyl Methyl Sulfone.

Presentations

"Comparing Computational Predictions and Experimental Results for Aluminum Triflate in Ethyl Methyl Sulfone", UC Merced, Chemistry and Chemical Biology Seminar, February 5, 2021.

"Potential Electrolytes for Al-ion Batteries", 259th American Chemical Society National Meeting, 2020.

"Potential nonaqueous Aluminum-ion Batteries", UC Merced, Chemistry and Chemical Biology Graduate Student Symposium, 2018.

List of Figures

Figure 2.1 Optimized structures of (a) Al(EMS)23+ and, (b) Al(EMS)33+, pink: aluminum,.... 22

Figure 2.2 Optimized structures (hydrogens shown as white) of (A) Free triflate, (B) Contact ion paired [Al(EMS)3][triflate]12+, (C) Bound-triflate [Al(EMS)3][triflate]12+. Pink: Al, grey: carbon, red: oxygen, blue: fluorine, yellow: sulfur. 23
Figure 2.3 FTIR spectra of Al-triflate/EMS solutions (A) CF_3 symmetric deformation region, (B) SO_3 antisymmetric stretch region, and (C) SO_3 symmetric stretch region. 26
Figure 2.4 Display of the first three cycles of cyclic voltammograms for Al-triflate/EMS electrolytes at different concentrations and temperatures with sweep rates of 100 mV/s and 2 mV/s: (A, B) 0.01 M on a gold WE at 40c and 60°C at a scan rate of 100 mV/s. (C, D) 0.01 M on a gold WE at 40°C and 60°C at a scan rate of 2 mV/s. (E, F) 0.1 M on a gold WE at 40°C and 60°C at a scan rate of 100 mV/s. (G, H) 0.1 M on a gold WE at 40°C and 60°C at a scan rate of 2 mV/s. The first scan is blue, the second is orange, and the third is green. 30
Figure 2.5 Ionic conductivity of the concentration dependence of the potential electrolyte 31
Figure 3.1 Optimized structures of (a) $Al(PC)_3^{3+}$, (b) $Al(PC)_4^{3+}$, pink: aluminum, grey: carbon, red: oxygen, white: hydrogen. 45
Figure 3.2 Optimized structures (hydrogens shown in white) of (A) bound triflate $[Al(PC)_4][triflate]_1^{2+}$, SO3 symmetric stretch (B) SO_3 symmetric stretch $[Al(PC)_4][triflate]^{2+}$, (C) SO_3 antisymmetric stretch $[Al(PC)_4][triflate]_2^{+}$. Pink: aluminum, grey: carbon, red: oxygen, blue: fluorine, yellow: sulfur. 45
Figure 3.3 FTIR spectra of Al-triflate/PC solutions reveal (A) CF_3 symmetric deformation region, (B) SO_3 symmetric stretch region, and (C) SO_3 antisymmetric stretch region. 49
Figure 3.4 Display of the first three cycles of cyclic voltammograms for Al-triflate/PC electrolytes at different concentrations and different sweep rates of 10 mV/s and 100 mV/s: (A) 100 mV/s 0.05 M on gold WE. (B) 10 mV/s 0.05 M on gold WE. (C) 100 mV/s 0.1 M on gold WE. (D) 10 mV/s0.1 M on gold WE. The first scan is red, the second is blue, and the third is green. 52
Figure 3.5 Ionic conductivity of the solution as a function of aluminum triflate concentration. 53
Figure 3.6 24 hr Chronoamperometry on a 0.05M aluminum propylene carbonate electrolyte 54
Figure 3.7 SEM images of (a, b) untreated Cu substrate, Al electrodeposits on Cu substrate (vs Al/Al^{3+}) obtained from (c, d) 0.1 M Al(OTF)3/PC at 0 V for 24 h. 55
Figure 3.8 X-ray photoelectron spectroscopy (XPS) spectra of Al-deposits from Al(OTF)3 Electrolyte. Showing (a) XPS survey for the deposit on Cu substrate (b) Al2p region (c) O1s region (d) F1s region (e) Cu2p for Al deposit obtained by electrodeposition of aluminum from a 0.1M Al(OTF)+⁄PC electrolyte at 0 V vs. Al wire for 24 hours. 56
Figure 4.1 Cyclic voltammogram on a golf working electrode for 1:3 Al(OTF)3:LiAlH4/PC (first scan is red, second is green, and third is blue). 71
Figure 4.2 Cyclic voltammogram on gold working electrode fork LiAlH4/PC (first scan is red, second is green, and third is blue) 71

List of Schemes

Scheme 2.1 Born-Haber cycle used to calculate the changes in the standard solvation Gibbs Free Energy in EMS……28
Scheme 3.1 Born-Haber cycle used to calculate the changes in the standard solvation Gibbs Free Energy in PC……51

List of Tables

Table 1.1 Intrinsic properties of various anodes. Standard potential, gravimetric and volumetric capacity, abundance, cost, and cation radius of lithium (Li), sodium (Na), magnesium (Mg), aluminum (Al), potassium (K), and calcium (Ca).[6] 1
Table 2.1 Measured and Computed Vibrational Frequencies (cm-1) of CF3 symmetric deformation, SO3 symmetric, and antisymmetric stretching modes. 24
Table 2.2 Gibbs Free Energies and Absolute Reduction Potentials of Solvent, Anion, and Complex 28
Table 3.1 Measured and Computed Vibrational Frequencies Measured and Computed Vibrational Frequencies 47
Table 3.2 Gibbs Free Energies and Absolute Reduction Potentials of Solvent, Anion, and Complexes 51

Abstract

Extensive research has been devoted to multivalent ions such as Al^{3+} for the advancement of rechargeable batteries, which play a pivotal role in powering mobile electronic devices that makeup 80% of practical renewable energy. Electrical devices such as portable electronics and electric vehicles are primarily powered by lithium-ion batteries. Lithium, the primary component of lithium-ion batteries is scarce in the earth's crust. The lack of Li availability raises doubts about its capability to meet future energy needs. Aluminum has garnered significant interest for its potential to bridge this energy storage gap for many reasons. One of Al's greatest attributes is being abundant in the earth's crust. Al anode materials can also theoretically provide high charge capacities, gravimetric as well as volumetric, in comparison to common metal salts utilized for the advancement of rechargeable-ion batteries such as lithium. Due to the utilization of chloride-rich solutions, there is a lack of non-corrosive electrolytes in development for practical use in aluminum-based battery research. Essentially, the work presented in this dissertation illustrates an effective method to understand reversible Al electrodeposition in an organic non-corrosive environment, which is currently a roadblock in synthesizing electrolytes that can be practically utilized. Through evaluating the aluminum-triflate active halide-free electrolyte in ethyl methyl sulfone and propylene carbonate, this work presents a method for the electrodeposition of aluminum-ions in a halogen-free environment which is a quintessential step in synthesizing an electrolyte that is ideal for the purpose of constructing a reversible aluminum-ion battery.

Chapter one is comprised of an extensive review of the foundation that has led up to the current improvements in non-aqueous electrolytes for advanced rechargeable aluminum batteries. This

section provides the framework for a battery system and the additives in an electrolyte that have been studied for their electrochemical and physiochemical qualities.

Chapter two discusses the results of an $Al(OTF)_3$ in ethyl methyl sulfone (EMS) electrolyte. Gaussian DFT calculation assisted in computational modeling couples with various experimental methods were utilized to analyze electrochemical and spectroscopic attributes of the electrolyte. The results suggest that Al is electrochemically active in EMS, as well as IR spectra revealing two distinct regions that explain the ionic association of triflate. This work provides a comprehensive method to relate computational predictions to electrochemical results from cyclic voltammetry and FTIR.

Chapter three reports on the results of an electrolyte that is comprised of $Al(OTF)_3$ in propylene carbonate. Computational results illustrate the exceptionally high oxidative stability as well as the electrochemical window. Also, electrochemical experiments indicate the Al activity in solution; evidence being the reduction of aluminum at various concentrations of the electrolyte. Chronoamperometry was utilized to provide spectroscopic evidence of Al species plating along with electrical impedance spectroscopy and FTIR. The surface morphology of the copper substrate in the chronoamperometry experiment was evaluated with a scanning electron microscope and x-ray photoelectron spectroscopy.

Chapter 4 is an overview of potential pathways for the advancement of this research in future work. Various additives have been incorporated to improve aluminum-ion batteries such as the addition of chlorides, hydrides, and borohydrides. These previous reports can be studied for the purpose of improving the aluminum-triflate non-aqueous electrolyte in propylene carbonate and ethyl methyl sulfone.

Chapter 1: Aluminum Battery Literature Review

1.1 Theory and background relevant to battery systems.

Global energy storage derived from fossil fuels has resulted in the formation of CO_2 gas, which accounts for about three-quarters of the annual anthropogenic greenhouse gas emissions. [1] To correct for climate change challenges, wind, and solar power have been proposed as alternative energy storage methods. [2] There is a desire to pursue the possibilities of sustainable energy storage to meet the needs of the ever-growing technological advancements that do not involve fossil fuels. [3] Rechargeable-ion batteries are electrochemical storage devices suited to be a vessel that meets these energy storage needs. [4] Lithium-ion (Li-ion) batteries have primarily been the device designated to provide reusable energy for practical use over an extended life cycle. [5] Society's utilization of portable electronics is growing exponentially, and this growth births the need for advanced devices other than the lithium-based standard. The concern regarding lithium's future capabilities stems from its lack of abundance, cost-effectiveness, and volumetric capacity.

Table 1.1 Intrinsic properties of various anodes. Standard potential, gravimetric and volumetric capacity, abundance, cost, and cation radius of lithium (Li), sodium (Na), magnesium (Mg), aluminum (Al), potassium (K), and calcium (Ca).[6]

Metal	Standard Potential (V vs SHE)	Gravimetric capacity (mAh/g)	Volumetric capacity (mAh/g)	Abundance (ppm)	Cost (USD/kg)	Cation radius (Å)
Li	-3.042	3861	2042	65	19.2	0.76
Na	-2.71	1166	1050	22700	3.1	1.02
Mg	-2.37	2205	3868	23000	2.2	0.72
Al	-1.66	2980	8046	82000	1.9	0.535
K	-2.925	685	609	18400	13.1	1.38
Ca	-2.87	1340	2071	41000	2.4	1

Aluminum (Al) has been chosen as an alternative to lithium due to naturally being the most abundant metal in the earth's crust, as well as being the third most abundant of all earthly elements. In comparison to various metals that are studied for their potential as rechargeable battery anode material Al displays the greatest theoretical volumetric charge capacity (8046 mAh/cm^3), this value is exceedingly greater than the most prevalent material utilized in rechargeable ion batteries today, lithium. Evidence of this comparison can be seen in the table above (Table 1.1). The vast abundance and superior volumetric capacity make Al an intriguing alternative to be investigated for its potential to advance the possibilities of portable electronics. Aluminum is one of the most abundant elements in the earth’s crust which is essential in the efforts of decreasing the cost and increasing practical manufacturing. Cation Radius also plays a part in the kinetics of the metal-ion and its ability to intercalate and deintercalate into cathode materials. Aluminum has one

of the smaller radiuses at (0.535 Å), in comparison to other studied metal ions. [7] These advantageous attributes of aluminum has encouraged the field of energy storage and rechargeable ion batteries to invest in the development of aluminum-based electrolytes as well as electrode materials that can take full advantage of their trivalent nature.

To make use of aluminum's advantageous qualities mentioned previously, a reversible electrolyte that has a high coulombic efficiency over a 100-cycle life or greater is necessary. Previous studies that have set the foundation for this research have suggested that there are only a few electrolyte environments that can produce this reversibility and facilitate aluminum ion mobility to and from the electrode material. Al-halide systems are an example of an electrolyte that meets the criteria for reversibly electrodepositing Aluminum. [7–14] The problem that reveals itself in terms of the practical use of halides is their corrosive nature towards the electrode materials. [15–18] Chlorine gas evolution is also an example of a side reaction that can result in corrosion due to its propensity to oxidize at very low potentials. [19,20] Overcoming the obstacle of gas evolution is a pivotal step in realizing aluminum's ability to take lithium's place as the dominant material for portable electronics.

Lithium-ion batteries have proven successful for rechargeable battery applications, yet still flawed due to the lack of abundance and volumetric capacity. Therefore, Aluminum has been chosen as a vessel to meet the needs of the advancements being made in portable electronics. In comparison to the previous research involving halide-rich electrolytes, this study is geared towards a halide-free approach due to the corrosive tendency. [11,16] Halide-fee refers to an environment that is free of halogen ions, and halo-aluminate complexes such as ($AlCl_4^-$, $Al_2Cl_7^-$) while still having the ability to reduce and oxidize aluminum ions in a reversible manner. A wide voltage range in between the oxidation and reduction of peaks known as the electrochemical window is also a factor that should be present in order to facilitate stability. Aluminum chloride-based organic solvents have been extensively studied. However, currently there is a lack of understanding the capability of Al electrolytes in a halogen-free environment. [21–25, 26] This body of work will discuss the research that has led to the intrigue and synthesis of Aluminum trifluormethanesulfonate, also known as Al-triflate ($Al(OTF)_3$), in ethyl methyl sulfone (EMS) [27] as well as propylene carbonate (PC).

1.2 Developing aluminum batteries

Since the 1850's aluminum has been characterized as being applicable for battery materials, firstly as a cathode coupled with a Zinc anode by Hulot.[8] The idea of Aluminum as an anode material was introduced in a Buff cell in 1857. [28] Aluminum can be electrochemically oxidized in an aqueous solution to form an oxide layer that is thicker than the native layer is the crux of what Buff found. [29] Later, a halogen-rich electrolyte was reported to produce substantial voltage, However, utilizing $AlCl_3$ resulted in the corrosion of the electrode materials as well as the evolution of chlorine gas (Cl_2). This inevitably hindered the system's ability to safely produce a rechargeable environment. In 1951 a cell was designed with various electrolytes in a Leclanché-type

dry cell where Al was the active anode material with a MnO_2 cathode to prevent halogen gas evolution. [30] Each cell setup incorporated a separator and either a NaOH plus ZnO or a manganese chloride tetrahydrate electrolyte. The synthesis of these batteries did not come to fruition for practical application for many reasons, one being aluminum's inclination to form an oxide layer which greatly hinders the voltage. Through the addition of incorporating highly concentrated KOH, the battery was able to remove the oxide layer and allow for an increase in voltage. [31] However, increasing this concentration leads to the electrode materials corroding due to the evolution of H_2 gas caused by side reactions. [32]

Research conducted by Del Duca in 1971 presented the framework for the kinetics of electrodeposition of Al from high-temperature molten salts that are free of hydrides and the H_2 gas evolution that includes hydride. This electrolyte consists of Cl in compounds such as $AlCl_3$, NaCl, LiCl, and KCl.[33]A few research documents on $AlCl_3$ – KCl – NaCl melts were conducted by Holleck and Griner later that year, firstly studying $AlCl_3$ anodic limitations. [34] Following this research article, Holleck shifted to a focus on the kinetics of chlorine reduction in such melts. [35] Much of this research produced results of improved energy storage. However, these melt-based electrolytes have not become prevalent in the mass production of batteries due to the heightened temperatures required for optimal electrochemical activity, and side reactions that result in dendrite formation during the electrodeposition process. Lastly, the propensity of Cl_2 gas formation, and the health risks that accompany Cl_2 gas.

To correct for the necessity of extreme temperatures to maximize these melts, a room-temperature molten salt was proposed as a potential electrolyte in 1988. This study asserts an investigation of a novel $AlCl_2$ rechargeable electrochemical cell that employs an Al anode in a room-temperature molten salt electrolyte of 1.5:1 $AlCl_3$: 1, 2 – dimethyl – 3 – propylimidazolium chloride. The cell studied in this work possesses a discharge voltage of 1.7V for currents of 1–10 mA/g graphite and over 150 cycles. The graphite electrode allows for the reversible intercalation of Al ions which removes the need for a separator in this system design. [36] A potential high energy density rechargeable aluminum/aluminum-ion (Al-ion) that can correct for the evolution of H_2 gas and the introduction of the oxide layer sparked interest in using an Al/Mn_2O_4 cell in a study conducted by Paranthaman et al in 2010. [37] In this cell Mn_2O_4 is the cathode material in a room temperature chloroaluminate melt which consists of $AlCl_3$ and 3-ethyl-1-methyl-imidizolium chloride EMIC:$AlCl_3$ at 1.2:1 mole ratio. This system revealed a reduction of H_2 evolution, as well as redox peaks according to cyclic voltammetry while no observation of intercalation capacity was present. [37]

In 2011 there was a report of a novel aluminum-ion rechargeable battery consisting of an electrolyte that contains $AlCl_3$ in the same ionic liquid mentioned previously, 1-ethyl-3-methylimidazolium chloride. However, a V_2O_5 nano-wire cathode was measured against an aluminum metal anode. The battery delivered a discharge capacity of 305 mAh g^{-1} in the first cycle and a 273 mAh g^{-1} gravimetric capacity after 20 cycles. [38] These results suggest the possibilities of a rechargeable Al-ion battery into V_2O_5, in terms of capacity

and the lengthened cycle life. In 2013, this idea was asserted to be untrue by Reed and Menke, who would suggest that V_2O_5 was inactive. The capacities that were presented were potentially attributed to side reactions at the stainless steele current collector. [17]

The early 2000s devoted a great deal of attention to developing an in-depth understanding of Al-ion battery electrolytes as well as the cathode materials. The groundwork that was mentioned earlier has shaped research projects for many studies on room temperature as well as high-temperature molten salts. [36, 38] The intercalation of aluminum ions in V_2O_5, EMIC, and other cathode materials has suggested a method for reversibility. While these systems have observed elimination of the native oxide layer, and increased capacity over a long cycle life, the obstacles that halide-rich environments present inspired Reed and Menke to focus on active-halide-free organic potential electrolytes. They reported an $Al(OTF)_3$ in diethylene glycol dimethyl ether (diglyme) electrolyte and copper hexacyanoferrate cathode in 2015. [23] This battery returned reversible intercalation behavior in the cathode materials. However, low discharge capacity and unsatisfactory capacity retention were observed. The results were not perfect, but this study provides pathways for advancements that are possible due to the wide electrochemical window and reversibility in a halide-free organic electrolyte.

1.3 Haloaluminate ionic liquids

Ionic liquids were first observed by Paul Walden in 1914. In this study, there was a report of the physical properties of ethylammonium nitrate ($[EtNH_3][NO_3]$), synthesized by neutralization of ethylamine with concentrate nitric acid. [39] This novel class of liquids' advantageous attributes was not produced until 1982.[40] During this time dialkylimidazolium chloroaluminate melts were reported. [41] This period is the first generation of ILs. Building on the foundation of the first generation, rigorous studies would follow and reveal a hindrance that was derived from water sensitivity stemming from chloroaluminate (III) anion. This sensitivity is an obstacle to potential industrial applications. [39] The electrolytes in question were synthesized by adding AlX_3 to RX, in this case, R is an organic cation. X is typically a halogen (Cl, Br, or I). [7, 42]

Hurley and Wier conducted studies on the early possibilities of electrodeposition of aluminum on various metals at room temperature. [43] Mixing two moles of anhydrous aluminum chloride with one mole of ethyl pyridinium in a dry oxygen-free atmosphere. [43] In 1978 Gale et al. reported on a similar systems speciation by way of Raman spectroscopy. [44] This Ramen spectral study asserts that the formation of Al_2Cl_7 ionic species is improved in $AlCl_3$-1-butylpyridinium chloride melts compared to the higher temperature $AlCl_3$-alkali metal chloride molten systems.

High-temperature molten salts mentioned earlier were studied by Del Duca in the 1970s. [33] High-temperature chloroaluminate molten salts are typically derived from a reaction of binary or ternary mixtures of AlX_3, with M^+X^-, where M is an alkali metal (such as Li, K or Na) and X is a halogen such as (Cl or Br). [12, 42] The framework that is being mentioned here is the background to a vast knowledge of rechargeable ion battery investigations

built on the chemical behavior of mixing an Al-halide salt with a halogenated source at various concentrations at increased temperatures to achieve the desired electrochemical activity and intercalation behavior.

The Al present in the aforementioned solutions is in the Al-complex variety, not necessarily free Al that is found in the mixtures. [13] Aluminum is present in the solution and does not result in adequate electrochemical activity for aluminum electrodeposition. Schematics of the conditions for the speciation of room and high-temperature molten salts have been thoroughly investigated and shown here:

In chloroaluminate melts with varied pH, or when the mole ratio of $AlCl_3$ compared to chloride is less than or equal to one, the system is governed by the following reaction. [42]

$$AlCl + Cl^- \leftrightarrows AlCl^-$$

Present-day electrolytes that incorporate ionic liquids have shown many promising characteristics. In 2019, the only non-ambiguous electrolytes that allow aluminum plating and stripping in a room temperature environment are the deep eutectic solvents comprised of aluminum halides such as (aluminum chloride $AlCl_3$ or aluminum bromide $AlBr_3$) and corresponding halides such as imidazolium, pyridinium, and ammonium. [16, 7] These deep eutectic chloroaluminate electrolytes have an important role in cathode material development, however, it is important to note the hindrance and faulty data that can be gathered in their presence. [16, 47] A few characteristics that may not be overlooked are low anodic stability, the evolution of chlorine gas and side reactions that lead to damaging products, and corrosion. These electrolytes are also extremely hygroscopic, and developing methods to completely remove the corrosive nature are still in progress. [20, 42]

1.4 Aluminum halide

The addition of a halides group plays a critical role in establishing a foundation for Aluminum electrodeposition on an industrial scale. Crouch and Brenner played a vital part in the process of development for the deposition of aluminum from aluminum chloride and a metal hydride, such as 0.5 to 1.0M lithium hydride (LiH) or lithium aluminum hydride. The most favorable deposits were derived from an ethyl ether solution concentrated at 2 to 3M. Building from this framework numerous studies were conducted on aluminum deposition and the impact hydride has on the system. [48]

The addition of $LiAlH_4$, and its impact on the electrochemical and physiochemical properties of the electrolyte is an intriguing potential additive for the purpose of incorporating reversibility. The goal here is to evaluate details regarding hydrides' impact on the specific electrolytes in question while mentioning the assortment of solvents and co-solvents Crouch and Brenner have covered. An example of further investigation into this behavior is a study by Ishibashi and Yoshio, where they report on the electrodeposition of aluminum from aluminum chloride and lithium hydride in a

tetrahydrofuran-benzene mixture. This study asserts the addition of $AlCl_3$/$LiAlH_4$ at molar ratios of 3:1 there is low volatility and increased stability compared to the pure tetrahydrofuran bath excellent aluminum deposits as well and a significant increase in operating life was established. [49] There have been reports on the heightened current density capabilities of THF previously in the literature, as well as in our lab in studies done by Zaher Slim. Current density is one of the many qualities that lead Ishibashi and others to THF as the primary solvent in the solution.

Hydrides were also investigated by Graef, who studied the electrochemical behavior of $AlCl_3$ and $LiAlH_4$ ability to electrodeposit aluminum in THF. [50] This report is instrumental to this work by setting a roadmap to realize the possibilities of a rechargeable aluminum ion battery. In this work, there is a shift from the previous electrolytes which were chloride-rich in the presence of excess $AlCl_3$. Rather this solution is consisting of abundant $LiAlH_4$. The reaction of 1:3 mole ratio of $AlCl_3$ to $LiAlH_4$ shown below [51]:

$$AlCl_3 + LiAlH_4^- \rightarrow 4AlH_3 + 3LiCl$$

The overall electrochemical mechanism suggested by Graef is according to the reaction below:

$$4AlX_3 + 3e^- \rightarrow Al + 3AlX_4^-$$

(X is H or Cl)

In previous literature, Daenen reported incorporating AlH_3, Et_3N, and $LiAlH_4$ in diethyl ether shows a decrease in the overpotential in comparison to ACl_3 rich environment due to H- catalyzing the transfer process of the transporting Al deposits.

To understand non-Lithium electrodeposition systems, diversifying the metal salts that are investigated is essential. This births the need to understand aluminum electrodeposition from organic electrolytes in contrast to melts for rechargeable ion batteries. Although we aspire to develop a halogen-free electrolyte due to corrosion among other factors, it is important to understand $AlCl_3$-based organic systems as they are well-studied and can provide critical insight. An electrolyte consisting of LiCl and $AlCl_3$ in sulfone-based solvents such as dimethylsulfone ($DMSO_2$) was reported by Legrand et al. [52–55] In this study the cathodic and anodic behavior of aluminum was analyzed, and reversibility was reported. $DMSO_2$'snature required for high-temperature operation which also coincides with degradation of the passivating layer. Miyake et al. reported on Al electrodeposition onto an Mg allow substrate in a dimethyl sulfone-aluminum chloride bath. This study suggested the possibility of dense Al deposition while having poor adhesion. Lastly, at room temperature (25 °C) $DMSO_2$-$AlCl_3$ baths are shown to effectively prevent rapid corrosion. [56] Different variations of the $AlCl_3$ electrolyte were studied to understand the aluminum speciation physiochemical and electrochemical behavior, examining temperature dependence as well as concentration

dependence. Work done by Nakayama et al. reports on a potential noncorrosive reversible room temperature aluminum electrolyte. The low chloride concentration in this system allows doe the use of Al metal anodes without corrosion. This work came to the conclusion that sulfone-based electrolytes would open the door to future Al rechargeable battery developments. [57]

Many different studies have been conducted on $AlCl_3$/glyme mixtures, this report has played an important role in the foundation of research done in our group. [58–60] Diglyme was the only glyme mixture that successfully deposited Aluminum. The reason behind this may be due to the lack of free Al ions in triglyme and tetraglyme mixtures. [58] A study by Wen et al. reported on an $AlCl_3$ solution in γ-butyrolactone (GBL), using electrochemical, spectroscopic, and computational methods. The electrochemical deposition of Al is present in the room temperature environment.

The electrochemical activity of the $Al_3Cl_{10}^-$ anion is created from the electrolytes with an $AlCl_3$/GBL ratio greater than 1 at room temperature to achieve Al deposition. This study provides a new method to manufacture electrolytes for Al electrodeposition without utilizing ionic liquids. The potential to open the door for similar mechanisms to yield active chloroaluminate species in similar systems with $AlCl_3$ and organic solvent electrolytes containing oxygen atoms with lone pair electrons was presented in this report.

1.4.1 Active-halide-free

Aluminum triflate was chosen as the designated aluminum salt for the work presented in this dissertation due to the aluminum ion association in this case. The interaction with the halogen F (fluorine) in aluminum triflate is bound therefore being a protection against the evolution of free halogen ions in solution. Al-triflate was also chosen to remove the necessity to include halo-aluminate compounds such as $AlCl_4^-,\ and\ Al_2Cl_7^-$. When constructing a stable non-volatile electrolyte, its components must have stable redox potentials to prevent the evolution of free halogens. [61]

In a study I mentioned earlier by Jayaprakash et al. where there was a report on an $AlCl_3$-[AMIm]Cl electrolyte system yielding an effect of electrodeposition and dissolution of aluminum, there is also mention of a potential active-halide-free electrolyte. [38] This same battery utilizing V_2O_5 nanowire battery was investigated with aluminum troflouromethanesulfonate (Al triflate) which was dissolved in an aprotic liquid's mixture of propylene carbonate and tetrahydrofuran PC/THF (1:1 v/v). [38] In comparison to the $AlCl_3$ electrolyte system, no electrochemical activity was observed in the voltage range of (-0.75 to 4.2 V). The cyclic voltammetry experiments presented in the study mentioned above showed what could be attributed to aluminum reduction at 0V vs Al/Al^{3+} of the 1:1 v/v of Al triflate in PC/THF would suggest the presence of electrochemical activity of aluminum ions while still appearing to be irreversible. The behavior of Al in the

voltammograms resembles studies conducted in our group that incorporate one of either THF or PC, rather than a mixture with Al-tiflate.[62]

Due to the sensitivity of haloaluminate-based electrolytes, finding an appropriate electrode material has yet to materialize. This births the need for the study conducted in 2015 by Mandai and Johansson investigating aluminum trifluoromethanesulfonate ($Al[TfO]_3$), N-methyl acetamide (NMA), and urea. [21] Although this electrolyte would provide satisfactory ionic conductivities, it could not be shown that Al could be electrochemically stripped or plated in this system.

While this work is taking place, $Al(OTF)_3$ was being investigated in diglyme. Previously, I mentioned Reed and Menke's work with Prussian blue analog utilizing this same electrolyte. In this report, there is a study of the physiochemical and electrochemical properties of the electrolyte while comparing these findings with the computational data. The Al-triflate/diglyme electrolyte was shown to have excellent ionic conductivity (25 mS/cm) shown by the electrical impedance spectroscopy experiments. However, aluminum electrodeposition was not apparent according to the cyclic voltammetry experiments which may be due to the chelating and passivation at the electrode. [22]

Mandai and Johnson reported on a halo aluminate-free cationic aluminum complex $[AlnX_{3n+1}]^-$ influence on the landscape of energy storage. This electrolyte was studied in DMSO, which has a significantly high melting point because the electrolyte exhibits anodic and cathodic currents. Although this electrolyte was not proven to be reversible, reduction of aluminum was present from $[Al(DMSO)_6][TFSI]$ and $[Al(DMSO)_6][OTF]_3$ in sulfone. Aluminum was not reduced from $[Al(MIm)_6][TFSI]_3$ in acetonitrile electrolytes shown by the lack of Al electrodeposition. The report concluded that decomposition of the electrolyte took place from electrodeposition from 1-butyl imidazole (BIm) based electrolyte $[Al(BIm)_6][TFSI]_3$ was conducted.

Li-ion batteries have been synthesized from active-halide-free systems in $TFSI^-$ and PF_6^- based electrolytes. [63–65] TFSI and PF_6 have also shown the potential to be rechargeable in magnesium-based electrolytes. [66, 67] An example of the promise of a TFSI-based electrolyte with aluminum was reported by Chiku et al. where aluminum bis(trifluoromethane sulfonyl)imide ($Al(TFSI)_3$) was shown to be rechargeable and increase the width of the electrochemical window. The EW was extended from 2.5V to 3.6V with the electrolyte in AN. [26]

1.5 Solvents

An electrolyte is a mixture of a metal salt, which we have discussed in detail, and the solvent the metal salt is dissolved in. The solvent plays a vital role in synthesizing an electrolyte that exhibits excellent stability along with other characteristics. Sulfone-based electrolytes show stability at high voltage according to a study by Wang et al. in 2013. The ab initio calculations of the oxidation potential (E_{ox}) of free sulfones appear to be lower than free carbonates, while the practical use of sulfone-based electrolytes has

shown higher oxidative stability. Wang et al. utilized density functional theory to investigate this contradiction between the ab initio data and the actual electrochemical experiments. In this report, it was found that not all sulfones behave the same, various sulfones behave with distinct levels of stability in comparison to the others. Gaussian was utilized to run DFT on various sulfone-based solvents such as fluorophenyl methyl sulfone (FPMS), ethyl iso-butyl sulfone (EiBS), methoxyethyl methyl sulfone (MEMS), ethyl methoxyethyl sulfone (EMES), ethylmethoxyethoxyethyl sulfone (EMEES), and ethyl methyl sulfone (EMS). These calculations show high stability toward the presence of anions and neighboring solvents which would agree with sulfones' actual potential for oxidative stability that can now be calculated. [68]

A study conducted by Peter Hilbig et al. has investigated one of the few reports on the potential of an EMS-based electrolyte utilizing Lithium-ion batteries. [27] In 2017, this research was conducted to utilize sulfone-based electrolytes for higher oxidative stability. Fluoroethylene carbonate (FEC) is an additive utilized in the synthesis of a $LiPF_6$ ethyl methyl sulfone (EMS) electrolyte. This additive can assist with correcting for the high viscosity of EMS and improve the intercalation behavior with the cathode material. EMS revealed improved overall nickel cobalt manganese oxide (NMC)/graphite cell performance with the addition of ethyl acetate (EA) as a co-solvent. Ethyl methyl sulfone's solid at room temperature nature presents obstacles of viscosity and practical use while having qualities of heightened capacity over 100 cycles.

Propylene carbonate is another solvent studied for potential rechargeable ion batteries. PC has been utilized as a cosolvent in aluminum ion battery reports, but only thoroughly investigated in lithium-ion batteries as the primary solvent. A study by Xing et al. in 2009 reported on theoretical insight into the oxidative decomposition of PC in lithium-ion batteries. [69] In this study density functional theory (DFT) was utilized at the level of B3LYP/6-311++G(d), in the gas and solvent phase. Here there is a report on the detailed mechanism for the oxidative decomposition which gives insight into radical generation that is reduced at the anode that is terminated by including trans-2-ethyl-4-methyl-1,3-dioxolane, cis-2-ethyl-4-methyl-1,3-dioxolane, and 2,5-dimethyl-1,4-dioxane.

1.6 Cathode materials

Although the concept of how lithium-ion batteries and aluminum-ion rechargeable batteries are similar, the components of the standard cells for each have their own distinct characteristics and electrochemical reactions. A Li-ion battery is typically constructed with a graphite anode electrode material while using a lithium-based cathode material made from layered metal oxide such as ($LiCoO_2$, $LiMnO_2$, $LiNiO_2$, and $LiFeO_2$). [5,70,71] In this cell setup, Li-ions are being transported involving intercalation and de-intercalation between both electrodes.

In a rechargeable aluminum-ion battery cell, the anode is comprised of aluminum where reversible aluminum plating and stripped is occurring. The intercalation/de-intercalation behavior is taking place at the given cathode material that new studies are being reported

on frequently at the present time. [6,7,9,11] The cathode material designated for a rechargeable aluminum-ion battery is typically a transition metal sulfide. [15,72] The appropriate cathode materials for a practical rechargeable aluminum-ion battery for mass use is one of the few components that are still not completely understood, along with understanding the proper electrolyte to take advantage of aluminum's advantageous attributes as anode material. A few of the common studies cathodes are graphitic foam[73], natural graphite[74], pyrolytic graphite[75], Mo_6S_8[76–78], and V_2O_5[17,38,79]. The proper cathode material capable of intercalating aluminum and the intercalation pathway is an area of advancement that is currently in development.

A rechargeable aluminum battery that exhibits high-rate capability is comprised of an aluminum anode and a three-dimensional graphitic-foam cathode was proposed by Lin et al. [73] In 2015 this study describes a battery that is capable of electrochemical deposition and dissolution of aluminum at the anode, as well as the intercalation/de-intercalation of the chloroaluminate complex into the cathode in the presence of a non-flammable ionic liquid. Herein, there are reports of this electrolyte and cell set up with explicit discharge voltage plateaus near 2 volts while exhibiting a specific capacity of around 70 $mAhg^{-1}$ and a Coulombic efficiency of nearly 98%. The Al/graphitic-foam cells show a current density of 4000 mA g^{-1}.

Previously mentioned in this review is a report on V_2O_5 as an initial cathode material to be studied for aluminum rechargeable batteries. Jayaprakash et al. also investigated a similar cell environment containing $AlCl_3$ in an ionic liquid, where in this report it was stated that aluminum intercalation was exhibited here. [38] Reed and Menke concluded that this was not the case, rather no electrochemical activity toward the aluminum. They assert the activity is iron and chromium in the stainless-steel current collector. This reaction leads to the cell potential declining due to side reactions and dendrite formation, resulting in the failure of the cell around 20 cycles. [17]

Wang et al. have also devoted considerable attention to the possibilities of a V_2O_5 cathode for greener rechargeable aluminum-ion batteries. [79] This study has reported on a different variation of this cathode in comparison to the V_2O_5 nanowires, this binder-free cathode was reported to have an increased initial discharge capacity of 239 mAh/g, as well as a slightly higher voltage of 0.6V. Counter to this cathode material, Mo_6S_8 was proposed as an electrode material capable of practical electrochemical intercalation. [76] According to this report Mo_6S_8 shows the unambiguous electrochemical activity of the aluminum intercalation and de-intercalation behavior coupled with an elongated cycle life. The results reported here appear to show the possibility of a practical battery with about 90 Wh/kg. Many of these cathode materials are under investigation currently to optimize aluminum's advantageous attributes to understand the trapping mechanism and correct for the irreversible capacity.

Cathodes that are based on chalcogens are another material that has been proposed to intercalate aluminum ions. CuS[80], FeS_2[81], and Ni_3S_2[82] are examples of these

chalcogen-based cathodes. Halogen-based cathodes have also been studied such as $FeCl_3$[83], VCl_3[84], $NiCl_2$[85], and PVP-iodine.[86] Further investigation into these cathode materials as well as understanding the electrolyte that will be optimized in the presence of said cathode. Current cathode materials that have been proposed for practical use are chloroaluminate ionic liquids or halogen-rich electrolytes that lead to many complications such as corrosion. The work presented in this dissertation is concentrated on specifically gaining a better understanding of the proper electrolyte for a cathode material for a practical aluminum ion battery.

References 1.7

(1) Erickson, P.; Lazarus, M.; Piggot, G. Limiting Fossil Fuel Production as the next Big Step in Climate Policy. *Nat. Clim. Change* **2018**, *8* (12), 1037–1043. https://doi.org/10.1038/s41558-018-0337-0.

(2) Cherp, A.; Vinichenko, V.; Tosun, J.; Gordon, J. A.; Jewell, J. National Growth Dynamics of Wind and Solar Power Compared to the Growth Required for Global Climate Targets. *Nat. Energy* **2021**, *6* (7), 742–754. https://doi.org/10.1038/s41560-021-00863-0.

(3) Larcher, D.; Tarascon, J.-M. Towards Greener and More Sustainable Batteries for Electrical Energy Storage. *Nat. Chem.* **2015**, *7* (1), 19–29. https://doi.org/10.1038/nchem.2085.

(4) Goodenough, J. B. Electrochemical Energy Storage in a Sustainable Modern Society. *Energy Environ. Sci.* **2013**, *7* (1), 14–18. https://doi.org/10.1039/C3EE42613K.

(5) Goodenough, J. B.; Park, K.-S. The Li-Ion Rechargeable Battery: A Perspective. *J. Am. Chem. Soc.* **2013**, *135* (4), 1167–1176. https://doi.org/10.1021/ja3091438.

(6) Tu, J.; Song, W.-L.; Lei, H.; Yu, Z.; Chen, L.-L.; Wang, M.; Jiao, S. Nonaqueous Rechargeable Aluminum Batteries: Progresses, Challenges, and Perspectives. *Chem. Rev.* **2021**, *121* (8), 4903–4961. https://doi.org/10.1021/acs.chemrev.0c01257.

(7) Elia, G. A.; Marquardt, K.; Hoeppner, K.; Fantini, S.; Lin, R.; Knipping, E.; Peters, W.; Drillet, J.-F.; Passerini, S.; Hahn, R. An Overview and Future Perspectives of Aluminum Batteries. *Adv. Mater.* **2016**, *28* (35), 7564–7579. https://doi.org/10.1002/adma.201601357.

(8) Li, Q.; Bjerrum, N. J. Aluminum as Anode for Energy Storage and Conversion: A Review. *J. Power Sources* **2002**, *110* (1), 1–10. https://doi.org/10.1016/S0378-7753(01)01014-X.

(9) Zhang, Y.; Liu, S.; Ji, Y.; Ma, J.; Yu, H. Emerging Nonaqueous Aluminum-Ion Batteries: Challenges, Status, and Perspectives. *Adv. Mater. Deerfield Beach Fla* **2018**, *30* (38), e1706310. https://doi.org/10.1002/adma.201706310.

(10) Li, M.; Lu, J.; Ji, X.; Li, Y.; Shao, Y.; Chen, Z.; Zhong, C.; Amine, K. Design Strategies for Nonaqueous Multivalent-Ion and Monovalent-Ion Battery Anodes. *Nat. Rev. Mater.* **2020**, *5* (4). https://doi.org/10.1038/s41578-019-0166-4.

(11) *The Rechargeable Aluminum Battery: Opportunities and Challenges - Yang - 2019 - Angewandte Chemie International Edition - Wiley Online Library*. https://onlinelibrary.wiley.com/doi/10.1002/anie.201814031 (accessed 2023-04-27).

(12) Elia, G. A.; Kravchyk, K. V.; Kovalenko, M. V.; Chacón, J.; Holland, A.; Wills, R. G. A. An Overview and Prospective on Al and Al-Ion Battery Technologies. *J. Power Sources* **2021**, *481*, 228870. https://doi.org/10.1016/j.jpowsour.2020.228870.
(13) Faegh, E.; Ng, B.; Hayman, D.; Mustain, W. Practical Assessment of the Performance of Aluminium Battery Technologies. *Nat. Energy* **2020**, *6*. https://doi.org/10.1038/s41560-020-00728-y.
(14) Leung, O. M.; Schoetz, T.; Prodromakis, T.; Leon, C. P. de. Review—Progress in Electrolytes for Rechargeable Aluminium Batteries. *J. Electrochem. Soc.* **2021**, *168* (5), 056509. https://doi.org/10.1149/1945-7111/abfb36.
(15) *Cathode materials for rechargeable aluminum batteries: current status and progress - Journal of Materials Chemistry A (RSC Publishing)*. https://pubs.rsc.org/en/content/articlelanding/2017/ta/c7ta00282c (accessed 2023-04-27).
(16) Shi, J.; Zhang, J.; Guo, J. Avoiding Pitfalls in Rechargeable Aluminum Batteries Research. *ACS Energy Lett.* **2019**, *4* (9), 2124–2129. https://doi.org/10.1021/acsenergylett.9b01285.
(17) Reed, L. D.; Menke, E. The Roles of V_2O_5 and Stainless Steel in Rechargeable Al–Ion Batteries. *J. Electrochem. Soc.* **2013**, *160* (6), A915–A917. https://doi.org/10.1149/2.114306jes.
(18) Wang, H.; Gu, S.; Bai, Y.; Chen, S.; Zhu, N.; Wu, C.; Wu, F. Anion-Effects on Electrochemical Properties of Ionic Liquid Electrolytes for Rechargeable Aluminum Batteries. *J. Mater. Chem. A* **2015**, *3* (45), 22677–22686. https://doi.org/10.1039/C5TA06187C.
(19) Lai, P. K.; Skyllas-Kazacos, M. Electrodeposition of Aluminium in Aluminium Chloride/1-Methyl-3-Ethylimidazolium Chloride. *J. Electroanal. Chem. Interfacial Electrochem.* **1988**, *248* (2), 431–440. https://doi.org/10.1016/0022-0728(88)85103-9.
(20) Zhang, M.; Watson, J. S.; Counce, R. M.; Trulove, P. C.; Zawodzinski, T. A. Electrochemistry and Morphology Studies of Aluminum Plating/Stripping in a Chloroaluminate Ionic Liquid on Porous Carbon Materials. *J. Electrochem. Soc.* **2014**, *161* (4), D163. https://doi.org/10.1149/2.048404jes.
(21) Mandai, T.; Johansson, P. Al Conductive Haloaluminate-Free Non-Aqueous Room-Temperature Electrolytes. *J. Mater. Chem. A* **2015**, *3* (23), 12230–12239. https://doi.org/10.1039/C5TA01760B.
(22) Reed, L. D.; Arteaga, A.; Menke, E. J. A Combined Experimental and Computational Study of an Aluminum Triflate/Diglyme Electrolyte. *J. Phys. Chem. B* **2015**, *119* (39), 12677–12681. https://doi.org/10.1021/acs.jpcb.5b08501.
(23) Reed, L. D.; Ortiz, S. N.; Xiong, M.; Menke, E. J. A Rechargeable Aluminum-Ion Battery Utilizing a Copper Hexacyanoferrate Cathode in an Organic Electrolyte. *Chem. Commun.* **2015**, *51* (76), 14397–14400. https://doi.org/10.1039/C5CC06053B.
(24) Mandai, T.; Johansson, P. Haloaluminate-Free Cationic Aluminum Complexes: Structural Characterization and Physicochemical Properties. *J. Phys. Chem. C* **2016**, *120* (38), 21285–21292. https://doi.org/10.1021/acs.jpcc.6b07235.
(25) Wen, X.; Zhang, J.; Luo, H.; Shi, J.; Tsay, C.; Jiang, H.; Lin, Y.-H.; Schroeder, M. A.; Xu, K.; Guo, J. Synthesis and Electrochemical Properties of Aluminum

Hexafluorophosphate. *J. Phys. Chem. Lett.* **2021**, *12* (25), 5903–5908. https://doi.org/10.1021/acs.jpclett.1c01236.
(26) Chiku, M.; Matsumura, S.; Takeda, H.; Higuchi, E.; Inoue, H. Aluminum Bis(Trifluoromethanesulfonyl)Imide as a Chloride-Free Electrolyte for Rechargeable Aluminum Batteries. *J. Electrochem. Soc.* **2017**, *164* (9), A1841. https://doi.org/10.1149/2.0701709jes.
(27) Hilbig, P.; Ibing, L.; Wagner, R.; Winter, M.; Cekic-Laskovic, I. Ethyl Methyl Sulfone-Based Electrolytes for Lithium Ion Battery Applications. *Energies* **2017**, *10* (9), 1312. https://doi.org/10.3390/en10091312.
(28) Avoundjian, A.; Galvan, V.; Gomez, F. An Inexpensive Paper-Based Aluminum-Air Battery. *Micromachines* **2017**, *8*. https://doi.org/10.3390/mi8070222.
(29) Lee, W.; Park, S.-J. Porous Anodic Aluminum Oxide: Anodization and Templated Synthesis of Functional Nanostructures. *Chem. Rev.* **2014**, *114* (15), 7487–7556. https://doi.org/10.1021/cr500002z.
(30) *Voltaic cell*. studylib.net. https://studylib.net/doc/18820455/voltaic-cell (accessed 2023-04-29).
(31) Zaromb, S. The Use and Behavior of Aluminum Anodes in Alkaline Primary Batteries. *J. Electrochem. Soc.* **1962**, *109* (12), 1125. https://doi.org/10.1149/1.2425257.
(32) Faegh, E.; Shrestha, S.; Zhao, X.; Mustain, W. In-Depth Structural Understanding of Zinc Oxide Addition to Alkaline Electrolytes to Protect Aluminum against Corrosion and Gassing. *J. Appl. Electrochem.* **2019**, *49*. https://doi.org/10.1007/s10800-019-01330-1.
(33) Duca, B. S. D. Electrochemical Behavior of the Aluminum Electrode in Molten Salt Electrolytes. *J. Electrochem. Soc.* **1971**, *118* (3), 405. https://doi.org/10.1149/1.2408069.
(34) Holleck, G. L.; Giner, J. The Aluminum Electrode in AlCl[Sub 3]-Alkali-Halide Melts. *J. Electrochem. Soc.* **1972**, *119* (9), 1161. https://doi.org/10.1149/1.2404433.
(35) Holleck, G. L. The Reduction of Chlorine on Carbon in AlCl3 - KCl - NaCl Melts. *J. Electrochem. Soc.* **1972**, *119* (9), 1158. https://doi.org/10.1149/1.2404432.
(36) Gifford, P. R.; Palmisano, J. B. An Aluminum/Chlorine Rechargeable Cell Employing a Room Temperature Molten Salt Electrolyte. *J. Electrochem. Soc.* **1988**, *135* (3), 650. https://doi.org/10.1149/1.2095685.
(37) Paranthaman, M. P.; Brown, G.; Sun, X.-G.; Nanda, J.; Manthiram, A.; Manivannan, A. A Transformational, High Energy Density, Secondary Aluminum Ion Battery. *ECS Meet. Abstr.* **2010**, *MA2010-02* (4), 314. https://doi.org/10.1149/MA2010-02/4/314.
(38) Jayaprakash, N.; Das, S. K.; Archer, L. A. The Rechargeable Aluminum-Ion Battery. *Chem. Commun.* **2011**, *47* (47), 12610–12612. https://doi.org/10.1039/C1CC15779E.
(39) V. Plechkova, N.; R. Seddon, K. Applications of Ionic Liquids in the Chemical Industry. *Chem. Soc. Rev.* **2008**, *37* (1), 123–150. https://doi.org/10.1039/B006677J.
(40) Pena-Pereira, F.; Namieśnik, J. Ionic Liquids and Deep Eutectic Mixtures: Sustainable Solvents for Extraction Processes. *ChemSusChem* **2014**, *7* (7), 1784–1800. https://doi.org/10.1002/cssc.201301192.

(41) Wilkes, J. S.; Levisky, J. A.; Wilson, R. A.; Hussey, C. L. Dialkylimidazolium Chloroaluminate Melts: A New Class of Room-Temperature Ionic Liquids for Electrochemistry, Spectroscopy and Synthesis. *Inorg. Chem.* **1982**, *21* (3), 1263–1264. https://doi.org/10.1021/ic00133a078.
(42) Zhao, Y.; VanderNoot, T. J. Electrodeposition of Aluminium from Nonaqueous Organic Electrolytic Systems and Room Temperature Molten Salts. *Electrochimica Acta* **1997**, *42* (1), 3–13. https://doi.org/10.1016/0013-4686(96)00080-1.
(43) Hurley, F. H.; WIer, T. P. The Electrodeposition of Aluminum from Nonaqueous Solutions at Room Temperature. *J. Electrochem. Soc.* **1951**, *98* (5), 207. https://doi.org/10.1149/1.2778133.
(44) Gale, R. J.; Gilbert, B.; Osteryoung, R. A. Raman Spectra of Molten Aluminum Chloride: 1-Butylpyridinium Chloride Systems at Ambient Temperatures. *Inorg. Chem.* **1978**, *17* (10), 2728–2729. https://doi.org/10.1021/ic50188a008.
(45) Wang, C.; Creuziger, A.; Stafford, G.; Hussey, C. L. Anodic Dissolution of Aluminum in the Aluminum Chloride-1-Ethyl-3-Methylimidazolium Chloride Ionic Liquid. *J. Electrochem. Soc.* **2016**, *163* (14), H1186. https://doi.org/10.1149/2.1061614jes.
(46) *PII: 0022-0728(88)85103-9 | Elsevier Enhanced Reader*. https://doi.org/10.1016/0022-0728(88)85103-9.
(47) Oh, Y.; Lee, G.; Tak, Y. Stability of Metallic Current Collectors in Acidic Ionic Liquid for Rechargeable Aluminum-Ion Batteries. *ChemElectroChem* **2018**, *5*, 3348–3352. https://doi.org/10.1002/celc.201801396.
(48) Couch, D. E.; Brenner, A. A Hydride Bath for the Electrodeposition of Aluminum. *J. Electrochem. Soc.* **1952**, *99* (6), 234. https://doi.org/10.1149/1.2779711.
(49) Ishibashi, N.; Yoshio, M. Electrodeposition of Aluminium from the NBS Type Bath Using Tetrahydrofuran—Benzene Mixed Solvent. *Electrochimica Acta* **1972**, *17* (8), 1343–1352. https://doi.org/10.1016/0013-4686(72)80080-X.
(50) Graef, M. W. M. The Mechanism of Aluminum Electrodeposition from Solutions of AlCl3 and LiAlH4 in THF. *J. Electrochem. Soc.* **1985**, *132* (5), 1038. https://doi.org/10.1149/1.2114011.
(51) Finholt, A. E.; Bond, A. C. Jr.; Schlesinger, H. I. Lithium Aluminum Hydride, Aluminum Hydride and Lithium Gallium Hydride, and Some of Their Applications in Organic and Inorganic Chemistry1. *J. Am. Chem. Soc.* **1947**, *69* (5), 1199–1203. https://doi.org/10.1021/ja01197a061.
(52) Legrand, L.; Tranchant, A.; Messina, R. Behaviour of Aluminium as Anode in Dimethylsulfone-Based Electrolytes. *Electrochimica Acta* **1994**, *39* (10), 1427–1431. https://doi.org/10.1016/0013-4686(94)85054-2.
(53) Legrand, L.; Tranchant, A.; Messina, R. Electrodeposition Studies of Aluminum on Tungsten Electrode from DMSO 2 Electrolytes: Determination of AlIII Species Diffusion Coefficients. *J. Electrochem. Soc.* **1994**, *141* (2), 378. https://doi.org/10.1149/1.2054735.
(54) Legrand, L.; Heintz, M.; Tranchant, A.; Messina, R. Sulfone-Based Electrolytes for Aluminum Electrodeposition. *Electrochimica Acta* **1995**, *40* (11), 1711–1716. https://doi.org/10.1016/0013-4686(95)00019-B.

(55) Legrand, L.; Tranchant, A.; Messina, R. Aluminium Behaviour and Stability in AlCl3DMSO2 Electrolyte. *Electrochimica Acta* **1996**, *41* (17), 2715–2720. https://doi.org/10.1016/0013-4686(96)00126-0.
(56) Miyake, M.; Fujii, H.; Hirato, T. Electroplating of Al on Mg Alloy in a Dimethyl Sulfone–Aluminum Chloride Bath. *Surf. Coat. Technol.* **2015**, *277*, 160–164. https://doi.org/10.1016/j.surfcoat.2015.07.047.
(57) Nakayama, Y.; Senda, Y.; Kawasaki, H.; Koshitani, N.; Hosoi, S.; Kudo, Y.; Morioka, H.; Nagamine, M. Sulfone-Based Electrolytes for Aluminium Rechargeable Batteries. *Phys. Chem. Chem. Phys.* **2015**, *17* (8), 5758–5766. https://doi.org/10.1039/C4CP02183E.
(58) Kitada, A.; Nakamura, K.; Fukami, K.; Murase, K. Electrochemically Active Species in Aluminum Electrodeposition Baths of AlCl3/Glyme Solutions. *Electrochimica Acta* **2016**, *211*, 561.
(59) Zhang, Z.; Kitada, A.; Gao, S.; Fukami, K.; Tsuji, N.; Yao, Z.; Murase, K. A Concentrated AlCl3–Diglyme Electrolyte for Hard and Corrosion-Resistant Aluminum Electrodeposits. *ACS Appl. Mater. Interfaces* **2020**, *12* (38), 43289–43298. https://doi.org/10.1021/acsami.0c12602.
(60) Kitada, A.; KATO, Y.; Fukami, K.; Murase, K. Room Temperature Electrodeposition of Flat and Smooth Aluminum Layers from An AlCl3/Diglyme Bath. *J. Surf. Finish. Soc. Jpn.* **2018**, *69*, 310–311. https://doi.org/10.4139/sfj.69.310.
(61) Howells, R. D.; Mc Cown, J. D. Trifluoromethanesulfonic Acid and Derivatives. *Chem. Rev.* **1977**, *77* (1), 69–92. https://doi.org/10.1021/cr60305a005.
(62) Slim, Z.; Menke, E. J. Comparing Computational Predictions and Experimental Results for Aluminum Triflate in Tetrahydrofuran. *J. Phys. Chem. B* **2020**, *124* (24), 5002–5008. https://doi.org/10.1021/acs.jpcb.0c02570.
(63) Hu, J. J.; Long, G. K.; Liu, S.; Li, G. R.; Gao, X. P. A LiFSI–LiTFSI Binary-Salt Electrolyte to Achieve High Capacity and Cycle Stability for a Li–S Battery. *Chem. Commun.* **2014**, *50* (93), 14647–14650. https://doi.org/10.1039/C4CC06666A.
(64) Yang, H.; Zhuang, G.; Ross, P. Thermal Stability of LiPF 6 Salt and Li-Ion Battery Electrolytes Containing LiPF 6. *J. Power Sources - J POWER SOURCES* **2006**, *161*, 573–579. https://doi.org/10.1016/j.jpowsour.2006.03.058.
(65) Younesi, R.; Veith, G. M.; Johansson, P.; Edström, K.; Vegge, T. Lithium Salts for Advanced Lithium Batteries: Li–Metal, Li–O2, and Li–S. *Energy Environ. Sci.* **2015**, *8* (7), 1905–1922. https://doi.org/10.1039/C5EE01215E.
(66) Ha, S.-Y.; Lee, Y.-W.; Woo, S. W.; Koo, B.; Kim, J.-S.; Cho, J.; Lee, K. T.; Choi, N.-S. Magnesium(II) Bis(Trifluoromethane Sulfonyl) Imide-Based Electrolytes with Wide Electrochemical Windows for Rechargeable Magnesium Batteries. *ACS Appl. Mater. Interfaces* **2014**, *6* (6), 4063–4073. https://doi.org/10.1021/am405619v.
(67) Keyzer, E. N.; Glass, H. F. J.; Liu, Z.; Bayley, P. M.; Dutton, S. E.; Grey, C. P.; Wright, D. S. Mg(PF6)2-Based Electrolyte Systems: Understanding Electrolyte-Electrode Interactions for the Development of Mg-Ion Batteries. *J. Am. Chem. Soc.* **2016**, *138* (28), 8682–8685. https://doi.org/10.1021/jacs.6b04319.
(68) Wang, Y.; Xing, L.; Li, W.; Bedrov, D. Why Do Sulfone-Based Electrolytes Show Stability at High Voltages? Insight from Density Functional Theory. *J. Phys. Chem. Lett.* **2013**, *4* (22), 3992–3999. https://doi.org/10.1021/jz401726p.

(69) Xing, L.; Wang, C.; Li, W.; Xu, M.; Meng, X.; Zhao, S. Theoretical Insight into Oxidative Decomposition of Propylene Carbonate in the Lithium Ion Battery. *J. Phys. Chem. B* **2009**, *113* (15), 5181–5187. https://doi.org/10.1021/jp810279h.
(70) Dunn, B.; Kamath, H.; Tarascon, J.-M. Electrical Energy Storage for the Grid: A Battery of Choices. *Science* **2011**, *334* (6058), 928–935. https://doi.org/10.1126/science.1212741.
(71) Manthiram, A. A Reflection on Lithium-Ion Battery Cathode Chemistry. *Nat. Commun.* **2020**, *11* (1), 1550. https://doi.org/10.1038/s41467-020-15355-0.
(72) Wu, F.; Yang, H.; Bai, Y.; Wu, C. Paving the Path toward Reliable Cathode Materials for Aluminum-Ion Batteries. *Adv. Mater. Deerfield Beach Fla* **2019**, *31* (16), e1806510. https://doi.org/10.1002/adma.201806510.
(73) Lin, M.-C.; Gong, M.; Lu, B.; Wu, Y.; Wang, D.-Y.; Guan, M.; Angell, M.; Chen, C.; Yang, J.; Hwang, B.-J.; Dai, H. An Ultrafast Rechargeable Aluminium-Ion Battery. *Nature* **2015**, *520* (7547), 324–328. https://doi.org/10.1038/nature14340.
(74) Kravchyk, K. V.; Wang, S.; Piveteau, L.; Kovalenko, M. V. Efficient Aluminum Chloride–Natural Graphite Battery. *Chem. Mater.* **2017**, *29* (10), 4484–4492. https://doi.org/10.1021/acs.chemmater.7b01060.
(75) Greco, G.; Tatchev, D.; Hoell, A.; Krumrey, M.; Raoux, S.; Hahn, R.; Elia, G. A. Influence of the Electrode Nano/Microstructure on the Electrochemical Properties of Graphite in Aluminum Batteries. *J. Mater. Chem. A* **2018**, *6* (45), 22673–22680. https://doi.org/10.1039/C8TA08319C.
(76) Geng, L.; Lv, G.; Xing, X.; Guo, J. Reversible Electrochemical Intercalation of Aluminum in Mo6S8. *Chem. Mater.* **2015**, *27* (14), 4926–4929. https://doi.org/10.1021/acs.chemmater.5b01918.
(77) Lee, B.; Lee, H. R.; Yim, T.; Kim, J. H.; Lee, J. G.; Chung, K. Y.; Cho, B. W.; Oh, S. H. Investigation on the Structural Evolutions during the Insertion of Aluminum Ions into Mo6S8 Chevrel Phase. *J. Electrochem. Soc.* **2016**, *163* (6), A1070. https://doi.org/10.1149/2.0011607jes.
(78) *X-MOL*. x-mol.net. https://www.x-mol.net/paper/article/1356342681998311424 (accessed 2023-05-09).
(79) Wang, H.; Bai, Y.; Chen, S.; Luo, X.; Wu, C.; Wu, F.; Lu, J.; Amine, K. Binder-Free V2O5 Cathode for Greener Rechargeable Aluminum Battery. *ACS Appl. Mater. Interfaces* **2015**, *7* (1), 80–84. https://doi.org/10.1021/am508001h.
(80) Wang, S.; Jiao, S.; Wang, J.; Chen, H.-S.; Tian, D.; Lei, H.; Fang, D.-N. High-Performance Aluminum-Ion Battery with CuS@C Microsphere Composite Cathode. *ACS Nano* **2017**, *11* (1), 469–477. https://doi.org/10.1021/acsnano.6b06446.
(81) Mori, T.; Orikasa, Y.; Nakanishi, K.; Kezheng, C.; Hattori, M.; Ohta, T.; Uchimoto, Y. Discharge/Charge Reaction Mechanisms of FeS2 Cathode Material for Aluminum Rechargeable Batteries at 55°C. *J. Power Sources* **2016**, *313*, 9–14. https://doi.org/10.1016/j.jpowsour.2016.02.062.
(82) Wang, S.; Yu, Z.; Tu, J.; Wang, J.; Tian, D.; Liu, Y.; Jiao, S. A Novel Aluminum-Ion Battery: Al/AlCl $_3$ -[EMIm]Cl/Ni $_3$ S $_2$ @Graphene. *Adv. Energy Mater.* **2016**, *6* (13), 1600137. https://doi.org/10.1002/aenm.201600137.

(83) Donahue, F. M.; Mancini, S. E.; Simonsen, L. Secondary Aluminium-Iron (III) Chloride Batteries with a Low Temperature Molten Salt Electrolyte. *J. Appl. Electrochem.* **1992**, *22* (3), 230–234. https://doi.org/10.1007/BF01030182.
(84) Suto, K.; Nakata, A.; Murayama, H.; Hirai, T.; Yamaki, J.; Ogumi, Z. Electrochemical Properties of Al/Vanadium Chloride Batteries with AlCl3-1-Ethyl-3-Methylimidazolium Chloride Electrolyte. *J. Electrochem. Soc.* **2016**, *163* (5), A742. https://doi.org/10.1149/2.0991605jes.
(85) Nakaya, K.; Nakata, A.; Hirai, T.; Ogumi, Z. Oxidation of Nickel in AlCl3-1-Butylpyridinium Chloride at Ambient Temperature. *J. Electrochem. Soc.* **2014**, *162* (1), D42. https://doi.org/10.1149/2.0401501jes.
(86) Tian, H.; Zhang, S.; Meng, Z.; He, W.; Han, W.-Q. Rechargeable Aluminum/Iodine Battery Redox Chemistry in Ionic Liquid Electrolyte. *ACS Energy Lett.* **2017**, *2* (5), 1170–1176. https://doi.org/10.1021/acsenergylett.7b00160.
(87) Armand, M.; Tarascon, J.-M. Building Better Batteries. *Nature* **2008**, *451* (7179), 652–657. https://doi.org/10.1038/451652a.
(88) Gao, X.-P.; Yang, H.-X. Multi-Electron Reaction Materials for High Energy Density Batteries. *Energy Environ. Sci.* **2010**, *3* (2), 174–189. https://doi.org/10.1039/B916098A.
(89) *2 – Past, Present and Future of Lithium-Ion Batteries: Can New Technologies Open up New Horizons? | Elsevier Enhanced Reader*. https://doi.org/10.1016/B978-0-444-59513-3.00002-9.
(90) Hu, Y.; Sun, D.; Luo, B.; Wang, L. Recent Progress and Future Trends of Aluminum Batteries. *Energy Technol.* **2019**, *7* (1), 86–106. https://doi.org/10.1002/ente.201800550.
(91) Shkrob, I. A.; Wishart, J. F.; Abraham, D. P. What Makes Fluoroethylene Carbonate Different? *J. Phys. Chem. C* **2015**, *119* (27), 14954–14964. https://doi.org/10.1021/acs.jpcc.5b03591.
(92) Tseng, C.-H.; Chang, J.-K.; Chen, J.-R.; Tsai, W. T.; Deng, M.-J.; Sun, I.-W. Corrosion Behaviors of Materials in Aluminum Chloride–1-Ethyl-3-Methylimidazolium Chloride Ionic Liquid. *Electrochem. Commun.* **2010**, *12* (8), 1091–1094. https://doi.org/10.1016/j.elecom.2010.05.036.
(93) *Gaussian 09 Citation | Gaussian.com*. https://gaussian.com/g09citation/ (accessed 2022-12-06).
(94) Becke, A. D. Density-functional Thermochemistry. III. The Role of Exact Exchange. *J. Chem. Phys.* **1993**, *98* (7), 5648–5652. https://doi.org/10.1063/1.464913.
(95) Krishnan, R.; Binkley, J. S.; Seeger, R.; Pople, J. A. Self-consistent Molecular Orbital Methods. XX. A Basis Set for Correlated Wave Functions. *J. Chem. Phys.* **1980**, *72* (1), 650–654. https://doi.org/10.1063/1.438955.
(96) Marenich, A. V.; Cramer, C. J.; Truhlar, D. G. Universal Solvation Model Based on Solute Electron Density and on a Continuum Model of the Solvent Defined by the Bulk Dielectric Constant and Atomic Surface Tensions. *J. Phys. Chem. B* **2009**, *113* (18), 6378–6396. https://doi.org/10.1021/jp810292n.
(97) Roy, L. E.; Jakubikova, E.; Guthrie, M. G.; Batista, E. R. Calculation of One-Electron Redox Potentials Revisited. Is It Possible to Calculate Accurate Potentials

with Density Functional Methods? *J. Phys. Chem. A* **2009**, *113* (24), 6745–6750. https://doi.org/10.1021/jp811388w.
(98) Jafari, S.; Tavares Santos, Y. A.; Bergmann, J.; Irani, M.; Ryde, U. Benchmark Study of Redox Potential Calculations for Iron–Sulfur Clusters in Proteins. *Inorg. Chem.* **2022**, *61* (16), 5991–6007. https://doi.org/10.1021/acs.inorgchem.1c03422.
(99) Shao, N.; Sun, X.-G.; Dai, S.; Jiang, D. Electrochemical Windows of Sulfone-Based Electrolytes for High-Voltage Li-Ion Batteries. *J. Phys. Chem. B* **2011**, *115* (42), 12120–12125. https://doi.org/10.1021/jp204401t.
(100) Yan, C.; Lv, C.; Wang, L.; Cui, W.; Zhang, L.; Dinh, K. N.; Tan, H.; Wu, C.; Wu, T.; Ren, Y.; Chen, J.; Liu, Z.; Srinivasan, M.; Rui, X.; Yan, Q.; Yu, G. Architecting a Stable High-Energy Aqueous Al-Ion Battery. *J. Am. Chem. Soc.* **2020**, *142* (36), 15295–15304. https://doi.org/10.1021/jacs.0c05054.
(101) *Lithium-Ion Batteries*. https://shop.elsevier.com/books/lithium-ion-batteries/pistoia/978-0-444-59513-3 (accessed 2022-12-20).
(102) Zu, C.-X.; Li, H. Thermodynamic Analysis on Energy Densities of Batteries. *Energy Environ. Sci.* **2011**, *4* (8), 2614–2624. https://doi.org/10.1039/C0EE00777C.
(103) Leisegang, T.; Meutzner, F.; Zschornak, M.; Münchgesang, W.; Schmid, R.; Nestler, T.; Eremin, R. A.; Kabanov, A. A.; Blatov, V. A.; Meyer, D. C. The Aluminum-Ion Battery: A Sustainable and Seminal Concept? *Front. Chem.* **2019**, *7*.
(104) Fan, H.; Liu, X.; Luo, L.; Zhong, F.; Cao, Y. All-Climate High-Voltage Commercial Lithium-Ion Batteries Based on Propylene Carbonate Electrolytes. *ACS Appl. Mater. Interfaces* **2022**, *14* (1), 574–580. https://doi.org/10.1021/acsami.1c16767.
(105) Hu, C.-C.; Chiu, P.-H.; Wang, S.-J.; Cheng, S.-H. Isobaric Vapor–Liquid Equilibria for Binary Systems of Diethyl Carbonate + Propylene Carbonate, Diethyl Carbonate + Propylene Glycol, and Ethanol + Propylene Carbonate at 101.3 KPa. *J. Chem. Eng. Data* **2015**, *60* (5), 1487–1494. https://doi.org/10.1021/acs.jced.5b00064.
(106) Xing, L.; Zheng, X.; Schroeder, M.; Alvarado, J.; von Wald Cresce, A.; Xu, K.; Li, Q.; Li, W. Deciphering the Ethylene Carbonate–Propylene Carbonate Mystery in Li-Ion Batteries. *Acc. Chem. Res.* **2018**, *51* (2), 282–289. https://doi.org/10.1021/acs.accounts.7b00474.
(107) Becke, A. D. Density-Functional Thermochemistry. III. The Role of Exact Exchange. *J. Chem. Phys.* **1993**, *98*, 5648–5652. https://doi.org/10.1063/1.464913.
(108) Jay, A.; Huet, C.; Salles, N.; Gunde, M.; Martin-Samos, L.; Richard, N.; Landa, G.; Goiffon, V.; De Gironcoli, S.; Hémeryck, A.; Mousseau, N. Finding Reaction Pathways and Transition States: R-ARTn and d-ARTn as an Efficient and Versatile Alternative to String Approaches. *J. Chem. Theory Comput.* **2020**, *16* (10), 6726–6734. https://doi.org/10.1021/acs.jctc.0c00541.
(109) Bauernschmitt, R.; Ahlrichs, R. Stability Analysis for Solutions of the Closed Shell Kohn-Sham Equation. *J. Chem. Phys.* **1996**, *104*, 9047–9052. https://doi.org/10.1063/1.471637.
(110) Menges, F. *Spectragryph - optical spectroscopy software*. Spectroscopy. http://spectragryph.com/ (accessed 2022-12-08).
(111) Konezny, S. J.; Doherty, M. D.; Luca, O. R.; Crabtree, R. H.; Soloveichik, G. L.; Batista, V. S. Reduction of Systematic Uncertainty in DFT Redox Potentials of

Transition-Metal Complexes. *J. Phys. Chem. C* **2012**, *116* (10), 6349–6356. https://doi.org/10.1021/jp300485t.
(112) Huang, W.; Frech, R.; Wheeler, R. A. Molecular Structures and Normal Vibrations of Trifluoromethane Sulfonate (CF3SO3-) and Its Lithium Ion Pairs and Aggregates. *J. Phys. Chem.* **1994**, *98* (1), 100–110. https://doi.org/10.1021/j100052a018.
(113) Frech, R.; Huang, W. Anion-Solvent and Anion-Cation Interactions in Lithium and Tetrabutylammonium Trifluoromethanesulfonate Solutions. *J. Solut. Chem.* **1994**, *23* (4), 469–481. https://doi.org/10.1007/BF00972613.
(114) Frech, R.; Huang, W. Ionic Association in Poly (Propylene Oxide) Complexed with Divalent Metal Trifluoromethanesulfonate Salts. *Solid State Ion.* **1993**, *66* (1), 183–188. https://doi.org/10.1016/0167-2738(93)90042-2.
(115) Huang, W.; Frech, R. Dependence of Ionic Association on Polymer Chain Length in Poly(Ethylene Oxide)-Lithium Triflate Complexes. *Polymer* **1994**, *35* (2), 235–242. https://doi.org/10.1016/0032-3861(94)90684-X.
(116) Bernson, A.; Lindgren, J.; Huang, W.; Frech, R. Coordination and Conformation in PEO, PEGM and PEG Systems Containing Lithium or Lanthanum Triflate. *Polymer* **1995**, *36* (23), 4471–4478. https://doi.org/10.1016/0032-3861(95)96855-3.
(117) Wendsjö, Å.; Lindgren, J.; Thomas, J. O.; Farrington, G. C. The Effect of Temperature and Concentration on the Local Environment in the System M(CF3SO3)2PEOn for M=Ni, Zn and Pb. *Solid State Ion.* **1992**, *53–56*, 1077–1082. https://doi.org/10.1016/0167-2738(92)90293-X.

Chapter 2: Comparing Computational Predictions and Experimental Results for Aluminum Triflate in Ethyl Methyl Sulfone

2.1 Introduction

To achieve a green and energy-sustainable society, developing non-fossil fuel energy storage options is vital. Investigating stable, post-lithium secondary battery chemistries have become necessary to meet the increase in energy storage needs. [87] Portable electronics have relied greatly on lithium-ion batteries since the early '90s, 90% of current rechargeable-ion battery devices. [88] A problem arises with the availability of lithium being scarce in the earth's crust. [89] This lack of abundance of lithium being only 0.0065% of the earth's crust leads to the belief that lithium will not be able to meet future energy storage needs.

To solve the problem of unavailable lithium, aluminum ion batteries have been proposed as a promising alternative capable of replacing lithium-ion batteries as the dominant pathway to store energy soon. Extensive investigation of cathode materials and electrolytes for aluminum ion batteries has been motivated by aluminum's advantageous attributes of abundance, low cost (~1.4 USD/kg), high theoretical volumetric charge density (8042 mAh/ml), and the trivalent nature of aluminum. [7, 90]

To fully utilize these promising attributes, it is important to partner aluminum with a stable electrolyte that allows a conductive environment that will allow for the transportation of aluminum ions, therefore, allowing reversible plating and stripping. An ideal solvent plays an essential role in establishing the electrolyte's stability through understanding the electrochemical window. The electrolyte that we are specifically focused on in this project is ethyl methyl sulfone. A study conducted by Peter Hilbig et al. reports on the potential of an EMS-based electrolyte utilizing Lithium-ion batteries. [27] In 2017, EMS was utilized as a sulfone-based electrolyte capable of high oxidative stability. This investigation into the possibilities of a sulfone-based electrolyte for the purpose of a rechargeable ion battery has shown to have a wide temperature range, allowing reversible stripping and plating above 100°C. Stable capacitance was also shown over 100 cycles was also present for the Li-ion battery in EMS. The effectiveness EMS has shown in the presence of lithium encouraged the research conducted in this project in the interest of comparison with aluminum's advantageous attributes.

Electrochemical deposition of pure aluminum (Al) has drawn significant attention around the world during the last decade. It is well known that aluminum is one of the most abundant metals on earth, being light and inexpensive while having excellent thermal and electrical conductivities, and exceptional corrosion resistance thanks to its native oxide

layer, which can be further anodized. [17,92] Aluminum's value has risen due to industrial demand for advancements in the field of energy storage. All efforts to gain an understanding of aluminum-based electrolytes are geared towards the desire to improve the efficiency of energy storage and conversion devices, including batteries.

Density functional theory (DFT) derived physicochemical properties of aluminum trifluoromethane sulfonate (Al-triflate) in ethyl methyl sulfone (EMS) was conducted to theoretically predict the most present and stable species in solution and predict the stability and ionic association. The electrochemical activity of aluminum ions was revealed by cyclic voltammetry measurements on a gold working electrode at various concentrations and temperatures, then compared to the stability predictions gathered by DFT. Fourie transform infrared Spectroscopy measurements reveal ionic association as it is related to the concentration-dependent behavior for the triflate/Al-complex with the presence of an Al-triflate bond and contact ion paired aluminum/triflate being present in the most concentrated solutions. These vibrational modes that are revealed in the FTIR spectra can then be compared to the vibrational frequencies gathered by DFT in Gaussian. Furthermore, electrochemical impedance spectroscopy measurements demonstrate the ionic conductivity profile as a function of molar concentrations, where an increase in ionic conductivity is observed up to the point of saturation to establish the optimal concentration that can allow maximum conductivity.

2.2 Materials and Methods

2.2.1 Density Functional Theory. Calculations

Calculations were performed using the Gaussian 09 suite of electronic structure programs. [93] The B3PW91 density functional was administered using the unrestricted spin-formalism for all open-shell cases along with the 6-311+G(d) basis set. [94,95] Geometry optimizations were conducted using standard methods, and the natures of the stationary points on the potential energy surfaces were confirmed using second-derivative calculations.21 A solvation model density (SMD) continuum solvation model was utilized to investigate the solvation-free energies based on the self-consistent reaction field (SCRF) approach, [96] and DMSO was used for all SMD calculations. Lastly, the stability of the SCF was verified in all cases.

2.2.2 Experimental Details.

Aluminum triflate and ethyl methyl sulfone were purchased from Sigma-Aldrich. The aluminum triflate was used without further purification, while the ethyl methyl sulfone was purified in a commercial purification system and transferred to a glovebox under argon. All chemical preparations and electrochemical measurements were carried out in an argon-filled glovebox (VAC) with water and oxygen levels held below 1.5 and 0.5 ppm, respectively. The solutions described below were prepared by dissolving various amounts of aluminum-triflate in ethyl methyl sulfone. Stirring overnight was the method used to promote complete dissolution.

Cyclic voltammetry measurements were performed using a potentiostat (Gamry). The electrochemical cells for cyclic voltammetry measurements consisted of a gold working electrode, an aluminum wire counter electrode, and an aluminum wire pseudo reference electrode set up in a standard three-electrode cell configuration. Scan rates of 2 mV/s, 10 mV/s, 50 mV/s, and 100 mV/s were used.

Ionic conductivity measurements were performed using a ParStat 2273 by means of electrochemical impedance spectroscopy. A 10 mV ac signal with a 0 V dc offset was used over a 0.1−4 kHz frequency range. The impedance cell was prepared in the lab and consisted of two platinum wires encased in flint glass tubing that were polished with 0.3 μm alumina. The cell was calibrated using a 0.01 M KCl standard solution at 20°C.

Fourier transform infrared (FTIR) spectra were measured using a Nicolet iS50R FT-IR in ATR. Resolutions of 4 cm^{-1} were used for concentrated solutions and 1 cm^{-1} for the most dilute. The spectra were normalized and smoothed using Spectragryph software.

2.3 Results and Discussion

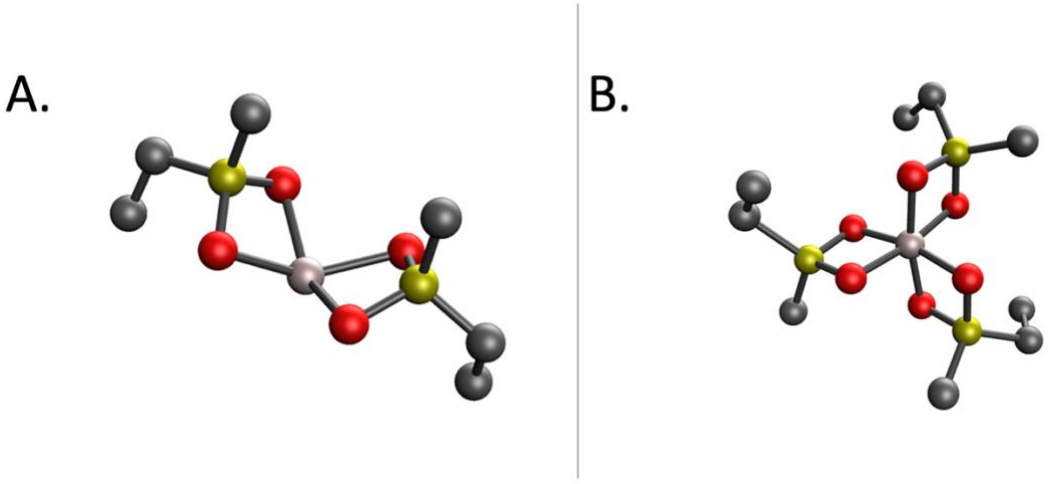

Figure 2.1 Optimized structures of (a) $Al(EMS)_2^{3+}$ and, (b) $Al(EMS)_3^{3+}$, pink: aluminum, grey: carbon, red: oxygen, yellow: sulfur, white: hydrogen

2.3.1 Coordination Structures.

DFT calculations were utilized to understand the coordination structures of the gas and solvent phase Al^{3+}/EMS complexes. The theoretical Gibbs free energy of the reactions resulting in an Al^{3+} cation coordinated by two and three ethyl methyl sulfone molecules was evaluated.

Reaction 1: $Al^{3+} + 2\ EMS \rightarrow Al(EMS)_2^{3+}$ ΔG_1= -483.22 kJ/mol

Reaction 2: $Al^{3+} + 3\ EMS \rightarrow Al(EMS)_3^{3+}$ ΔG_2= -483.49 kJ/mol

The reactions that produce $Al(EMS)_2^{3+}$ and $Al(EMS)_3^{3+}$ are shown to be the most thermodynamically favorable with solvent phase Gibbs free energy of nearly -500 kJ/mol that was calculated using density functional theory. We expect these configurations of the Al-EMS complex to be most present in the solution due to their entropic attributes. These optimized structures will be used as the focus of our computational analysis.

To understand the impact triflate anions are having in solution and on the geometry of $Al(EMS)_3^{3+}$, spectroscopic measurements were performed and compared to results from the DFT calculations with different numbers of coordinated triflate anions around the aluminum core.
Figure 2.2A-C are examples of geometries created using density functional theory calculations that were all revealed as stable structures. The vibrational frequencies gathered from the optimized structures in Figure 2.2B-C show two ways in which triflate interacts with the aluminum core. Figure 2B shows triflate ion-paired interaction via contact-ion pairing, while in Figure 2.2C triflate is directly bound to aluminum. After analyzing various configurations of triflate around the aluminum core, interestingly only one triflate will be bound to the core while the other triflate molecules are either free or contact ion paired. Figure 2.2A shows the presence of free triflate, the vibrational frequencies of each can be gathered in Gaussian. Al-triflate bonds in these electrolytes and the specific regions of the triflate anions provide insight for intricate analyses of the anion-dependent physiochemical properties.

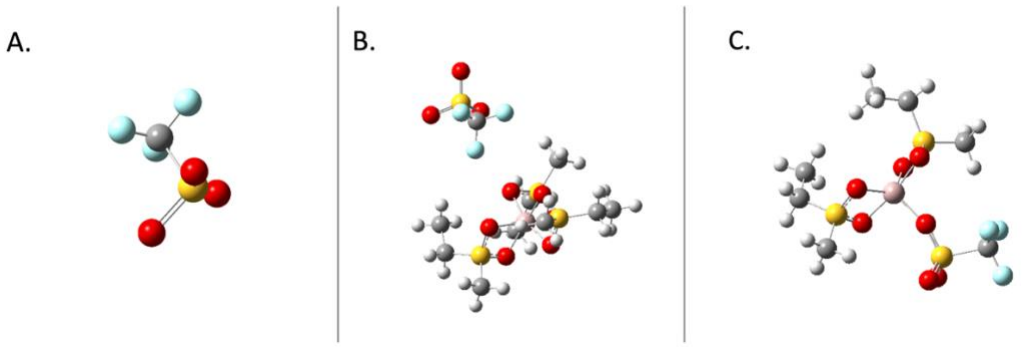

Figure 2.2 Optimized structures (hydrogens shown as white) of (A) Free triflate, (B) Contact ion paired $[Al(EMS)_3][triflate]_1^{2+}$, (C) Bound-triflate $[Al(EMS)_3][triflate]_1^{2+}$. Pink: Al, grey: carbon, red: oxygen, blue: fluorine, yellow: sulfur.

2.3.2 Determining the ionic association interaction between aluminum and triflate in EMS using infrared spectroscopy

Table 2.1 Measured and Computed Vibrational Frequencies (cm^{-1}) of CF_3 symmetric deformation, SO_3 symmetric, and antisymmetric stretching modes.

Species	Free triflate		Contact ion pair		Bound triflate	
Mode	computed	measured	computed	measured	computed	measured
CF_3 symmetric deformation	768.1	768	772.8	770	759.3	
SO_3 symmetric stretch	1178.9		998.3		989.6	986
SO_3 antisymmetric stretch	1204	1205	1210.4	1210	1215.9	1200-1240

The FTIR spectra show the concentration bands of the distinct regimes are in agreement with the predicted IR-Spectra gathered in Gaussian through utilizing density functional theory calculations on $[Al(EMS)_3][triflate]1^{2+}$, this complex exhibits vibrational frequencies around 770 cm-1 which is related to the $\delta s(CF_3)$ vibrational mode of the Al-bound triflates. Analysis of triflate ionic association was also reported in previous studies done by Reed, Slim, and others. Similar vibrational frequencies of triflate anions were presented in these reports on the $\delta s(CF_3)$ vibrational mode for Al-bound triflate. One peak that isn't present in this study or the previous studies in our lab referring to aluminum triflate in organic solvents is the peak at 751 cm^{-1} which is related to the CF_3 vibrational frequency of free triflate in solution. The lack of this free triflate peak suggests that $Al(EMS)_3^{3+}$ is more available to be paired with triflate anions in comparison to the work investigating triflate's behavior in diglyme.

Within the region that encompasses the frequency range of 750-775 cm^{-1} for the CF_3 symmetric deformation mode, there is an absence of the peak near 750 that is designated as free triflate. However, the free triflate does strictly manifest as a CF_3 stretch. Figure 2.2C is evidence of another region where free triflate can be observed around 985 cm^{-1} which can be assigned to the non-degenerate symmetric stretch of the SO_3 in free triflate $\nu_s SO_3$. When observing the band in Figure 2.2C the free triflate peak does not shift position, relatively staying at the same wavenumber as the concentration is increased from 0.1 to 1.0M.

A.

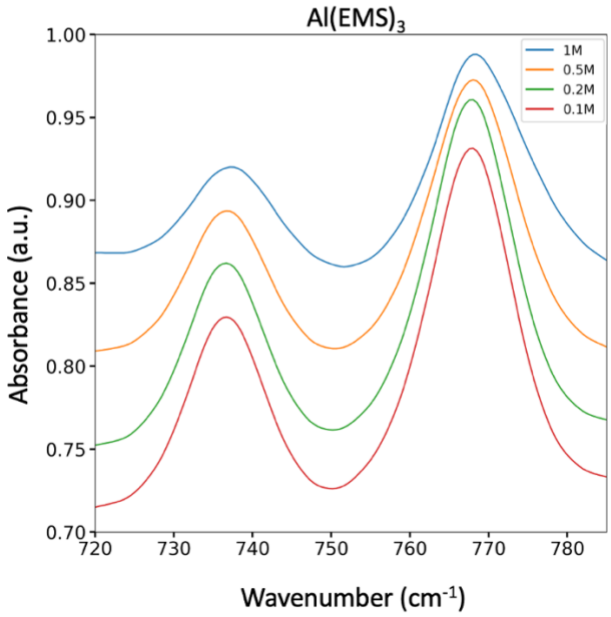
Al(EMS)3
1M
0.5M
0.2M
0.1M
Absorbance (a.u.)
1.00
0.95
0.90
0.85
0.80
0.75
0.70
720
730
740
750
760
770
780
Wavenumber (cm-1)

B.

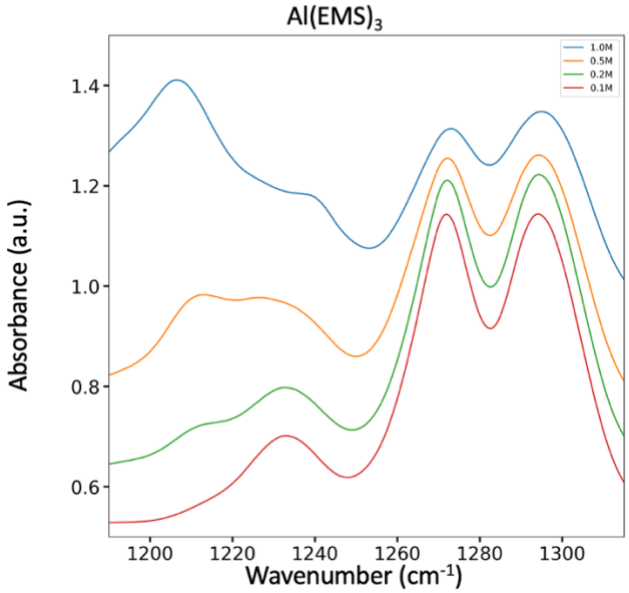
Al(EMS)3
1.0M
0.5M
0.2M
0.1M
Absorbance (a.u.)
1.4
1.2
1.0
0.8
0.6
1200
1220
1240
1260
1280
1300
Wavenumber (cm-1)

C.

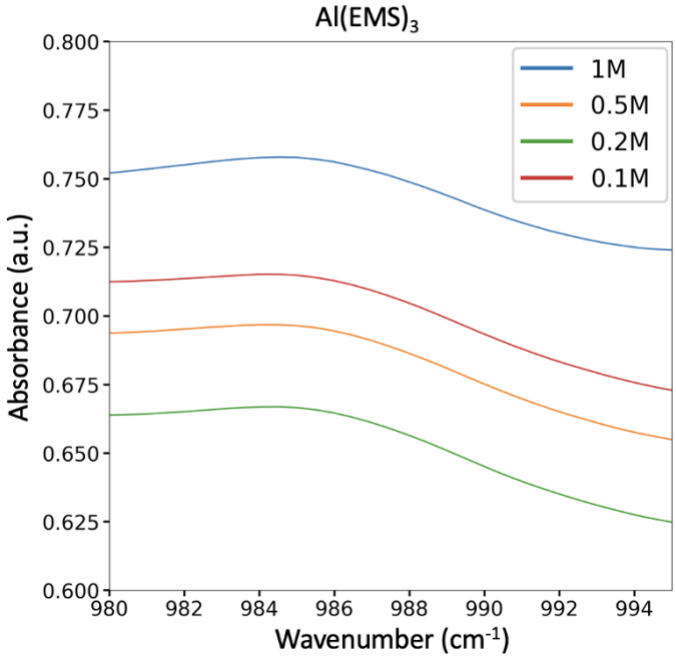

Figure 2.3 FTIR spectra of Al-triflate/EMS solutions (A) CF_3 symmetric deformation region, (B) SO_3 antisymmetric stretch region, and (C) SO_3 symmetric stretch region.

Figure 2.2A shows the absorption bands of the $\delta s(CF_3)$ for four different concentrations. Analysis of triflate ionic association has been compartmentalized into two distinct regions of triflate anion interaction. High-intensity downfield peaks near 770 cm^{-1} that appear more pronounced as concentration is increased to 1M are attributed to the $\delta s(CF_3)$ mode for Al-bound triflate anions. The spectra in Figure 2.2A also reveal a peak near 740 cm^{-1} that is shifted too far downfield to be assigned to free triflate bands but rather is attributed to ion aggregates.

The most influential region in the IR spectra is seen when investigating bands at 1200 and 1400 cm^{-1}, where the best indication of the strength of ionic association can be understood. Previous studies on lithium triflate ionic interaction in solutions comprising tetrahydrofuran, triethylene glycol dimethyl ether, acetone, and acetonitrile have shown a splitting of the doubly degenerate antisymmetric SO_3 mode, $v_{as}SO_3$ into two peaks. The degree of wavelength band splitting is indicative of the strength of ionic association, $\Delta v_{as}(SO_3)$.

Lithium-triflate in THF shows a frequency separation of 54 cm^{-1}, separating peaks at 1254 and 1308 cm^{-1}. This study is focused on aluminum-triflate, which has been studied

in a previous report by Slim in THF where the split between the designated peaks positioned at 1238 and 1309 cm^{-1} at a $\Delta\nu_{as}(SO_3)$ near 71 cm^{-1}. The difference when comparing Al-triflate/THF and Li-triflate/THF can be attributed to an increase in the charge density of the Al-cation.

The IR spectra and computational results for $[Al(EMS)_3][triflate]_1^{2+}$ reveal an exceedingly wide band splitting in this region at 1210 and 1300 cm^{-1}, with a frequency separation of 90 cm^{-1} which is indicative of two separate environments of triflate which are contact ion paired triflate and bound triflate of the doubly-degenerate, which differs from the actual splitting that Frech and Huang suggested.

2.3.3 Stability Predictions and electrochemical profiling

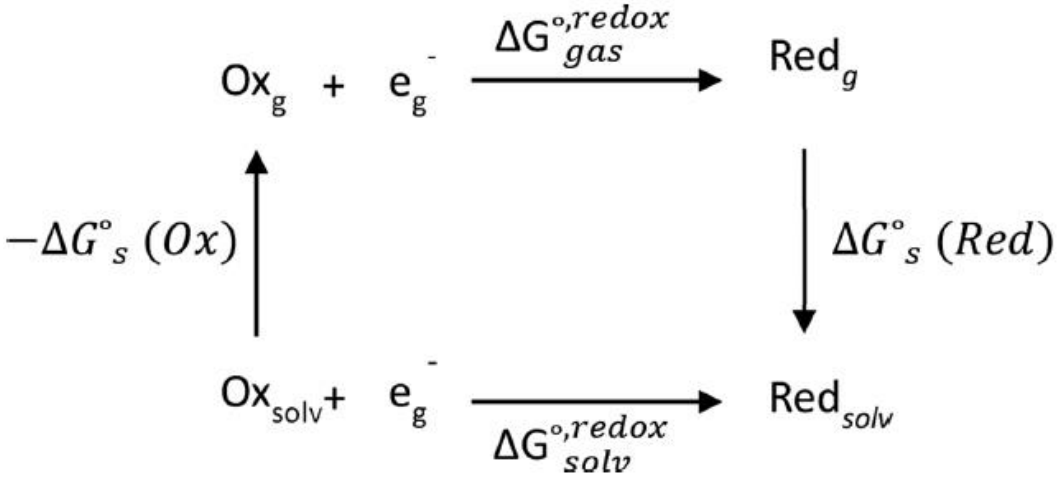

Scheme 2.1 Born-Haber cycle is used to calculate the changes in the standard solvation Gibbs Free Energy.

$$\Delta G^{\circ,redox}_{solv} = \Delta G^{\circ,redox}_{gas} + \Delta G^{\circ}_s(Red) - \Delta G^{\circ}_s(Ox) \quad (1)$$

To understand to electrochemical behavior of Al^{3+} in EMS, the free energies of each species are a valuable tool to solve for the total free energy of the redox for the desired component in the electrolyte. Utilizing the Born-Haber Cycle shown in scheme 1[97–99] to understand the reduction of one electron process In order to estimate the redox potentials, E^{abs}_{calc} . The following approach is necessary to solve for the total Gibbs free energy in the solvent phase ($\Delta G^{\circ,redox}_{solv}$) shown in equation (1). This method includes calculating for the solvation-free energies of the oxidized species, $\Delta G^{\circ}_S(Ox)$, reduced species, $\Delta G^{\circ}_S(Red)$, and the gas phase standard Gibbs free Energies $\Delta G \Delta G^{redox}_{gas}$

$$E_{calc}^{abs} = -\frac{\Delta G_{solv}^{\circ,redox}}{nF} \quad (2)$$

The Nernst equation seen in equation (2) can then be used to solve for E_{calc}^{abs} , where F is Faraday's constant, and n is the number of electrons. With the help of these calculations, it is possible to solve for the absolute redox potentials, which allows us to predict the electrochemical window of species in solution. Table 2.2 is a summary of the free energies that are necessary to solve for the absolute redox potentials for these calculations.

Table 2.2 Gibbs Free Energies and Absolute Reduction Potentials of Solvent, Anion, and Complex

Reaction	$\Delta G_s^{\circ,Ox}$ (kJ/mol)	$\Delta G^{\circ redox}_{gas}$ (kJ/mol)	$\Delta G_s^{\circ(Red)}$ (kJ/mol)	E_{calc}^{abs} (V)	E_{calc} (V vs Al/Al^{+3})
$EMS^+ + e^- \rightarrow$ EMS	-286.2	-893.4	-69.5	7.01	2.2
$EMS + e^- \rightarrow EMS^-$	-69.5	607.2	-919.2	2.51	-2.4
$triflate + e^- \rightarrow triflate^-$	-15.5	-489.7	-187.2	6.86	1.9
$triflate^- + e^- \rightarrow triflate^{-2}$	-187.3	457.1	-598.3	-0.5	-5.3
$Al(EMS)_3^{+4} + e^- \rightarrow Al(EMS)_3^{+3}$	-56.7	402.8	-1378.7	9.5	4.7
$Al(EMS)_3^{+3} + e^- \rightarrow Al(EMS)_3^{+2}$	-1378.7	-1204.9	-643.1	4.9	0

The electrochemical window of the EMS, triflate, and Al(EMS)$_3^{3+}$ as predicted from the DFT calculations are 4.5V, 7.3V, and 4.5V respectively. These EW's suggest the stability of the electrolyte is dependent upon the oxidation of the solvent (EMS) and the reduction of the overall electrolyte Al(EMS)$_3^{3+}$. The overall electrochemical window for this system is nearly 2.5V. reduction of Al^{3+} to Al metal should take place near 0 volts vs the aluminum wire. With this knowledge, the correction can be made for the computation of absolute redox predictions. In Table 2.2 the calculated predictions are shown and can be compared to the experimental data gathered. These results suggest that the stability that is governed by a specific range from the oxidation of ethyl methyl sulfone to the reduction of Al(EMS)$_3^{3+}$, which would imply that the electrochemical window is around 2.51V as calculated here. [22, 99]

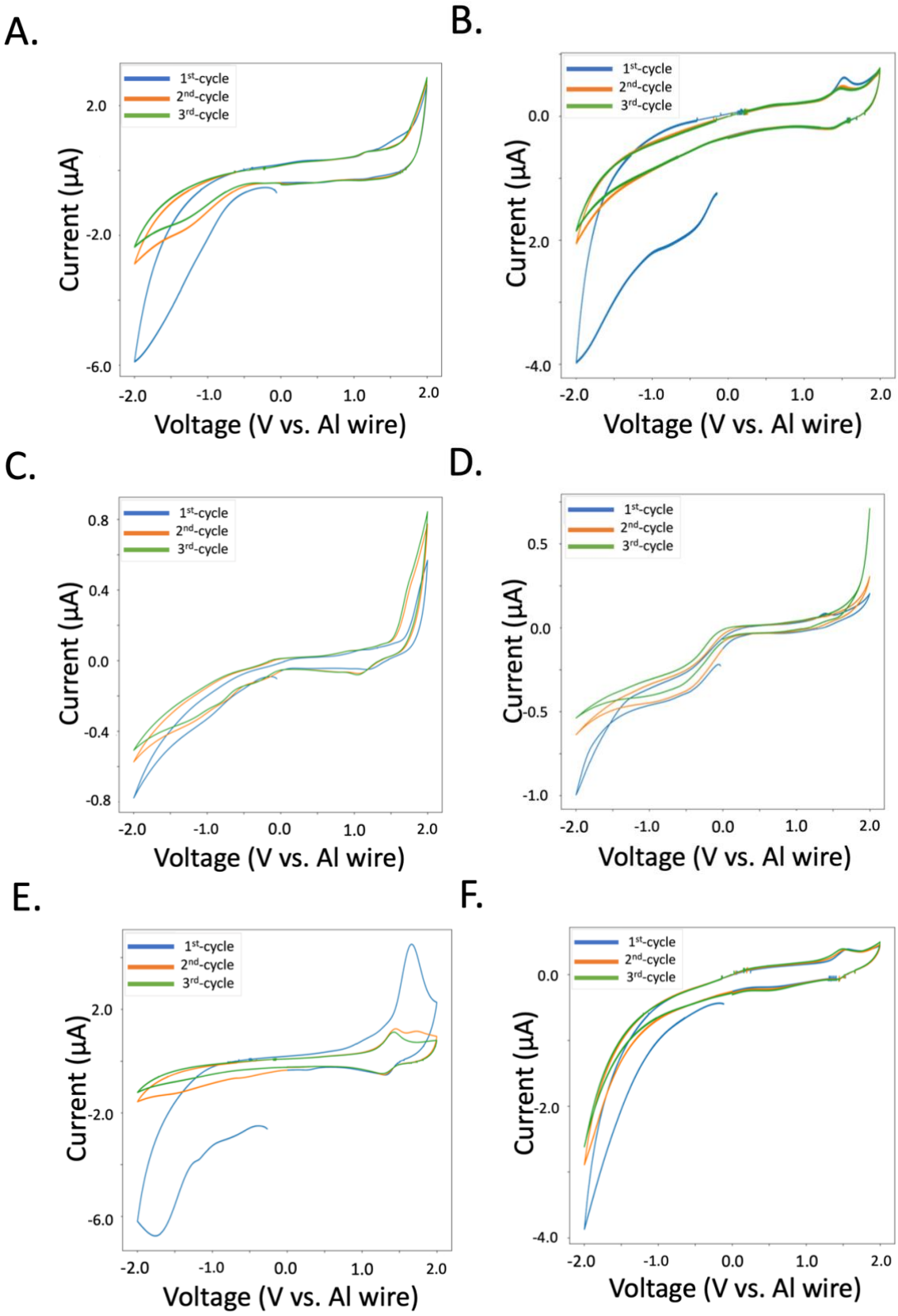
A.
B.
C.
D.
E.
F.
1st-cycle
2nd-cycle
3rd-cycle
Current (μA)
Voltage (V vs. Al wire)

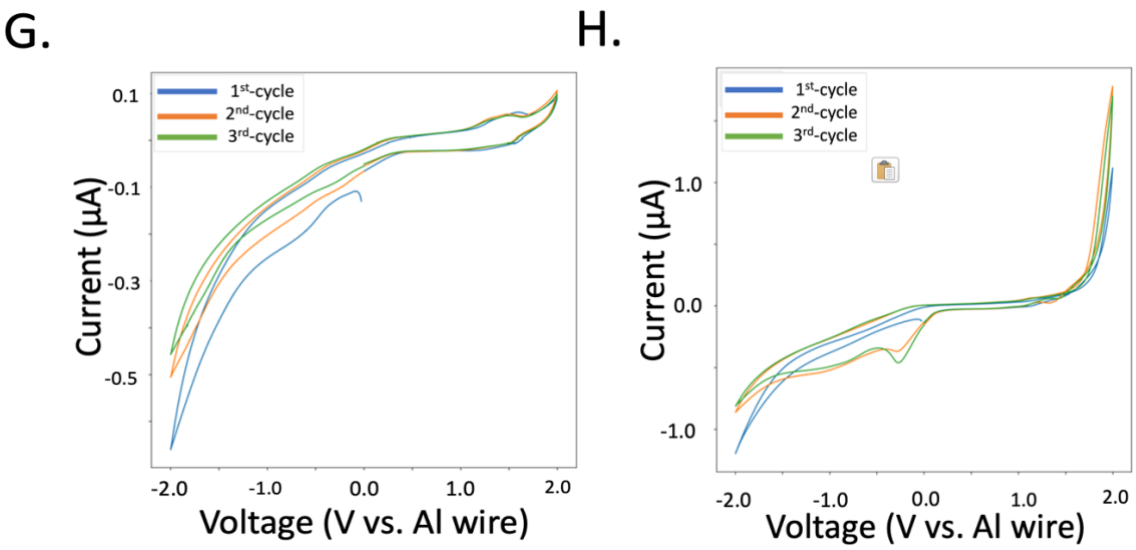

Figure 2.4 Display of the first three cycles of cyclic voltammograms for Al-triflate/EMS electrolytes at different concentrations and temperatures with sweep rates of 100 mV/s and 2 mV/s: (A, B) 0.01 M on a gold WE at 40c and 60°C at a scan rate of 100 mV/s. (C, D) 0.01 M on a gold WE at 40°C and 60°C at a scan rate of 2 mV/s. (E, F) 0.1 M on a gold WE at 40°C and 60°C at a scan rate of 100 mV/s. (G, H) 0.1 M on a gold WE at 40°C and 60°C at a scan rate of 2 mV/s. The first scan is blue, the second is orange, and the third is green.

Cyclic voltammetry was performed using a gold working electrode to examine the I−V polarization curves. Figure 2.3 show oxidation peaks occurring around 2 V, which agrees with the computational predictions shown in Table 2. The onset potentials for the reduction reactions show electrochemical activity around 0 V for 40°C and 60°C when measured on a gold working electrode. We attribute this activity to the reduction of $Al(EMS)_3^{3+\cdot}$ We hypothesize that this reduction indicates aluminum reducing to aluminum metal. The cyclic voltammogram shows a lack of an anodic current that would be attributed to aluminum stripping when sweeping positively is likely due to the lack of a strong Lewis base in this electrolyte. This idea coincides with previous research by Graef, who proposed a mechanism for reversibly depositing/dissolving aluminum from an $AlCl_3$−$LiAlH_4$/THF bath.

To confirm the computational predictions gathered through DFT, cyclic voltammetry was conducted to analyze the electrochemical activity of the electrolyte using a gold working electrode. Figure 2.4A-H reveals redox potentials of the I-V polarization curves on the gold working electrode as we compare the temperature and scan rate dependence on the deposition. Relatively independent of concentration, reduction, and oxidation of EMS is shown at -2 and 2 V respectively. Also, the onset potentials for the reduction reactions show electrochemical activity around 0 V for 40°C and 60°C when measured on a gold working electrode. We attribute this activity to the reduction of aluminum. We hypothesize that this reduction indicates aluminum reducing to aluminum metal. The

cyclic voltammogram shows a lack of an anodic current that would be attributed to aluminum stripping when sweeping positively is likely due to the lack of a strong Lewis base in this electrolyte. This idea coincides with previous research by Graef, who proposed a mechanism for reversibly depositing/dissolving aluminum from an $AlCl_3$−$LiAlH_4$/THF bath.

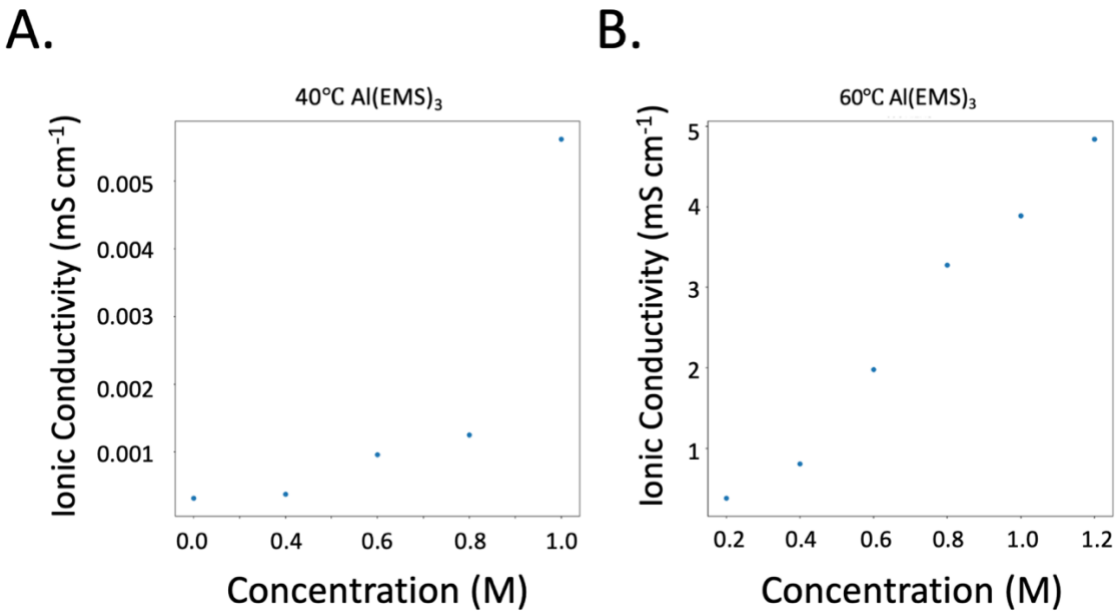

Figure 2.5 Ionic conductivity of the concentration dependence of the potential electrolyte.

To gain a deeper understanding of the electrochemical behavior of the Al-EMS electrolyte, and the concentration dependence shown when increasing the concentration of the electrolyte, electrochemical impedance spectroscopy was conducted to measure the ionic conductivities at increased molar concentrations at 40 and 60°C to also study the temperature dependence. Increasing the temperature of an EMS-based electrolyte is necessary due to the solid nature of EMS at room temperature. Figure 2.5 shows that the ionic conductivity for these electrolytes increases as a function of concentration and temperature up to the point of saturation ~1.0 M, with conductivities as high as 5 mS/cm at 60°C, before the ionic conductivity starts to decrease ~1.2 M, which may be attributed to an increase in viscosity and ion pairing. [22] At 40°C the point of saturation is reached at a lower conductivity of 0.006 mS/cm, which agrees with EMS's solid at room temperature nature that requires to be heated up to show optimal electrochemical behavior.

2.4 Conclusion

The electrochemical and physiochemical behavior of aluminum triflate in ethyl methyl sulfone has been investigated computationally as well as experimentally. Ethyl methyl sulfone's advantageous qualities such as nonvolatility and the ability to strip and play

lithium ions at extreme temperatures. Due to these advantageous properties of EMS, there is a desire to investigate the potential this solvent has when partnered with aluminum-triflate. Firstly, the foundation of this project is built on the computational data collected utilizing Gaussian to solve for the free energies in solution as well as optimizing the coordinated structures. DFT calculations were conducted at the B3PW91/6-311G(d) level of theory to calculate structural, spectroscopic, electrochemical, and ionic association in solution. To further understand the computational data collected regarding the ionic association of triflate in solution FTIR spectra were measured at various concentrations. The IR spectra revealed 3 distinct regions which show bound, free, and contact ion paired triflate. The band region between 1200 to 1400 cm^{-1} revealed increased band splitting of the doubly degenerate SO_3 symmetric stretch which further agreed with the increase of charge density when pairing aluminum with EMS for exceptional capacity. Electrochemical experiments such as cyclic voltammetry were also collected to test the computational predictions to confirm the ab initio data gathered previously. The cyclic voltammograms collected to study the electrochemical activity and the effects of temperature and concentration dependence appear to show the electrochemical activity of aluminum ions in solution which agrees with the computational data. Using DFT calculations in unison with the experimental electrochemical and spectroscopic measurements allows for the framework of the electrolyte to be set. This foundation gives insight into the stability predictions, electrochemical window, and stability, as well as establishing the proper conductive environment based on the vibrational frequencies that help explain the ionic association. Although aluminum triflate-based electrolyte has shown to be an improvement of the dyglime electrolyte design, due to the lack of an oxidation peak presence, it is not clear that a reversible reaction is taking place. The lack of an oxidation peak along with the difficulty that was experienced in acquiring EMS and working with a solid solvent encourages this study to pivot to other solvent solutions as well as the possibilities of additives such as hydrides and chlorides to allow reversibility.

2.5 References

(1) Erickson, P.; Lazarus, M.; Piggot, G. Limiting Fossil Fuel Production as the next Big Step in Climate Policy. *Nat. Clim. Change* **2018**, *8* (12), 1037–1043. https://doi.org/10.1038/s41558-018-0337-0.

(2) Cherp, A.; Vinichenko, V.; Tosun, J.; Gordon, J. A.; Jewell, J. National Growth Dynamics of Wind and Solar Power Compared to the Growth Required for Global Climate Targets. *Nat. Energy* **2021**, *6* (7), 742–754. https://doi.org/10.1038/s41560-021-00863-0.

(3) Larcher, D.; Tarascon, J.-M. Towards Greener and More Sustainable Batteries for Electrical Energy Storage. *Nat. Chem.* **2015**, *7* (1), 19–29. https://doi.org/10.1038/nchem.2085.

(4) Goodenough, J. B. Electrochemical Energy Storage in a Sustainable Modern Society. *Energy Environ. Sci.* **2013**, *7* (1), 14–18. https://doi.org/10.1039/C3EE42613K.

(5) Goodenough, J. B.; Park, K.-S. The Li-Ion Rechargeable Battery: A Perspective. *J. Am. Chem. Soc.* **2013**, *135* (4), 1167–1176. https://doi.org/10.1021/ja3091438.

(6) Tu, J.; Song, W.-L.; Lei, H.; Yu, Z.; Chen, L.-L.; Wang, M.; Jiao, S. Nonaqueous Rechargeable Aluminum Batteries: Progresses, Challenges, and Perspectives. *Chem. Rev.* **2021**, *121* (8), 4903–4961. https://doi.org/10.1021/acs.chemrev.0c01257.
(7) Elia, G. A.; Marquardt, K.; Hoeppner, K.; Fantini, S.; Lin, R.; Knipping, E.; Peters, W.; Drillet, J.-F.; Passerini, S.; Hahn, R. An Overview and Future Perspectives of Aluminum Batteries. *Adv. Mater.* **2016**, *28* (35), 7564–7579. https://doi.org/10.1002/adma.201601357.
(8) Li, Q.; Bjerrum, N. J. Aluminum as Anode for Energy Storage and Conversion: A Review. *J. Power Sources* **2002**, *110* (1), 1–10. https://doi.org/10.1016/S0378-7753(01)01014-X.
(9) Zhang, Y.; Liu, S.; Ji, Y.; Ma, J.; Yu, H. Emerging Nonaqueous Aluminum-Ion Batteries: Challenges, Status, and Perspectives. *Adv. Mater. Deerfield Beach Fla* **2018**, *30* (38), e1706310. https://doi.org/10.1002/adma.201706310.
(10) Li, M.; Lu, J.; Ji, X.; Li, Y.; Shao, Y.; Chen, Z.; Zhong, C.; Amine, K. Design Strategies for Nonaqueous Multivalent-Ion and Monovalent-Ion Battery Anodes. *Nat. Rev. Mater.* **2020**, *5* (4). https://doi.org/10.1038/s41578-019-0166-4.
(11) *The Rechargeable Aluminum Battery: Opportunities and Challenges - Yang - 2019 - Angewandte Chemie International Edition - Wiley Online Library*. https://onlinelibrary.wiley.com/doi/10.1002/anie.201814031 (accessed 2023-04-27).
(12) Elia, G. A.; Kravchyk, K. V.; Kovalenko, M. V.; Chacón, J.; Holland, A.; Wills, R. G. A. An Overview and Prospective on Al and Al-Ion Battery Technologies. *J. Power Sources* **2021**, *481*, 228870. https://doi.org/10.1016/j.jpowsour.2020.228870.
(13) Faegh, E.; Ng, B.; Hayman, D.; Mustain, W. Practical Assessment of the Performance of Aluminium Battery Technologies. *Nat. Energy* **2020**, *6*. https://doi.org/10.1038/s41560-020-00728-y.
(14) Leung, O. M.; Schoetz, T.; Prodromakis, T.; Leon, C. P. de. Review—Progress in Electrolytes for Rechargeable Aluminium Batteries. *J. Electrochem. Soc.* **2021**, *168* (5), 056509. https://doi.org/10.1149/1945-7111/abfb36.
(15) *Cathode materials for rechargeable aluminum batteries: current status and progress - Journal of Materials Chemistry A (RSC Publishing)*. https://pubs.rsc.org/en/content/articlelanding/2017/ta/c7ta00282c (accessed 2023-04-27).
(16) Shi, J.; Zhang, J.; Guo, J. Avoiding Pitfalls in Rechargeable Aluminum Batteries Research. *ACS Energy Lett.* **2019**, *4* (9), 2124–2129. https://doi.org/10.1021/acsenergylett.9b01285.
(17) Reed, L. D.; Menke, E. The Roles of V_2O_5 and Stainless Steel in Rechargeable Al–Ion Batteries. *J. Electrochem. Soc.* **2013**, *160* (6), A915–A917. https://doi.org/10.1149/2.114306jes.
(18) Wang, H.; Gu, S.; Bai, Y.; Chen, S.; Zhu, N.; Wu, C.; Wu, F. Anion-Effects on Electrochemical Properties of Ionic Liquid Electrolytes for Rechargeable Aluminum Batteries. *J. Mater. Chem. A* **2015**, *3* (45), 22677–22686. https://doi.org/10.1039/C5TA06187C.
(19) Lai, P. K.; Skyllas-Kazacos, M. Electrodeposition of Aluminium in Aluminium Chloride/1-Methyl-3-Ethylimidazolium Chloride. *J. Electroanal. Chem. Interfacial*

Electrochem. **1988**, *248* (2), 431–440. https://doi.org/10.1016/0022-0728(88)85103-9.
(20) Zhang, M.; Watson, J. S.; Counce, R. M.; Trulove, P. C.; Zawodzinski, T. A. Electrochemistry and Morphology Studies of Aluminum Plating/Stripping in a Chloroaluminate Ionic Liquid on Porous Carbon Materials. *J. Electrochem. Soc.* **2014**, *161* (4), D163. https://doi.org/10.1149/2.048404jes.
(21) Mandai, T.; Johansson, P. Al Conductive Haloaluminate-Free Non-Aqueous Room-Temperature Electrolytes. *J. Mater. Chem. A* **2015**, *3* (23), 12230–12239. https://doi.org/10.1039/C5TA01760B.
(22) Reed, L. D.; Arteaga, A.; Menke, E. J. A Combined Experimental and Computational Study of an Aluminum Triflate/Diglyme Electrolyte. *J. Phys. Chem. B* **2015**, *119* (39), 12677–12681. https://doi.org/10.1021/acs.jpcb.5b08501.
(23) Reed, L. D.; Ortiz, S. N.; Xiong, M.; Menke, E. J. A Rechargeable Aluminum-Ion Battery Utilizing a Copper Hexacyanoferrate Cathode in an Organic Electrolyte. *Chem. Commun.* **2015**, *51* (76), 14397–14400. https://doi.org/10.1039/C5CC06053B.
(24) Mandai, T.; Johansson, P. Haloaluminate-Free Cationic Aluminum Complexes: Structural Characterization and Physicochemical Properties. *J. Phys. Chem. C* **2016**, *120* (38), 21285–21292. https://doi.org/10.1021/acs.jpcc.6b07235.
(25) Wen, X.; Zhang, J.; Luo, H.; Shi, J.; Tsay, C.; Jiang, H.; Lin, Y.-H.; Schroeder, M. A.; Xu, K.; Guo, J. Synthesis and Electrochemical Properties of Aluminum Hexafluorophosphate. *J. Phys. Chem. Lett.* **2021**, *12* (25), 5903–5908. https://doi.org/10.1021/acs.jpclett.1c01236.
(26) Chiku, M.; Matsumura, S.; Takeda, H.; Higuchi, E.; Inoue, H. Aluminum Bis(Trifluoromethanesulfonyl)Imide as a Chloride-Free Electrolyte for Rechargeable Aluminum Batteries. *J. Electrochem. Soc.* **2017**, *164* (9), A1841. https://doi.org/10.1149/2.0701709jes.
(27) Hilbig, P.; Ibing, L.; Wagner, R.; Winter, M.; Cekic-Laskovic, I. Ethyl Methyl Sulfone-Based Electrolytes for Lithium Ion Battery Applications. *Energies* **2017**, *10* (9), 1312. https://doi.org/10.3390/en10091312.
(28) Avoundjian, A.; Galvan, V.; Gomez, F. An Inexpensive Paper-Based Aluminum-Air Battery. *Micromachines* **2017**, *8*. https://doi.org/10.3390/mi8070222.
(29) Lee, W.; Park, S.-J. Porous Anodic Aluminum Oxide: Anodization and Templated Synthesis of Functional Nanostructures. *Chem. Rev.* **2014**, *114* (15), 7487–7556. https://doi.org/10.1021/cr500002z.
(30) *Voltaic cell*. studylib.net. https://studylib.net/doc/18820455/voltaic-cell (accessed 2023-04-29).
(31) Zaromb, S. The Use and Behavior of Aluminum Anodes in Alkaline Primary Batteries. *J. Electrochem. Soc.* **1962**, *109* (12), 1125. https://doi.org/10.1149/1.2425257.
(32) Faegh, E.; Shrestha, S.; Zhao, X.; Mustain, W. In-Depth Structural Understanding of Zinc Oxide Addition to Alkaline Electrolytes to Protect Aluminum against Corrosion and Gassing. *J. Appl. Electrochem.* **2019**, *49*. https://doi.org/10.1007/s10800-019-01330-1.

(33) Duca, B. S. D. Electrochemical Behavior of the Aluminum Electrode in Molten Salt Electrolytes. *J. Electrochem. Soc.* **1971**, *118* (3), 405. https://doi.org/10.1149/1.2408069.
(34) Holleck, G. L.; Giner, J. The Aluminum Electrode in AlCl[Sub 3]-Alkali-Halide Melts. *J. Electrochem. Soc.* **1972**, *119* (9), 1161. https://doi.org/10.1149/1.2404433.
(35) Holleck, G. L. The Reduction of Chlorine on Carbon in AlCl3 - KCl - NaCl Melts. *J. Electrochem. Soc.* **1972**, *119* (9), 1158. https://doi.org/10.1149/1.2404432.
(36) Gifford, P. R.; Palmisano, J. B. An Aluminum/Chlorine Rechargeable Cell Employing a Room Temperature Molten Salt Electrolyte. *J. Electrochem. Soc.* **1988**, *135* (3), 650. https://doi.org/10.1149/1.2095685.
(37) Paranthaman, M. P.; Brown, G.; Sun, X.-G.; Nanda, J.; Manthiram, A.; Manivannan, A. A Transformational, High Energy Density, Secondary Aluminum Ion Battery. *ECS Meet. Abstr.* **2010**, *MA2010-02* (4), 314. https://doi.org/10.1149/MA2010-02/4/314.
(38) Jayaprakash, N.; Das, S. K.; Archer, L. A. The Rechargeable Aluminum-Ion Battery. *Chem. Commun.* **2011**, *47* (47), 12610–12612. https://doi.org/10.1039/C1CC15779E.
(39) V. Plechkova, N.; R. Seddon, K. Applications of Ionic Liquids in the Chemical Industry. *Chem. Soc. Rev.* **2008**, *37* (1), 123–150. https://doi.org/10.1039/B006677J.
(40) Pena-Pereira, F.; Namieśnik, J. Ionic Liquids and Deep Eutectic Mixtures: Sustainable Solvents for Extraction Processes. *ChemSusChem* **2014**, *7* (7), 1784–1800. https://doi.org/10.1002/cssc.201301192.
(41) Wilkes, J. S.; Levisky, J. A.; Wilson, R. A.; Hussey, C. L. Dialkylimidazolium Chloroaluminate Melts: A New Class of Room-Temperature Ionic Liquids for Electrochemistry, Spectroscopy and Synthesis. *Inorg. Chem.* **1982**, *21* (3), 1263–1264. https://doi.org/10.1021/ic00133a078.
(42) Zhao, Y.; VanderNoot, T. J. Electrodeposition of Aluminium from Nonaqueous Organic Electrolytic Systems and Room Temperature Molten Salts. *Electrochimica Acta* **1997**, *42* (1), 3–13. https://doi.org/10.1016/0013-4686(96)00080-1.
(43) Hurley, F. H.; WIer, T. P. The Electrodeposition of Aluminum from Nonaqueous Solutions at Room Temperature. *J. Electrochem. Soc.* **1951**, *98* (5), 207. https://doi.org/10.1149/1.2778133.
(44) Gale, R. J.; Gilbert, B.; Osteryoung, R. A. Raman Spectra of Molten Aluminum Chloride: 1-Butylpyridinium Chloride Systems at Ambient Temperatures. *Inorg. Chem.* **1978**, *17* (10), 2728–2729. https://doi.org/10.1021/ic50188a008.
(45) Wang, C.; Creuziger, A.; Stafford, G.; Hussey, C. L. Anodic Dissolution of Aluminum in the Aluminum Chloride-1-Ethyl-3-Methylimidazolium Chloride Ionic Liquid. *J. Electrochem. Soc.* **2016**, *163* (14), H1186. https://doi.org/10.1149/2.1061614jes.
(46) *PII: 0022-0728(88)85103-9 | Elsevier Enhanced Reader*. https://doi.org/10.1016/0022-0728(88)85103-9.
(47) Oh, Y.; Lee, G.; Tak, Y. Stability of Metallic Current Collectors in Acidic Ionic Liquid for Rechargeable Aluminum-Ion Batteries. *ChemElectroChem* **2018**, *5*, 3348–3352. https://doi.org/10.1002/celc.201801396.

(48) Couch, D. E.; Brenner, A. A Hydride Bath for the Electrodeposition of Aluminum. *J. Electrochem. Soc.* **1952**, *99* (6), 234. https://doi.org/10.1149/1.2779711.
(49) Ishibashi, N.; Yoshio, M. Electrodeposition of Aluminium from the NBS Type Bath Using Tetrahydrofuran—Benzene Mixed Solvent. *Electrochimica Acta* **1972**, *17* (8), 1343–1352. https://doi.org/10.1016/0013-4686(72)80080-X.
(50) Graef, M. W. M. The Mechanism of Aluminum Electrodeposition from Solutions of AlCl3 and LiAlH4 in THF. *J. Electrochem. Soc.* **1985**, *132* (5), 1038. https://doi.org/10.1149/1.2114011.
(51) Finholt, A. E.; Bond, A. C. Jr.; Schlesinger, H. I. Lithium Aluminum Hydride, Aluminum Hydride and Lithium Gallium Hydride, and Some of Their Applications in Organic and Inorganic Chemistry1. *J. Am. Chem. Soc.* **1947**, *69* (5), 1199–1203. https://doi.org/10.1021/ja01197a061.
(52) Legrand, L.; Tranchant, A.; Messina, R. Behaviour of Aluminium as Anode in Dimethylsulfone-Based Electrolytes. *Electrochimica Acta* **1994**, *39* (10), 1427–1431. https://doi.org/10.1016/0013-4686(94)85054-2.
(53) Legrand, L.; Tranchant, A.; Messina, R. Electrodeposition Studies of Aluminum on Tungsten Electrode from DMSO 2 Electrolytes: Determination of AlIII Species Diffusion Coefficients. *J. Electrochem. Soc.* **1994**, *141* (2), 378. https://doi.org/10.1149/1.2054735.
(54) Legrand, L.; Heintz, M.; Tranchant, A.; Messina, R. Sulfone-Based Electrolytes for Aluminum Electrodeposition. *Electrochimica Acta* **1995**, *40* (11), 1711–1716. https://doi.org/10.1016/0013-4686(95)00019-B.
(55) Legrand, L.; Tranchant, A.; Messina, R. Aluminium Behaviour and Stability in AlCl3DMSO2 Electrolyte. *Electrochimica Acta* **1996**, *41* (17), 2715–2720. https://doi.org/10.1016/0013-4686(96)00126-0.
(56) Miyake, M.; Fujii, H.; Hirato, T. Electroplating of Al on Mg Alloy in a Dimethyl Sulfone–Aluminum Chloride Bath. *Surf. Coat. Technol.* **2015**, *277*, 160–164. https://doi.org/10.1016/j.surfcoat.2015.07.047.
(57) Nakayama, Y.; Senda, Y.; Kawasaki, H.; Koshitani, N.; Hosoi, S.; Kudo, Y.; Morioka, H.; Nagamine, M. Sulfone-Based Electrolytes for Aluminium Rechargeable Batteries. *Phys. Chem. Chem. Phys.* **2015**, *17* (8), 5758–5766. https://doi.org/10.1039/C4CP02183E.
(58) Kitada, A.; Nakamura, K.; Fukami, K.; Murase, K. Electrochemically Active Species in Aluminum Electrodeposition Baths of AlCl3/Glyme Solutions. *Electrochimica Acta* **2016**, *211*, 561.
(59) Zhang, Z.; Kitada, A.; Gao, S.; Fukami, K.; Tsuji, N.; Yao, Z.; Murase, K. A Concentrated AlCl3–Diglyme Electrolyte for Hard and Corrosion-Resistant Aluminum Electrodeposits. *ACS Appl. Mater. Interfaces* **2020**, *12* (38), 43289–43298. https://doi.org/10.1021/acsami.0c12602.
(60) Kitada, A.; KATO, Y.; Fukami, K.; Murase, K. Room Temperature Electrodeposition of Flat and Smooth Aluminum Layers from An AlCl3/Diglyme Bath. *J. Surf. Finish. Soc. Jpn.* **2018**, *69*, 310–311. https://doi.org/10.4139/sfj.69.310.
(61) Howells, R. D.; Mc Cown, J. D. Trifluoromethanesulfonic Acid and Derivatives. *Chem. Rev.* **1977**, *77* (1), 69–92. https://doi.org/10.1021/cr60305a005.

(62) Slim, Z.; Menke, E. J. Comparing Computational Predictions and Experimental Results for Aluminum Triflate in Tetrahydrofuran. *J. Phys. Chem. B* **2020**, *124* (24), 5002–5008. https://doi.org/10.1021/acs.jpcb.0c02570.
(63) Hu, J. J.; Long, G. K.; Liu, S.; Li, G. R.; Gao, X. P. A LiFSI–LiTFSI Binary-Salt Electrolyte to Achieve High Capacity and Cycle Stability for a Li–S Battery. *Chem. Commun.* **2014**, *50* (93), 14647–14650. https://doi.org/10.1039/C4CC06666A.
(64) Yang, H.; Zhuang, G.; Ross, P. Thermal Stability of LiPF 6 Salt and Li-Ion Battery Electrolytes Containing LiPF 6. *J. Power Sources - J POWER SOURCES* **2006**, *161*, 573–579. https://doi.org/10.1016/j.jpowsour.2006.03.058.
(65) Younesi, R.; Veith, G. M.; Johansson, P.; Edström, K.; Vegge, T. Lithium Salts for Advanced Lithium Batteries: Li–Metal, Li–O2, and Li–S. *Energy Environ. Sci.* **2015**, *8* (7), 1905–1922. https://doi.org/10.1039/C5EE01215E.
(66) Ha, S.-Y.; Lee, Y.-W.; Woo, S. W.; Koo, B.; Kim, J.-S.; Cho, J.; Lee, K. T.; Choi, N.-S. Magnesium(II) Bis(Trifluoromethane Sulfonyl) Imide-Based Electrolytes with Wide Electrochemical Windows for Rechargeable Magnesium Batteries. *ACS Appl. Mater. Interfaces* **2014**, *6* (6), 4063–4073. https://doi.org/10.1021/am405619v.
(67) Keyzer, E. N.; Glass, H. F. J.; Liu, Z.; Bayley, P. M.; Dutton, S. E.; Grey, C. P.; Wright, D. S. Mg(PF6)2-Based Electrolyte Systems: Understanding Electrolyte-Electrode Interactions for the Development of Mg-Ion Batteries. *J. Am. Chem. Soc.* **2016**, *138* (28), 8682–8685. https://doi.org/10.1021/jacs.6b04319.
(68) Wang, Y.; Xing, L.; Li, W.; Bedrov, D. Why Do Sulfone-Based Electrolytes Show Stability at High Voltages? Insight from Density Functional Theory. *J. Phys. Chem. Lett.* **2013**, *4* (22), 3992–3999. https://doi.org/10.1021/jz401726p.
(69) Xing, L.; Wang, C.; Li, W.; Xu, M.; Meng, X.; Zhao, S. Theoretical Insight into Oxidative Decomposition of Propylene Carbonate in the Lithium Ion Battery. *J. Phys. Chem. B* **2009**, *113* (15), 5181–5187. https://doi.org/10.1021/jp810279h.
(70) Dunn, B.; Kamath, H.; Tarascon, J.-M. Electrical Energy Storage for the Grid: A Battery of Choices. *Science* **2011**, *334* (6058), 928–935. https://doi.org/10.1126/science.1212741.
(71) Manthiram, A. A Reflection on Lithium-Ion Battery Cathode Chemistry. *Nat. Commun.* **2020**, *11* (1), 1550. https://doi.org/10.1038/s41467-020-15355-0.
(72) Wu, F.; Yang, H.; Bai, Y.; Wu, C. Paving the Path toward Reliable Cathode Materials for Aluminum-Ion Batteries. *Adv. Mater. Deerfield Beach Fla* **2019**, *31* (16), e1806510. https://doi.org/10.1002/adma.201806510.
(73) Lin, M.-C.; Gong, M.; Lu, B.; Wu, Y.; Wang, D.-Y.; Guan, M.; Angell, M.; Chen, C.; Yang, J.; Hwang, B.-J.; Dai, H. An Ultrafast Rechargeable Aluminium-Ion Battery. *Nature* **2015**, *520* (7547), 324–328. https://doi.org/10.1038/nature14340.
(74) Kravchyk, K. V.; Wang, S.; Piveteau, L.; Kovalenko, M. V. Efficient Aluminum Chloride–Natural Graphite Battery. *Chem. Mater.* **2017**, *29* (10), 4484–4492. https://doi.org/10.1021/acs.chemmater.7b01060.
(75) Greco, G.; Tatchev, D.; Hoell, A.; Krumrey, M.; Raoux, S.; Hahn, R.; Elia, G. A. Influence of the Electrode Nano/Microstructure on the Electrochemical Properties of Graphite in Aluminum Batteries. *J. Mater. Chem. A* **2018**, *6* (45), 22673–22680. https://doi.org/10.1039/C8TA08319C.

(76) Geng, L.; Lv, G.; Xing, X.; Guo, J. Reversible Electrochemical Intercalation of Aluminum in Mo6S8. *Chem. Mater.* **2015**, *27* (14), 4926–4929. https://doi.org/10.1021/acs.chemmater.5b01918.
(77) Lee, B.; Lee, H. R.; Yim, T.; Kim, J. H.; Lee, J. G.; Chung, K. Y.; Cho, B. W.; Oh, S. H. Investigation on the Structural Evolutions during the Insertion of Aluminum Ions into Mo6S8 Chevrel Phase. *J. Electrochem. Soc.* **2016**, *163* (6), A1070. https://doi.org/10.1149/2.0011607jes.
(78) *X-MOL*. x-mol.net. https://www.x-mol.net/paper/article/1356342681998311424 (accessed 2023-05-09).
(79) Wang, H.; Bai, Y.; Chen, S.; Luo, X.; Wu, C.; Wu, F.; Lu, J.; Amine, K. Binder-Free V2O5 Cathode for Greener Rechargeable Aluminum Battery. *ACS Appl. Mater. Interfaces* **2015**, *7* (1), 80–84. https://doi.org/10.1021/am508001h.
(80) Wang, S.; Jiao, S.; Wang, J.; Chen, H.-S.; Tian, D.; Lei, H.; Fang, D.-N. High-Performance Aluminum-Ion Battery with CuS@C Microsphere Composite Cathode. *ACS Nano* **2017**, *11* (1), 469–477. https://doi.org/10.1021/acsnano.6b06446.
(81) Mori, T.; Orikasa, Y.; Nakanishi, K.; Kezheng, C.; Hattori, M.; Ohta, T.; Uchimoto, Y. Discharge/Charge Reaction Mechanisms of FeS2 Cathode Material for Aluminum Rechargeable Batteries at 55°C. *J. Power Sources* **2016**, *313*, 9–14. https://doi.org/10.1016/j.jpowsour.2016.02.062.
(82) Wang, S.; Yu, Z.; Tu, J.; Wang, J.; Tian, D.; Liu, Y.; Jiao, S. A Novel Aluminum-Ion Battery: Al/AlCl $_3$ -[EMIm]Cl/Ni $_3$ S $_2$ @Graphene. *Adv. Energy Mater.* **2016**, *6* (13), 1600137. https://doi.org/10.1002/aenm.201600137.
(83) Donahue, F. M.; Mancini, S. E.; Simonsen, L. Secondary Aluminium-Iron (III) Chloride Batteries with a Low Temperature Molten Salt Electrolyte. *J. Appl. Electrochem.* **1992**, *22* (3), 230–234. https://doi.org/10.1007/BF01030182.
(84) Suto, K.; Nakata, A.; Murayama, H.; Hirai, T.; Yamaki, J.; Ogumi, Z. Electrochemical Properties of Al/Vanadium Chloride Batteries with AlCl3-1-Ethyl-3-Methylimidazolium Chloride Electrolyte. *J. Electrochem. Soc.* **2016**, *163* (5), A742. https://doi.org/10.1149/2.0991605jes.
(85) Nakaya, K.; Nakata, A.; Hirai, T.; Ogumi, Z. Oxidation of Nickel in AlCl3-1-Butylpyridinium Chloride at Ambient Temperature. *J. Electrochem. Soc.* **2014**, *162* (1), D42. https://doi.org/10.1149/2.0401501jes.
(86) Tian, H.; Zhang, S.; Meng, Z.; He, W.; Han, W.-Q. Rechargeable Aluminum/Iodine Battery Redox Chemistry in Ionic Liquid Electrolyte. *ACS Energy Lett.* **2017**, *2* (5), 1170–1176. https://doi.org/10.1021/acsenergylett.7b00160.
(87) Armand, M.; Tarascon, J.-M. Building Better Batteries. *Nature* **2008**, *451* (7179), 652–657. https://doi.org/10.1038/451652a.
(88) Gao, X.-P.; Yang, H.-X. Multi-Electron Reaction Materials for High Energy Density Batteries. *Energy Environ. Sci.* **2010**, *3* (2), 174–189. https://doi.org/10.1039/B916098A.
(89) *2 – Past, Present and Future of Lithium-Ion Batteries: Can New Technologies Open up New Horizons? | Elsevier Enhanced Reader*. https://doi.org/10.1016/B978-0-444-59513-3.00002-9.

(90) Hu, Y.; Sun, D.; Luo, B.; Wang, L. Recent Progress and Future Trends of Aluminum Batteries. *Energy Technol.* **2019**, *7* (1), 86–106. https://doi.org/10.1002/ente.201800550.
(91) Shkrob, I. A.; Wishart, J. F.; Abraham, D. P. What Makes Fluoroethylene Carbonate Different? *J. Phys. Chem. C* **2015**, *119* (27), 14954–14964. https://doi.org/10.1021/acs.jpcc.5b03591.
(92) Tseng, C.-H.; Chang, J.-K.; Chen, J.-R.; Tsai, W. T.; Deng, M.-J.; Sun, I.-W. Corrosion Behaviors of Materials in Aluminum Chloride–1-Ethyl-3-Methylimidazolium Chloride Ionic Liquid. *Electrochem. Commun.* **2010**, *12* (8), 1091–1094. https://doi.org/10.1016/j.elecom.2010.05.036.
(93) *Gaussian 09 Citation | Gaussian.com*. https://gaussian.com/g09citation/ (accessed 2022-12-06).
(94) Becke, A. D. Density-functional Thermochemistry. III. The Role of Exact Exchange. *J. Chem. Phys.* **1993**, *98* (7), 5648–5652. https://doi.org/10.1063/1.464913.
(95) Krishnan, R.; Binkley, J. S.; Seeger, R.; Pople, J. A. Self-consistent Molecular Orbital Methods. XX. A Basis Set for Correlated Wave Functions. *J. Chem. Phys.* **1980**, *72* (1), 650–654. https://doi.org/10.1063/1.438955.
(96) Marenich, A. V.; Cramer, C. J.; Truhlar, D. G. Universal Solvation Model Based on Solute Electron Density and on a Continuum Model of the Solvent Defined by the Bulk Dielectric Constant and Atomic Surface Tensions. *J. Phys. Chem. B* **2009**, *113* (18), 6378–6396. https://doi.org/10.1021/jp810292n.
(97) Roy, L. E.; Jakubikova, E.; Guthrie, M. G.; Batista, E. R. Calculation of One-Electron Redox Potentials Revisited. Is It Possible to Calculate Accurate Potentials with Density Functional Methods? *J. Phys. Chem. A* **2009**, *113* (24), 6745–6750. https://doi.org/10.1021/jp811388w.
(98) Jafari, S.; Tavares Santos, Y. A.; Bergmann, J.; Irani, M.; Ryde, U. Benchmark Study of Redox Potential Calculations for Iron–Sulfur Clusters in Proteins. *Inorg. Chem.* **2022**, *61* (16), 5991–6007. https://doi.org/10.1021/acs.inorgchem.1c03422.
(99) Shao, N.; Sun, X.-G.; Dai, S.; Jiang, D. Electrochemical Windows of Sulfone-Based Electrolytes for High-Voltage Li-Ion Batteries. *J. Phys. Chem. B* **2011**, *115* (42), 12120–12125. https://doi.org/10.1021/jp204401t.
(100) Yan, C.; Lv, C.; Wang, L.; Cui, W.; Zhang, L.; Dinh, K. N.; Tan, H.; Wu, C.; Wu, T.; Ren, Y.; Chen, J.; Liu, Z.; Srinivasan, M.; Rui, X.; Yan, Q.; Yu, G. Architecting a Stable High-Energy Aqueous Al-Ion Battery. *J. Am. Chem. Soc.* **2020**, *142* (36), 15295–15304. https://doi.org/10.1021/jacs.0c05054.
(101) *Lithium-Ion Batteries*. https://shop.elsevier.com/books/lithium-ion-batteries/pistoia/978-0-444-59513-3 (accessed 2022-12-20).
(102) Zu, C.-X.; Li, H. Thermodynamic Analysis on Energy Densities of Batteries. *Energy Environ. Sci.* **2011**, *4* (8), 2614–2624. https://doi.org/10.1039/C0EE00777C.
(103) Leisegang, T.; Meutzner, F.; Zschornak, M.; Münchgesang, W.; Schmid, R.; Nestler, T.; Eremin, R. A.; Kabanov, A. A.; Blatov, V. A.; Meyer, D. C. The Aluminum-Ion Battery: A Sustainable and Seminal Concept? *Front. Chem.* **2019**, *7*.
(104) Fan, H.; Liu, X.; Luo, L.; Zhong, F.; Cao, Y. All-Climate High-Voltage Commercial Lithium-Ion Batteries Based on Propylene Carbonate Electrolytes. *ACS*

Appl. Mater. Interfaces **2022**, *14* (1), 574–580. https://doi.org/10.1021/acsami.1c16767.
(105) Hu, C.-C.; Chiu, P.-H.; Wang, S.-J.; Cheng, S.-H. Isobaric Vapor–Liquid Equilibria for Binary Systems of Diethyl Carbonate + Propylene Carbonate, Diethyl Carbonate + Propylene Glycol, and Ethanol + Propylene Carbonate at 101.3 KPa. *J. Chem. Eng. Data* **2015**, *60* (5), 1487–1494. https://doi.org/10.1021/acs.jced.5b00064.
(106) Xing, L.; Zheng, X.; Schroeder, M.; Alvarado, J.; von Wald Cresce, A.; Xu, K.; Li, Q.; Li, W. Deciphering the Ethylene Carbonate–Propylene Carbonate Mystery in Li-Ion Batteries. *Acc. Chem. Res.* **2018**, *51* (2), 282–289. https://doi.org/10.1021/acs.accounts.7b00474.
(107) Becke, A. D. Density-Functional Thermochemistry. III. The Role of Exact Exchange. *J. Chem. Phys.* **1993**, *98*, 5648–5652. https://doi.org/10.1063/1.464913.
(108) Jay, A.; Huet, C.; Salles, N.; Gunde, M.; Martin-Samos, L.; Richard, N.; Landa, G.; Goiffon, V.; De Gironcoli, S.; Hémeryck, A.; Mousseau, N. Finding Reaction Pathways and Transition States: R-ARTn and d-ARTn as an Efficient and Versatile Alternative to String Approaches. *J. Chem. Theory Comput.* **2020**, *16* (10), 6726–6734. https://doi.org/10.1021/acs.jctc.0c00541.
(109) Bauernschmitt, R.; Ahlrichs, R. Stability Analysis for Solutions of the Closed Shell Kohn-Sham Equation. *J. Chem. Phys.* **1996**, *104*, 9047–9052. https://doi.org/10.1063/1.471637.
(110) Menges, F. *Spectragryph - optical spectroscopy software*. Spectroscopy. http://spectragryph.com/ (accessed 2022-12-08).
(111) Konezny, S. J.; Doherty, M. D.; Luca, O. R.; Crabtree, R. H.; Soloveichik, G. L.; Batista, V. S. Reduction of Systematic Uncertainty in DFT Redox Potentials of Transition-Metal Complexes. *J. Phys. Chem. C* **2012**, *116* (10), 6349–6356. https://doi.org/10.1021/jp300485t.
(112) Huang, W.; Frech, R.; Wheeler, R. A. Molecular Structures and Normal Vibrations of Trifluoromethane Sulfonate (CF3SO3-) and Its Lithium Ion Pairs and Aggregates. *J. Phys. Chem.* **1994**, *98* (1), 100–110. https://doi.org/10.1021/j100052a018.
(113) Frech, R.; Huang, W. Anion-Solvent and Anion-Cation Interactions in Lithium and Tetrabutylammonium Trifluoromethanesulfonate Solutions. *J. Solut. Chem.* **1994**, *23* (4), 469–481. https://doi.org/10.1007/BF00972613.
(114) Frech, R.; Huang, W. Ionic Association in Poly (Propylene Oxide) Complexed with Divalent Metal Trifluoromethanesulfonate Salts. *Solid State Ion.* **1993**, *66* (1), 183–188. https://doi.org/10.1016/0167-2738(93)90042-2.
(115) Huang, W.; Frech, R. Dependence of Ionic Association on Polymer Chain Length in Poly(Ethylene Oxide)-Lithium Triflate Complexes. *Polymer* **1994**, *35* (2), 235–242. https://doi.org/10.1016/0032-3861(94)90684-X.
(116) Bernson, A.; Lindgren, J.; Huang, W.; Frech, R. Coordination and Conformation in PEO, PEGM and PEG Systems Containing Lithium or Lanthanum Triflate. *Polymer* **1995**, *36* (23), 4471–4478. https://doi.org/10.1016/0032-3861(95)96855-3.
(117) Wendsjö, Å.; Lindgren, J.; Thomas, J. O.; Farrington, G. C. The Effect of Temperature and Concentration on the Local Environment in the System

M(CF3SO3)2PEOn for M=Ni, Zn and Pb. *Solid State Ion.* **1992**, *53–56*, 1077–1082. https://doi.org/10.1016/0167-2738(92)90293-X.

Chapter 3: Comparing Computational Predictions and Experimental Results for Aluminum Triflate in Propylene Carbonate

3.1 Introduction

An investigation into the behavior of an effective aluminum-ion battery calls for an in-depth analysis of the electrochemical and physiochemical properties of the electrolyte and electrode materials. A limited understanding of the appropriate electrolyte mixtures is a major barrier to actualizing a suitable aluminum-ion battery. Herein, we present a study on the behavior of potential electrolytes formed by dissolving aluminum-triflouromethanesulfonate (Al-triflate) in propylene carbonate (PC), due to its advantageous attributes such as high oxidative stability, wide temperature range, and excellent capacity. Density functional theory (DFT) calculations were used to optimize the coordinated structures, allowing us to predict characteristics of our electrolyte such as the speciation, species redox potentials, and vibrational frequencies. Cyclic Voltammetry (CV) measurements are consistent with the stability predictions DFT calculations provide, showing aluminum to be electrochemically active in PC with a reduction onset near 0 V versus Al/Al^{3+}. Fourier-transform infrared spectroscopy (FTIR) shows the Ionic association of triflate interaction with the aluminum core to understand a conductive medium suitable for the exchange of Al^{3+} ions. Scanning electron microscopy (SEM) images were captured to analyze the surface morphology of Al deposition on a Cu substrate. X-ray photoelectron spectroscopy (XPS) was utilized as a tool to gain an in-depth understanding of the species present on a copper substrate after deposition is carried out through chronoamperometry to confirm the aluminum plating suggested by cyclic voltammetry. Lastly, an ionic conductivity of ~5.4 mS/cm of ionic conductivity was measured at ~0.6M.

A green and energy-sustainable society requires the development of non-fossil fuel energy storage technologies. [100] Mastering stable post-lithium secondary batteries is necessary to meet the energy storage needs of the near future which will encompass 80% of the world's renewable energy source. Mobile electronic devices have relied heavily on lithium-ion batteries, comprising 90% of all rechargeable energy storage since the early ’90s. [101] There is significant concern that lithium will not be able to meet the needs of modern technology due to many factors, but firstly due to its lack of abundance in the earth’s crust. [88] Aluminum-ion batteries have been proposed to be a promising alternative capable of meeting these needs that lithium will not be able to account for. [102] Lack of understanding of cathode materials and electrolytes for aluminum-ion batteries necessitates the need to investigate aluminum’s advantageous attributes of abundance, low cost (~1.4 USD/kg), high theoretical volumetric density (8042 mAh/ml), and its trivalent nature. [90]

Employing these promising characteristics of aluminum requires a stable electrolyte that will allow for aluminum ion transport to and from the desired electrode material. The

electrodeposition of pure aluminum(Al) is gaining considerable interest from numerous research groups during the last decade. [103] Aluminum is light, inexpensive, and has excellent thermal and electrical conductivities. [103] In recent history aluminum ion batteries have been studied in the presence of harmful species such as halogens and hydrides which compromise the exceptional corrosion resistance of aluminum thanks to its native oxide layer, which can be further anodized. Aluminum-triflate has been chosen as the alternative to aluminum chloride to synthesize halide-free aluminum-ion batteries. Al value has risen due to industrial demand for advancements in the field of energy storage. Al can be utilized to improve the efficiencies of energy storage and conversion devices through the exchange of 3 electrons and a high theoretical charge capacity. [102]

The difficulties of delayed delivery of EMS coupled with difficulty working with a solvent that is solid at room temperature necessitates the need to pivot to a new solvent, Propylene carbonate (PC). PC-based electrolytes have many attractive attributes that lead to being superior to widely commercially used ethylene carbonate (EC)-based electrolytes such as a wider operating temperature as well as higher oxidative stability and relative permittivity. [104] Therefore, PC-based electrolytes are a potential candidate for aluminum-ion batteries capable of high energy density, and a long lifespan. [105, 106]

Density functional theory (DFT) derived physiochemical properties of Al-triflate in propylene carbonate to computationally optimize structures in solution. These optimized structures are beneficial in predicting the theoretical electrochemical window, redox potentials, and lastly understanding the ionic association. The electrochemical activity of aluminum ions in the Al-PC complex was revealed through the reduction onset at 0 V shown in the cyclic voltammetry measurements on a gold working electrode at various concentrations. These values were compared to the predicted redox potentials gathered from the DFT calculations. The ab-intio data was compared to electrochemical experiments conducted in an argon-filled glovebox. Fourier Transform Infrared spectroscopy was used as a tool to analyze the ionic association. Scanning electron microscopy assisted in evaluating the surface morphology of the aluminum deposition. Electrical impedance spectroscopy experiments were run to better understand the electrochemical activity of the $Al(PC)_4$ electrolyte based on the concentration dependence. Lastly, X-ray photoelectron spectroscopy allows for an in-depth view of the species present after chronoamperometry was run for 24 hours. and electrical impedance spectroscopy experiments were run to better understand the electrochemical activity of the $Al(PC)_4$ electrolyte.

3.2 Materials and Methods

3.2.1 Density Functional Theory Calculations

DFT calculations were performed using the Gaussian 09 suite of electronic structure program. [93] The cam-B3LYP density functional was administered using the unrestricted spin-formalism for all open-shell cases along with the 6-311+G(d) basis set. [107, and 95] Geometry optimizations were conducted using standard methods, and the natures of the stationary points on the potential energy surfaces were confirmed using second-derivative calculations. [108] A solvation model density (SMD) continuum solvation model was used to evaluate the solvation-free energies based on the self-consistent reaction field (SCRF) approach, and a modified cyclopentanone was used for all SMD calculations as PC isn't a preset solvent in gaussian. [96] The dielectric constant was changed to 64.9 to clarify that the solvent is propylene carbonate at 293.15 K. In all cases, the stability of the SCF solution was verified. [109, 95]

3.2.2 Experimental Details

Aluminum triflate and PC were purchased from Sigma-Aldrich and used as delivered. All chemical preparations and electrochemical measurements were conducted in an argon-filled glovebox (VAC) with water and oxygen levels held below 1.5 and 0.5 ppm, respectively. The solutions described below were prepared by dissolving appropriate amounts of Al-triflate in the PC.

Cyclic voltammetry measurements were performed using a potentiostat (Gamry). The electrochemical cells for cyclic voltammetry measurements consisted of a gold working electrode with a surface area of 0.02 cm^2, an aluminum wire counter electrode, and an aluminum wire pseudo reference electrode set up in a standard three-electrode cell configuration. Scan rates of 10 mV/s and 100 mV/s were used.

Ionic conductivity measurements were performed using a ParStat 2273 by means of electrochemical impedance spectroscopy. A 10 mV ac signal with a 0 V dc offset was used over a 1−10 kHz frequency range. The impedance cell was prepared in the lab and consisted of two platinum wires encased in flint glass tubing that were polished with 0.3 μm alumina. The cell was calibrated using a 0.01 M KCl standard solution at 20°C.

Fourier transform infrared (FTIR) spectra were measured using Nicolet iS5OR FT-IR spectrometer in ATR and 32 scans. Resolutions of 4 cm^{-1} were utilized for solutions at various concentrations. [110]

Chronoamperometry was carried out using a Cu substrate as the working electrode, an Al wire pseudoreference, and an Al wire counter electrode. The potential was set to 0 V (with a pre-step initial voltage of −0.1 V) for the $Al(OTF)_3$/PC electrolyte. Before and after the chronoamperometry experiments, the Cu electrodes were rinsed with acetone and dried for at least 30 min. Electron microscopy was conducted with a field emission scanning electron microscope (Zeiss Gemini SEM 500). X-ray photoelectron spectroscopy (XPS) measurements were carried out using a Nexsa spectrometer. The sample for the XPS analysis was prepared by holding the potential of a Cu substrate at 0

V vs the Al wire for 48h in a 0.1 M $Al(OTF)_3$/PC electrolyte, followed by rinsing the Cu substrate with acetone.

3.3 Results and Discussion

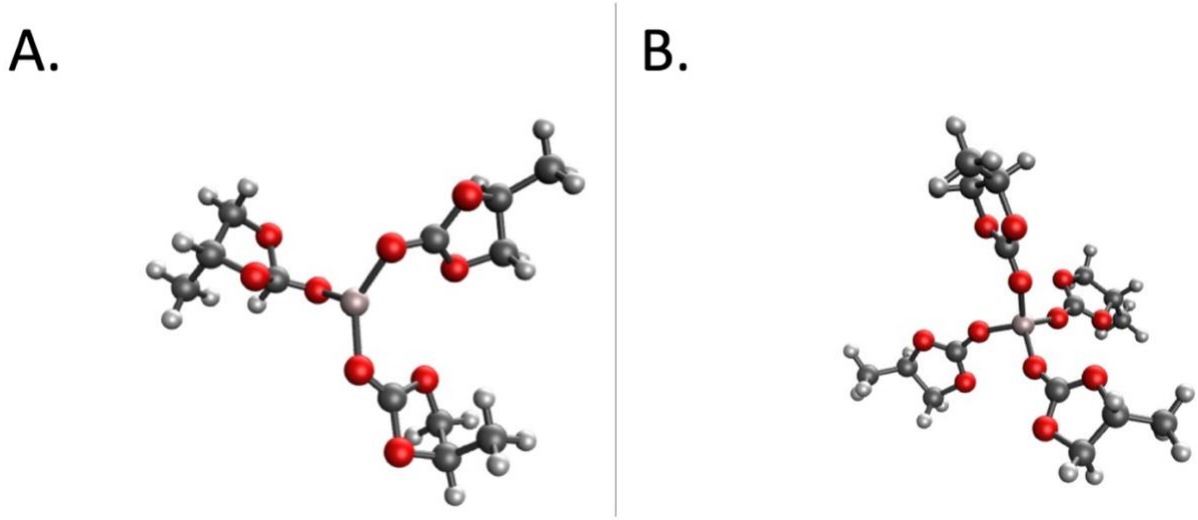

Figure 3.1 Optimized structures of (a) $Al(PC)_3^{3+}$, (b) $Al(PC)_4^{3+}$, pink: aluminum, grey: carbon, red: oxygen, white: hydrogen.

To understand the impact triflate anions are having in solution and on the geometry of $Al(PC)_3^{3+}$, spectroscopic measurements were carried out for the purpose of comparison to results from the DFT calculations with various numbers of coordinated triflate anions in propylene carbonate. Figure 3.1A-B are examples of geometries modeled using density functional theory calculations that produce stable structures.

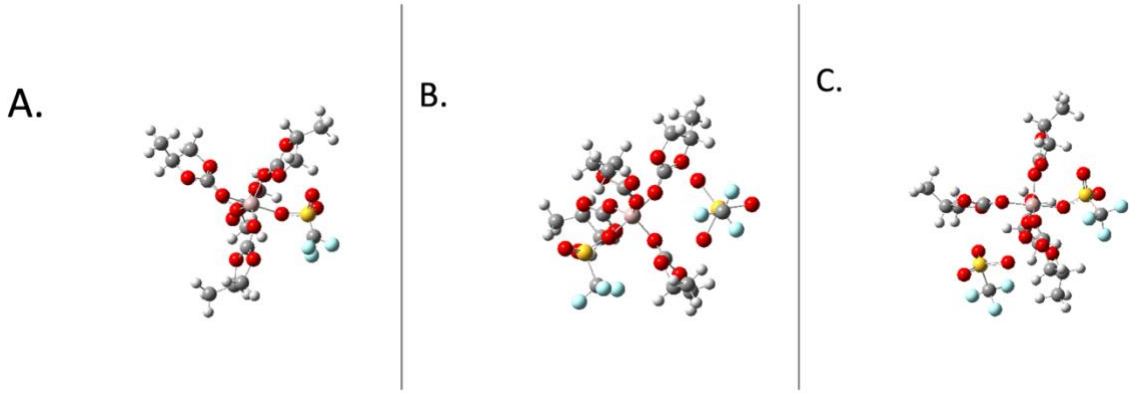

Figure 3.2 Optimized structures (hydrogens shown in white) of (A) bound triflate $[Al(PC)_4][triflate]_1^{2+}$, SO_3 symmetric stretch (B) SO_3 symmetric stretch

$[Al(PC)_4][triflate]^{2+}$, (C) SO_3 antisymmetric stretch $[Al(PC)_4][triflate]_2^{+}$. Pink: aluminum, grey: carbon, red: oxygen, blue: fluorine, yellow: sulfur.

The reactions that produce $Al(PC)_3^{3+}$ and $Al(PC)_4^{3+}$ are shown to be the most thermodynamically favorable with solvent phase Gibbs free energy of nearly -1386 and 1768 kJ/mol respectively that was calculated using density functional theory. The $Al(PC)_4^{3+}$ complex is anticipated to be the most present configuration of the Al-PC in the solution due to their entropic attributes of being most energetically favorable. Optimized structures will be used as the foundation of the computational analysis.

3.3.1 Coordination Structures.

DFT calculations were utilized to understand the coordination structures of the gas and solvent phase Al^{3+}-PC complexes. The theoretical Gibbs free energy of the reactions resulting in an Al^{3+} cation coordinated by three and four PC molecules was evaluated using Gaussian to optimize the potential electrolyte in the gas and solvent phase.

Reaction 1: $Al^{3+} + 3PC \rightarrow Al(PC)_3^{3+}$ $\Delta G_1 = -1386.79$ kJ/mol (1)

Reaction 2: $Al^{3+} + 4PC \rightarrow Al(PC)_4^{3+}$ $\Delta G_2 = -1768.52$ kJ/mol (2)

The vibrational frequencies gathered from the optimized structures in Figure 3.2B-C show ways in which triflate interacts with PC in solution. Figure 3.2A shows triflate ion-paired interaction as a bound triflate, while in Figure 3.2B triflate is paired with aluminum through contact-ion pairing. After analyzing various configurations of triflate around the aluminum core, triflate can interact with aluminum in multiple ways at a time. Figure 2.2A shows the presence of triflate being bounded to aluminum while another triflate anion is interacting through contact ion pairing which is indicative of the SO_3 antisymmetric stretch. This last region will prove to provide great insight by analyzing the splitting of vibrational frequency peaks.

3.3.2 Ionic association of triflate in PC through infrared spectroscopy

Table 3.1 Measured and Computed Vibrational Frequencies Measured and Computed Vibrational Frequencies

Species	**Free triflate**		**Contact ion pair**		**Bound triflate**	
mode	computed	measured	computed	measured	computed	measured
CF_3 symmetric deformation	759.3	740-755	762.5	735-755	776.70	775
SO_3 symmetric stretch	1008.9		1021.5	1020	995.7	
SO_3 antisymmetric stretch	1226.3	1225	1231.7		1235.3	1210-1220

The ionic association plays an important role in understanding an adequate environment necessary for the exchange of Al^{3+} ions. Infrared spectra were gathered to understand the complex-ion formation and ionic association of free triflate and $Al(PC)_4^{3+}$ at various concentrations. These results can be compared to the ab-initio data collected previously. The table above summarizes the results of the measurements and calculations. Frech and Huang have thoroughly investigated triflate's behavior in electrolytes, providing the groundwork to establish an understanding of known IR bands for electrolytes that incorporate triflate anions. [112, 113, 114, 115, 116, 114] Bands observed within the 750−775 cm^{-1} region of the IR spectra correspond to vibrational frequencies of the C−S stretch coupled with a C−F bending mode of the triflate anion, this is well known as the CF_3 symmetric deformation mode, $\delta s(CF_3)$. [113] Figure 3.3A shows an absorption band at 4 different concentrations near 775 cm^{-1} which agrees with the ab-initio results showing evidence of $\delta s(CF_3)$, which is the Al-bound triflate mode. As concentration is increased the bound triflate peak is relatively unaffected shown by the lack of shifting which would suggest that triflate is readily available to the aluminum core at dilute and concentrated mixtures.

A.

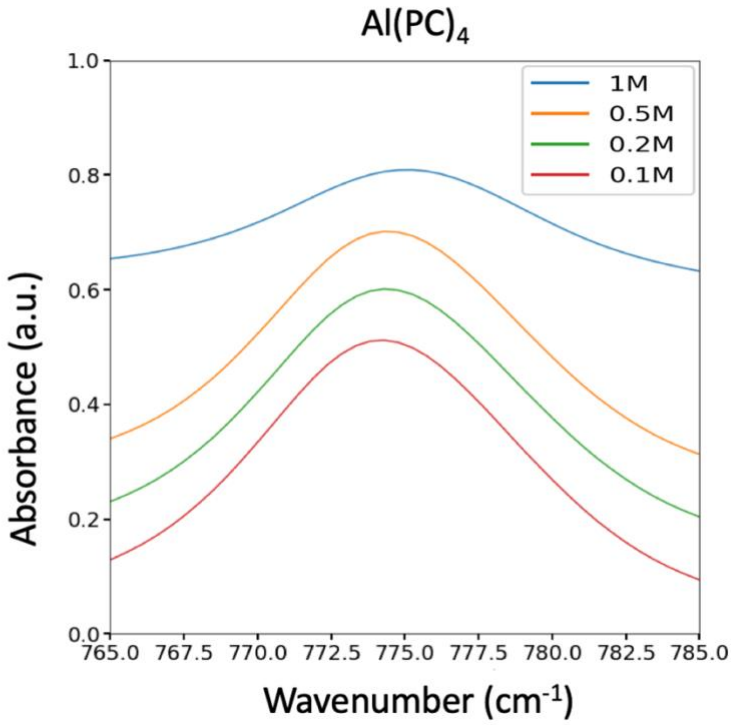
Al(PC)4
1M
0.5M
0.2M
0.1M
Absorbance (a.u.)
Wavenumber (cm-1)
0.0
0.2
0.4
0.6
0.8
1.0
765.0
767.5
770.0
772.5
775.0
777.5
780.0
782.5
785.0

B.

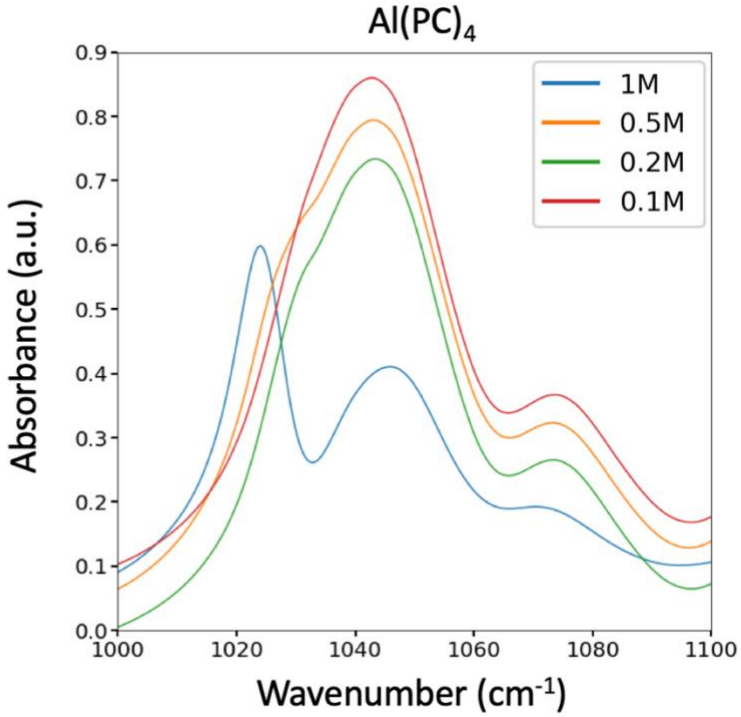
Al(PC)4
1M
0.5M
0.2M
0.1M
Absorbance (a.u.)
Wavenumber (cm-1)
0.0
0.1
0.2
0.3
0.4
0.5
0.6
0.7
0.8
0.9
1000
1020
1040
1060
1080
1100

C.

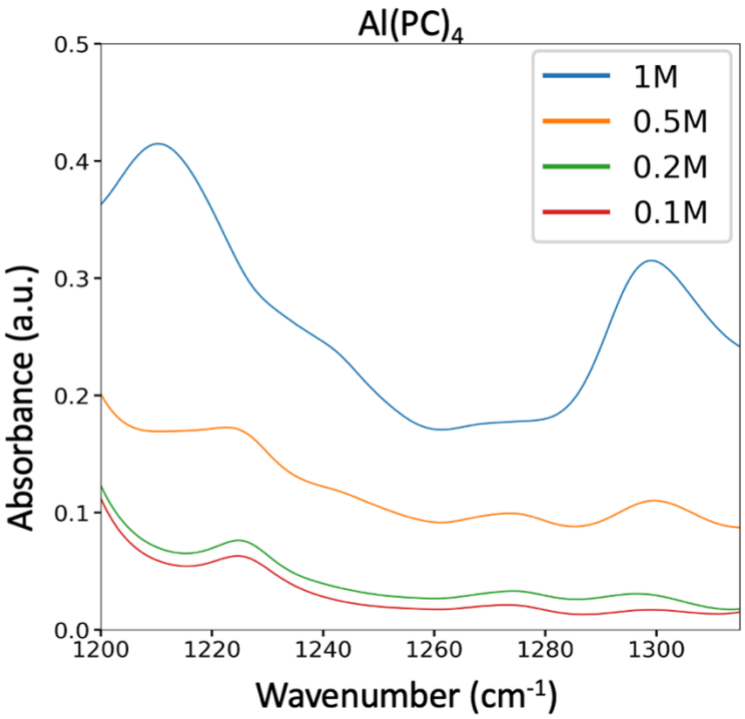

Figure 3.3 FTIR spectra of Al-triflate/PC solutions reveal (A) CF_3 symmetric deformation region, (B) SO_3 symmetric stretch region, and (C) SO_3 antisymmetric stretch region.

Predicted IR spectra collected via DFT calculations on $[Al(PC)_4][triflate]^{2+}$ and $[Al(PC)_4][triflate]_2^{+}$ agree with the aforementioned results. These complexes show evidence of vibrational frequencies at 776.70 and 775.29 cm^{-1} which corresponds to the CF_3 symmetric deformation mode of the complex-bound and Al-bound triflate. Previous literature by Reed, Slim, and myself in regards to the EMS-based solvent also produced results similar to the frequencies shown here including bands between 740-755 cm^{-1} that are in agreement with predicted vibrations of $\delta s(CF_3)$. [22] Free triflate demonstrates a vibrational frequency at 759.28 cm^{-1}. However, this peak is absent in the IR measurements in EMS, and PC at every concentration presented here. This suggests that $Al(PC)_4^{3+}$ is more readily available for an Al-bound triflate in comparison to previous work with Al-triflate with diglyme by Reed, and THF by Slim. [22]

As mentioned previously, the absorption bands at lower vibrational frequencies near 750 cm^{-1} were not present in the IR measurements, which appear to indicate the absence of free triflate entirely but that is not necessarily the case. Table 3.1 shows computational data that is linked to the presence of free triflate in solution near 760 cm^{-1}, while the IR spectra reveal free triflate peaks in the 740-755 cm^{-1} region. Figure 3.2B shows a spectral profile that is attributed to the absorption region of a nondegenerate symmetric stretch of SO_3, which is near 1020 cm^{-1}. [117] Spectral evidence of this can be described by the presence of the peak near 1020 cm^{-1} that is revealed as the concentration of the

electrolyte is increased due to the additional triflate in the solution. Triflate is now more readily available to encounter the aluminum core resulting in the contact-ion pairing peak. shows that the peak placement changes in the presence of added triflate in the contact ion paired mode.

The region that provides the most insight into the strength of ionic association is between 1200-1300 cm^{-1}. Previous literature states there is an ionic interaction prevalent in solutions synthesized by adding lithium and tetrabutylammonium triflate in a multitude of solvents showed that solutions consisting of Li-triflate in THF, trimethylene glycol dimethyl ether, acetone, and acetonitrile shown evidence of splitting in the doubly degenerate antisymmetric SO_3 mode $\nu_{as}SO_3$ into two fragments. [113] In comparing the significance of the band splitting we can infer the correlation to the strength of ionic association. The difference between the frequencies was shown to have a separation of 54 cm^{-1} for Li-triflate in THF. As mentioned previously, aluminum triflate has shown an increase in splitting for the purpose of comparison to lithium. In THF, the splitting of the doubly degenerate nearly 71 cm^{-1}, and in propylene carbonate, the splitting increased to 91 cm^{-1}. Finally, Figure 3.2C shows designated peaks at 1210 and 1300 cm^{-1}, which is like frequency splitting $\Delta_{vas}(SO_3)$ of around 90 cm^{-1}. The increase in separation between the bands for Al-triflate and Li-triflate-based electrolytes can be attributed to the higher charge density of the Al-cation due to the splitting of the doubly degenerate antisymmetric SO_3 mode $\nu_{as}SO_3$ into two fragments. [112-25]

3.3.3 Stability Predictions and Electrochemical Profiling

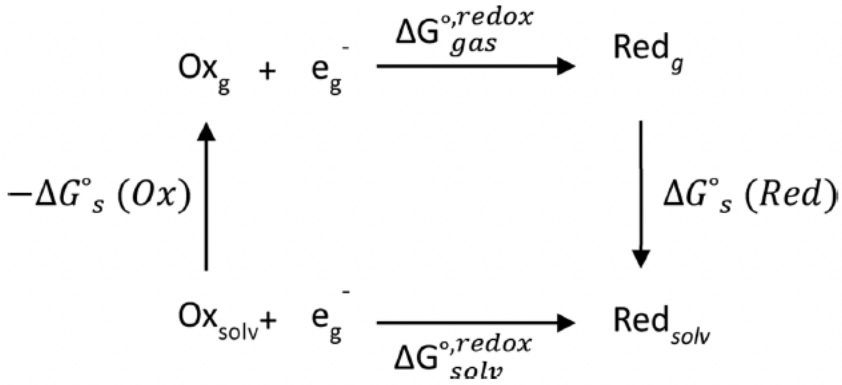

Scheme 3.1 Born-Haber Cycle Used to Calculate the Standard Solvation Gibbs Free Energy Changes.

$$\Delta G^{\circ,\mathrm{redox}}_{\mathrm{solv}} = -\Delta G^{\circ}_{\mathrm{s}}(\mathrm{Ox}) + \Delta G^{\circ,\mathrm{redox}}_{\mathrm{gas}} + \Delta G^{\circ}_{\mathrm{s}}(\mathrm{Red}) \quad (1)$$

To gain an understanding of the electrochemical behavior of the proposed electrolyte the Born-Haber cycle approach was used to evaluate the one-electron redox potentials shown in Scheme 1. [97, 111, 99] This cycle was used to calculate the absolute redox potentials. Before calculating the stability predictions, we solved for the change in solvent-phase Gibbs free energy ($\Delta G_{solv}^{\circ,redox}$) shown in equation 1, that can then be used to calculate for E_{calc}^{abs} as seen in equation 2. The Nernst equation was utilized to compute the absolute redox potentials for all species in solution that may impact the electrochemical activity.

$$E_{calc}^{abs} = -\frac{\Delta G_{solv}^{\circ,redox}}{nF} \quad (2)$$

After acquiring the solvent phase Gibbs free energy using equation 1, we can now solve for the absolute redox potentials using equation 2. In this Nernst equation n is 1 due to the exchange of one electron involved, and F is Faraday's constant. These redox potentials shown in Table 3.2 give us insight into the stability of the species in the electrolyte and the electrochemical window.

Table 3.2 Gibbs Free Energies and Absolute Reduction Potentials of Solvent, Anion, and Complexes

Reaction	$\Delta G_s^{\circ,Ox}$ **(kJ/mol)**	$\Delta G_{gas}^{\circ redox}$ **(kJ/mol)**	$\Delta G_s^{\circ(Red)}$ **(kJ/mol)**	E_{calc}^{abs} **(V)**	E_{calc} **(V vs Al/Al^{+3})**
$PC^+ + e^- \rightarrow PC$	-215.3	-997.7	-28.9	8.4	5.0
$PC + e^- \rightarrow PC^-$	-28.9	70.9	-230.3	1.3	-2.1
$triflate + e^- \rightarrow triflate^-$	-13.4	-489.3	-185.4	6.9	3.5
$triflate^- + e^- \rightarrow triflate^{-2}$	-185.4	459.6	-595.6	-0.5	-3.9
$Al(PC)_4^{+4} + e^- \rightarrow Al(PC)_4^{+3}$	-2076.0	-1792.2	-1175.9	9.3	6.9
$Al(PC)_4^{+3} + e^- \rightarrow Al(PC)_4^{+2}$	-1175.8	-850.1	-652.2	3.4	0

Propylene carbonate, triflate, and $Al(PC)_4^{3+}$ electrochemical window was predicted through density functional theory to be 7.1V, 7.4, and 5.9V respectively. The increase in theoretical electrochemical window depth agrees with propylene carbonate's stable attributes mentioned early. The stability of the electrolyte is described and governed by the oxidation of PC and the reduction of $Al(PC)_4^{3+}$. This results in an increase in the electrochemical window in comparison to lithium and aluminum in various solvents such as THF and diglyme. The PC electrolyte complex results in a theoretical electrochemical window of 5.0 V which doubles the previous materials and agrees with previous literature suggesting PC's advanced stability. The cell set up for the cyclic voltammetry measurements consists of an aluminum wire as a pseudo-reference electrode during the 3-cycle process, as suggested in Table 3.2, we hypothesize the reduction of $Al(PC)_4^{3+}$ involves Al^{3+} being reduced to aluminum metal. Therefore, the reduction peak of aluminum is expected to have an onset presence at 0V vs the aluminum wire, while the oxidation of propylene carbonate is expected at 5.0V.

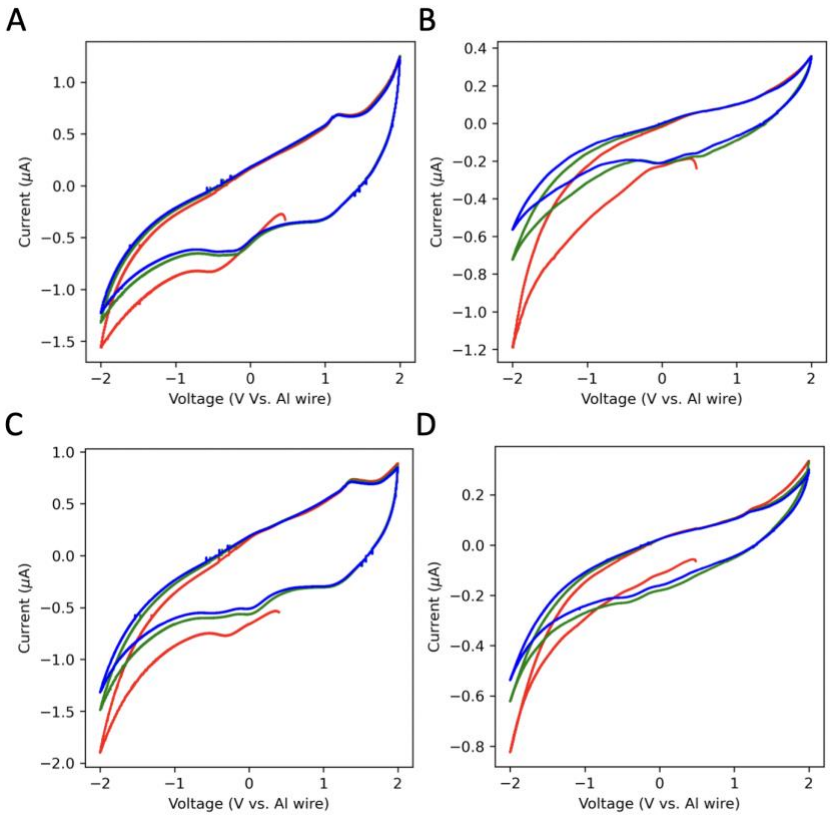

Figure 3.4 Display of the first three cycles of cyclic voltammograms for Al-triflate/PC electrolytes at different concentrations and different sweep rates of 10 mV/s and 100 mV/s: (A) 100 mV/s 0.05 M on gold WE. (B) 10 mV/s 0.05 M on gold WE. (C) 100 mV/s 0.1 M on gold WE. (D) 10 mV/s 0.1 M on gold WE. The first scan is red, the second is blue, and the third is green.

Cyclic voltammetry was performed using a gold working electrode to examine the I−V polarization curves to investigate any activity correlation between the DFT calculations and the actual CV measurements. Figure 3.3A-D show a reduction peak at approximately -2.0 V which agrees with the reduction of PC according to the DFT calculations. Cyclic voltammograms were measured on a gold working electrode shown above, revealing evidence of electrochemical activity around 0 V. We assign this electrochemical reduction at 0 to $Al(PC)_4^{3+}$ where Al^{3+} is reduced to aluminum metal. Observations of color change from gold to a silver-like color on the electrode surface area show possible plating. Looking at the CVs, there is a lack of an oxidation current due to the absence of aluminum stripping. This may be due to the electrolyte's lack of a strong Lewis base. This agrees with Graef's proposition of a mechanism for reversibly depositing/dissolving aluminum from an $AlCl_3$−$LiAlH_4$/THF bath. [50] It has been shown that a chloride-rich environment is necessary for the activation overpotential for the dissolution of aluminum. Realizing the full potential of the addition of a strong Lewis base is not the focus of this work, but rather the motivation of future research.

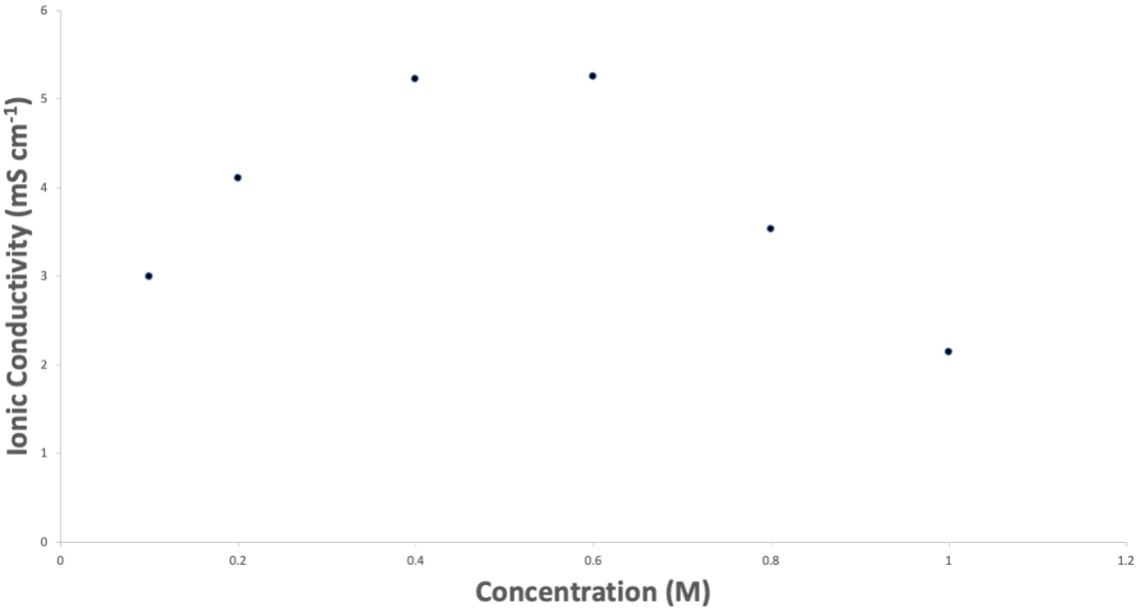

Figure 3.5 Ionic conductivity of the solution as a function of aluminum triflate concentration.

Another method to analyze the molar concentration dependence of the electrochemical properties of the electrolyte, electrical impedance spectroscopy was run to measure the ionic conductivities of the $Al(PC)_4^{3+}$ electrolyte to investigate the conductivity through its concentration dependence at room temperature. Figure 3.4 shows this electrolyte's ionic conductivity as concentration increases until the point of saturation ~0.6 M. The conductivity reaches as high as 5.4mS/cm before the ionic conductivity begins to decrease ~0.8 M. In comparison to the ionic conductivity of aluminum-triflate in THF

being 2.5 mS/cm, Propylene carbonate more than doubles the measured conductivity at a slightly lower concentration. These EIS measurements allow us to establish a conducive environment with optimal conductivity, also showing an improvement from the Al-EMS electrolyte in the previous chapter which required an increase in temperature to reach an ionic conductivity of 5 mS/cm at nearly double the concentration at 1.2 M. At 0.6 the electrolyte ionic conductivity begins to decrease at what we call the point of saturation due to the viscosity and ion pairing increasing. [22]

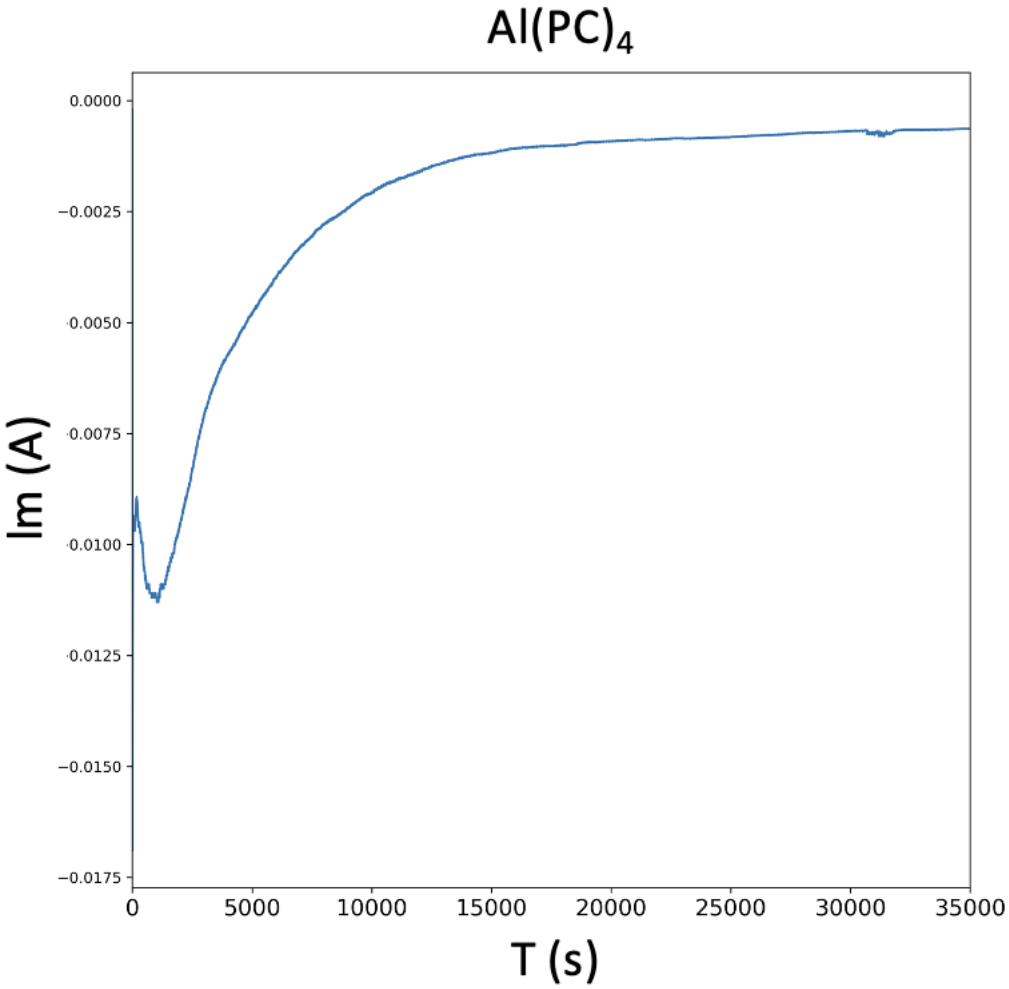

Figure 3.6 24 hr Chronoamperometry on a 0.05M aluminum propylene carbonate electrolyte

To confirm the reductive properties suggested by the electrochemical data collected through cyclic voltammetry which we hypothesize to correspond to the electrochemical reduction of Al-ions to Al-metal that agrees with the stability predictions gathered through the utilization of DFT, a scanning electron microscope (SEM) was used to

evaluate the surface morphology of the Cu substrates. Figure 3.6 shows a series of SEM images of an untreated Cu substrate at magnifications of 1 μm and 200 nm respectively (a, b), Al deposits obtained from $Al(OTF)_3$/PC (c, d). Figure 3.5 (a, b) images of untreated Cu shows a uniform morphology that resembles Cu substrate. Figure 3.5 shows a chronoamperometry graph of the process taken to treat the Cu substrate by applying a -0.5V to the $Al(PC)_4^{3+}$ electrolyte for 24 hours, allowing deposits to collect on the copper substrate for the purpose of studying the surface chemistry of what we suggest as aluminum deposition. Figure 3.6 (c, d) shows a non-homogenous morphology, free of uniformity that shows the deposition that we attribute to an Al species at low as well as high magnification (1 μm and 200 nm). A more in-depth analysis of the specific species present on the surface of the copper substrate can be examined through X-ray photoelectron spectroscopy.

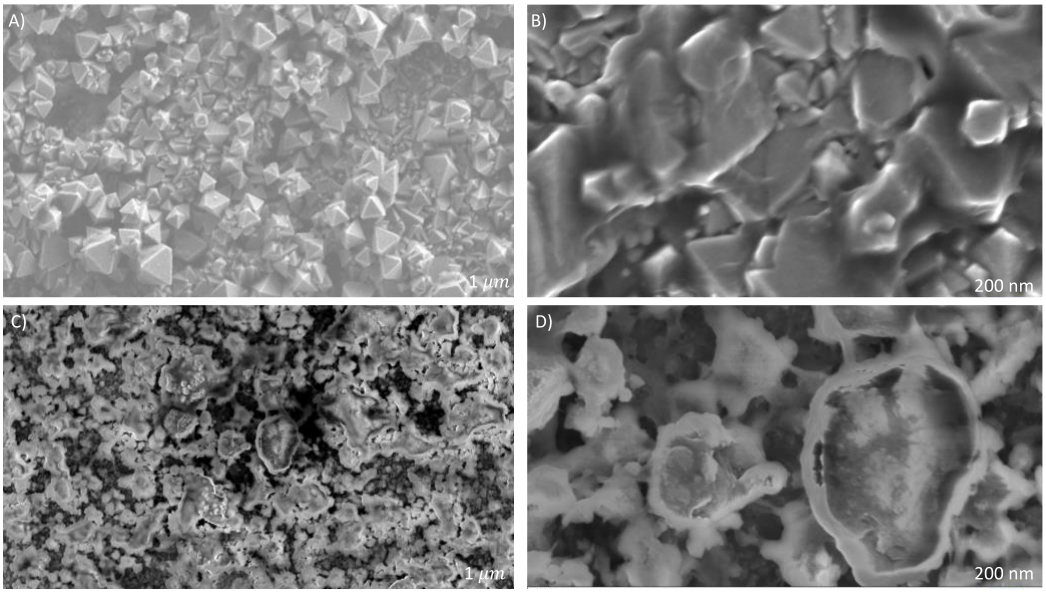

Figure 3.7 SEM images of (a, b) untreated Cu substrate, Al electrodeposits on Cu substrate (vs Al/Al^{3+}) obtained from (c, d) 0.1 M Al(OTF)3/PC at 0 V for 24 hr

To identify characteristics of the chemical composition of the electrodeposited Al films seen in the SEM images, depth-profile X-ray photoelectron spectroscopy analyses characterized the copper substrates shown in Figure 3.7. The XPS survey of the Al deposit on the Cu substrate in Figure 3.7A shows a broad survey that reveals the presence of various elements present on the Cu substrate after chronoamperometry. The presence of aluminum is evident due to the Al 2p peaks, while also showing other elements that can be found in an $Al(PC)_4$ electrolyte such as S2p, C1s, O1s, F1s, and Cu 2p3. The Cu peaks shown in Figure 3.7B can be attributed to the lack of complete coating of the metal Cu substrate. These copper peaks were anticipated to be present due to the solvent being an active halide-free electrolyte that would not incorporate chlorine. The addition of chlorine and hydride species in the electrolyte have shown to increase the coating surface

area. Still, this benefit comes with the addition of harmful corrosion to the potential battery which would greatly diminish the lifespan.

The Al 2p spectra shown in Figure 3.7C for the Al deposits obtained from the OTF^- electrolytes show peaks that are attributed to Al_2O_3 and Al metal at 75 eV and an AlF_3 at 77.5 eV, which is evidence of aluminum deposits from the $Al(PC)_4$ electrolyte.

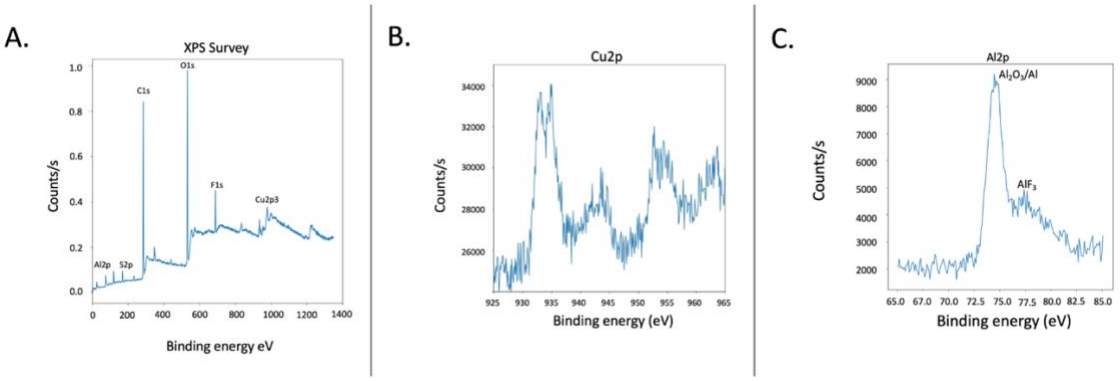

Figure 3.8 X-ray photoelectron spectroscopy (XPS) spectra of Al-deposits from $Al(OTF)_3$ Electrolyte. Showing (a) XPS survey for the deposit on Cu substrate (b) Al2p region (c) O1s region (d) F1s region (e) Cu2p for Al deposit obtained by electrodeposition of aluminum from a 0.1M Al(OTF)⁄PC electrolyte at 0 V vs. Al wire for 24 hours.

3.4 Conclusion

The physicochemical properties of Al-trif/PC electrolytes were investigated utilizing DFT calculations. These ab-initio experiments were conducted at the cam-b3lyp/6-311+g(d) level of theory to make stability predictions based on the absolute redox potentials of species in solution, and theoretical spectroscopic predictions regarding the ionic association of triflate with the core, as well as examine the electrochemical behavior. Spectroscopic experiments were also carried out to compare to the DFT calculations such as FTIR spectra of varied Al-triflate concentrations. Our results show peaks within 750-780 cm^{-1}, 1000-1100 cm^{-1}, and 1200-1300 cm^{-1} reveal congruent evidence of specific regions that give insight into the ionic environments for triflate anion contact Al-bound, free triflate, and contact ion paired respectively. Cyclic voltammetry measurements show the presence of electrochemical behavior of Al ions on a gold working electrode shown by the reduction when sweeping negatively from 0 V and the reduction of propylene carbonate was also observed near -2 V, which agrees with the DFT calculations for the reduction of PC and $Al(PC)_4^{3+}$. Understanding a conductive environment requires an in-depth study of the ionic conductivity, which reveals the concentration dependence of conductivity on the Al-PC electrolyte, showing a peak at 5.1 mS/cm near the expected point of saturation. The peak ionic conductivity was an

improvement on the previous electrolytes in THF and EMS, reaching the point of saturation at 0.6M at room temperature for a practical battery. SEM and XPS were utilized to study the surface chemistry and morphology that reveals evidence of Al plating without the presence of Cl in the solution, the Al deposit was shown in each case to be present which is promising but not fully coated on the Cu substrate. SEM revealed a change in the surface morphology after chronoamperometry was run on the copper substrate. Thereafter, XPS confirmed the presence of Al plating through the snapshot of the Al2p which suggests the presence of Al metal and other aluminum complexes. However, the copper peaks are present due to the lack of complete coating of the Cu substrate. Showing the possibility of plating aluminum and taking advantage of propylene carbonate stability in an active-halide-free electrolyte. There is a desire to increase coating as well as incorporate additives to promote reversibility for an electrolyte capable of playing an essential role in designing aluminum-ion batteries. This guides the direction of future work, incorporating hydrides such LiH and $LiAlH_4$ as well as chlorides to achieve this.

3.5 References

(1) Erickson, P.; Lazarus, M.; Piggot, G. Limiting Fossil Fuel Production as the next Big Step in Climate Policy. Nat. Clim. Change 2018, 8 (12), 1037–1043. https://doi.org/10.1038/s41558-018-0337-0.

(2) Cherp, A.; Vinichenko, V.; Tosun, J.; Gordon, J. A.; Jewell, J. National Growth Dynamics of Wind and Solar Power Compared to the Growth Required for Global Climate Targets. Nat. Energy 2021, 6 (7), 742–754. https://doi.org/10.1038/s41560-021-00863-0.

(3) Larcher, D.; Tarascon, J.-M. Towards Greener and More Sustainable Batteries for Electrical Energy Storage. Nat. Chem. 2015, 7 (1), 19–29. https://doi.org/10.1038/nchem.2085.

(4) Goodenough, J. B. Electrochemical Energy Storage in a Sustainable Modern Society. Energy Environ. Sci. 2013, 7 (1), 14–18. https://doi.org/10.1039/C3EE42613K.

(5) Goodenough, J. B.; Park, K.-S. The Li-Ion Rechargeable Battery: A Perspective. J. Am. Chem. Soc. 2013, 135 (4), 1167–1176. https://doi.org/10.1021/ja3091438.

(6) Tu, J.; Song, W.-L.; Lei, H.; Yu, Z.; Chen, L.-L.; Wang, M.; Jiao, S. Nonaqueous Rechargeable Aluminum Batteries: Progresses, Challenges, and Perspectives. Chem. Rev. 2021, 121 (8), 4903–4961. https://doi.org/10.1021/acs.chemrev.0c01257.

(7) Elia, G. A.; Marquardt, K.; Hoeppner, K.; Fantini, S.; Lin, R.; Knipping, E.; Peters, W.; Drillet, J.-F.; Passerini, S.; Hahn, R. An Overview and Future Perspectives of Aluminum Batteries. Adv. Mater. 2016, 28 (35), 7564–7579. https://doi.org/10.1002/adma.201601357.

(8) Li, Q.; Bjerrum, N. J. Aluminum as Anode for Energy Storage and Conversion: A Review. J. Power Sources 2002, 110 (1), 1–10. https://doi.org/10.1016/S0378-7753(01)01014-X.

(9) Zhang, Y.; Liu, S.; Ji, Y.; Ma, J.; Yu, H. Emerging Nonaqueous Aluminum-Ion Batteries: Challenges, Status, and Perspectives. Adv. Mater. Deerfield Beach Fla 2018, 30 (38), e1706310. https://doi.org/10.1002/adma.201706310.

(10) Li, M.; Lu, J.; Ji, X.; Li, Y.; Shao, Y.; Chen, Z.; Zhong, C.; Amine, K. Design Strategies for Nonaqueous Multivalent-Ion and Monovalent-Ion Battery Anodes. Nat. Rev. Mater. 2020, 5 (4). https://doi.org/10.1038/s41578-019-0166-4.
(11) The Rechargeable Aluminum Battery: Opportunities and Challenges - Yang - 2019 - Angewandte Chemie International Edition - Wiley Online Library. https://onlinelibrary.wiley.com/doi/10.1002/anie.201814031 (accessed 2023-04-27).
(12) Elia, G. A.; Kravchyk, K. V.; Kovalenko, M. V.; Chacón, J.; Holland, A.; Wills, R. G. A. An Overview and Prospective on Al and Al-Ion Battery Technologies. J. Power Sources 2021, 481, 228870. https://doi.org/10.1016/j.jpowsour.2020.228870.
(13) Faegh, E.; Ng, B.; Hayman, D.; Mustain, W. Practical Assessment of the Performance of Aluminium Battery Technologies. Nat. Energy 2020, 6. https://doi.org/10.1038/s41560-020-00728-y.
(14) Leung, O. M.; Schoetz, T.; Prodromakis, T.; Leon, C. P. de. Review—Progress in Electrolytes for Rechargeable Aluminium Batteries. J. Electrochem. Soc. 2021, 168 (5), 056509. https://doi.org/10.1149/1945-7111/abfb36.
(15) Cathode materials for rechargeable aluminum batteries: current status and progress - Journal of Materials Chemistry A (RSC Publishing). https://pubs.rsc.org/en/content/articlelanding/2017/ta/c7ta00282c (accessed 2023-04-27).
(16) Shi, J.; Zhang, J.; Guo, J. Avoiding Pitfalls in Rechargeable Aluminum Batteries Research. ACS Energy Lett. 2019, 4 (9), 2124–2129. https://doi.org/10.1021/acsenergylett.9b01285.
(17) Reed, L. D.; Menke, E. The Roles of V_2O_5 and Stainless Steel in Rechargeable Al–Ion Batteries. J. Electrochem. Soc. 2013, 160 (6), A915–A917. https://doi.org/10.1149/2.114306jes.
(18) Wang, H.; Gu, S.; Bai, Y.; Chen, S.; Zhu, N.; Wu, C.; Wu, F. Anion-Effects on Electrochemical Properties of Ionic Liquid Electrolytes for Rechargeable Aluminum Batteries. J. Mater. Chem. A 2015, 3 (45), 22677–22686. https://doi.org/10.1039/C5TA06187C.
(19) Lai, P. K.; Skyllas-Kazacos, M. Electrodeposition of Aluminium in Aluminium Chloride/1-Methyl-3-Ethylimidazolium Chloride. J. Electroanal. Chem. Interfacial Electrochem. 1988, 248 (2), 431–440. https://doi.org/10.1016/0022-0728(88)85103-9.
(20) Zhang, M.; Watson, J. S.; Counce, R. M.; Trulove, P. C.; Zawodzinski, T. A. Electrochemistry and Morphology Studies of Aluminum Plating/Stripping in a Chloroaluminate Ionic Liquid on Porous Carbon Materials. J. Electrochem. Soc. 2014, 161 (4), D163. https://doi.org/10.1149/2.048404jes.
(21) Mandai, T.; Johansson, P. Al Conductive Haloaluminate-Free Non-Aqueous Room-Temperature Electrolytes. J. Mater. Chem. A 2015, 3 (23), 12230–12239. https://doi.org/10.1039/C5TA01760B.
(22) Reed, L. D.; Arteaga, A.; Menke, E. J. A Combined Experimental and Computational Study of an Aluminum Triflate/Diglyme Electrolyte. J. Phys. Chem. B 2015, 119 (39), 12677–12681. https://doi.org/10.1021/acs.jpcb.5b08501.

(23) Reed, L. D.; Ortiz, S. N.; Xiong, M.; Menke, E. J. A Rechargeable Aluminum-Ion Battery Utilizing a Copper Hexacyanoferrate Cathode in an Organic Electrolyte. Chem. Commun. 2015, 51 (76), 14397–14400. https://doi.org/10.1039/C5CC06053B.
(24) Mandai, T.; Johansson, P. Haloaluminate-Free Cationic Aluminum Complexes: Structural Characterization and Physicochemical Properties. J. Phys. Chem. C 2016, 120 (38), 21285–21292. https://doi.org/10.1021/acs.jpcc.6b07235.
(25) Wen, X.; Zhang, J.; Luo, H.; Shi, J.; Tsay, C.; Jiang, H.; Lin, Y.-H.; Schroeder, M. A.; Xu, K.; Guo, J. Synthesis and Electrochemical Properties of Aluminum Hexafluorophosphate. J. Phys. Chem. Lett. 2021, 12 (25), 5903–5908. https://doi.org/10.1021/acs.jpclett.1c01236.
(26) Chiku, M.; Matsumura, S.; Takeda, H.; Higuchi, E.; Inoue, H. Aluminum Bis(Trifluoromethanesulfonyl)Imide as a Chloride-Free Electrolyte for Rechargeable Aluminum Batteries. J. Electrochem. Soc. 2017, 164 (9), A1841. https://doi.org/10.1149/2.0701709jes.
(27) Hilbig, P.; Ibing, L.; Wagner, R.; Winter, M.; Cekic-Laskovic, I. Ethyl Methyl Sulfone-Based Electrolytes for Lithium Ion Battery Applications. Energies 2017, 10 (9), 1312. https://doi.org/10.3390/en10091312.
(28) Avoundjian, A.; Galvan, V.; Gomez, F. An Inexpensive Paper-Based Aluminum-Air Battery. Micromachines 2017, 8. https://doi.org/10.3390/mi8070222.
(29) Lee, W.; Park, S.-J. Porous Anodic Aluminum Oxide: Anodization and Templated Synthesis of Functional Nanostructures. Chem. Rev. 2014, 114 (15), 7487–7556. https://doi.org/10.1021/cr500002z.
(30) Voltaic cell. studylib.net. https://studylib.net/doc/18820455/voltaic-cell (accessed 2023-04-29).
(31) Zaromb, S. The Use and Behavior of Aluminum Anodes in Alkaline Primary Batteries. J. Electrochem. Soc. 1962, 109 (12), 1125. https://doi.org/10.1149/1.2425257.
(32) Faegh, E.; Shrestha, S.; Zhao, X.; Mustain, W. In-Depth Structural Understanding of Zinc Oxide Addition to Alkaline Electrolytes to Protect Aluminum against Corrosion and Gassing. J. Appl. Electrochem. 2019, 49. https://doi.org/10.1007/s10800-019-01330-1.
(33) Duca, B. S. D. Electrochemical Behavior of the Aluminum Electrode in Molten Salt Electrolytes. J. Electrochem. Soc. 1971, 118 (3), 405. https://doi.org/10.1149/1.2408069.
(34) Holleck, G. L.; Giner, J. The Aluminum Electrode in AlCl[Sub 3]-Alkali-Halide Melts. J. Electrochem. Soc. 1972, 119 (9), 1161. https://doi.org/10.1149/1.2404433.
(35) Holleck, G. L. The Reduction of Chlorine on Carbon in AlCl3 - KCl - NaCl Melts. J. Electrochem. Soc. 1972, 119 (9), 1158. https://doi.org/10.1149/1.2404432.
(36) Gifford, P. R.; Palmisano, J. B. An Aluminum/Chlorine Rechargeable Cell Employing a Room Temperature Molten Salt Electrolyte. J. Electrochem. Soc. 1988, 135 (3), 650. https://doi.org/10.1149/1.2095685.
(37) Paranthaman, M. P.; Brown, G.; Sun, X.-G.; Nanda, J.; Manthiram, A.; Manivannan, A. A Transformational, High Energy Density, Secondary Aluminum Ion Battery. ECS Meet. Abstr. 2010, MA2010-02 (4), 314. https://doi.org/10.1149/MA2010-02/4/314.

(38) Jayaprakash, N.; Das, S. K.; Archer, L. A. The Rechargeable Aluminum-Ion Battery. Chem. Commun. 2011, 47 (47), 12610–12612. https://doi.org/10.1039/C1CC15779E.
(39) V. Plechkova, N.; R. Seddon, K. Applications of Ionic Liquids in the Chemical Industry. Chem. Soc. Rev. 2008, 37 (1), 123–150. https://doi.org/10.1039/B006677J.
(40) Pena-Pereira, F.; Namieśnik, J. Ionic Liquids and Deep Eutectic Mixtures: Sustainable Solvents for Extraction Processes. ChemSusChem 2014, 7 (7), 1784–1800. https://doi.org/10.1002/cssc.201301192.
(41) Wilkes, J. S.; Levisky, J. A.; Wilson, R. A.; Hussey, C. L. Dialkylimidazolium Chloroaluminate Melts: A New Class of Room-Temperature Ionic Liquids for Electrochemistry, Spectroscopy and Synthesis. Inorg. Chem. 1982, 21 (3), 1263–1264. https://doi.org/10.1021/ic00133a078.
(42) Zhao, Y.; VanderNoot, T. J. Electrodeposition of Aluminium from Nonaqueous Organic Electrolytic Systems and Room Temperature Molten Salts. Electrochimica Acta 1997, 42 (1), 3–13. https://doi.org/10.1016/0013-4686(96)00080-1.
(43) Hurley, F. H.; WIer, T. P. The Electrodeposition of Aluminum from Nonaqueous Solutions at Room Temperature. J. Electrochem. Soc. 1951, 98 (5), 207. https://doi.org/10.1149/1.2778133.
(44) Gale, R. J.; Gilbert, B.; Osteryoung, R. A. Raman Spectra of Molten Aluminum Chloride: 1-Butylpyridinium Chloride Systems at Ambient Temperatures. Inorg. Chem. 1978, 17 (10), 2728–2729. https://doi.org/10.1021/ic50188a008.
(45) Wang, C.; Creuziger, A.; Stafford, G.; Hussey, C. L. Anodic Dissolution of Aluminum in the Aluminum Chloride-1-Ethyl-3-Methylimidazolium Chloride Ionic Liquid. J. Electrochem. Soc. 2016, 163 (14), H1186. https://doi.org/10.1149/2.1061614jes.
(46) PII: 0022-0728(88)85103-9 | Elsevier Enhanced Reader. https://doi.org/10.1016/0022-0728(88)85103-9.
(47) Oh, Y.; Lee, G.; Tak, Y. Stability of Metallic Current Collectors in Acidic Ionic Liquid for Rechargeable Aluminum-Ion Batteries. ChemElectroChem 2018, 5, 3348–3352. https://doi.org/10.1002/celc.201801396.
(48) Couch, D. E.; Brenner, A. A Hydride Bath for the Electrodeposition of Aluminum. J. Electrochem. Soc. 1952, 99 (6), 234. https://doi.org/10.1149/1.2779711.
(49) Ishibashi, N.; Yoshio, M. Electrodeposition of Aluminium from the NBS Type Bath Using Tetrahydrofuran—Benzene Mixed Solvent. Electrochimica Acta 1972, 17 (8), 1343–1352. https://doi.org/10.1016/0013-4686(72)80080-X.
(50) Graef, M. W. M. The Mechanism of Aluminum Electrodeposition from Solutions of AlCl3 and LiAlH4 in THF. J. Electrochem. Soc. 1985, 132 (5), 1038. https://doi.org/10.1149/1.2114011.
(51) Finholt, A. E.; Bond, A. C. Jr.; Schlesinger, H. I. Lithium Aluminum Hydride, Aluminum Hydride and Lithium Gallium Hydride, and Some of Their Applications in Organic and Inorganic Chemistry1. J. Am. Chem. Soc. 1947, 69 (5), 1199–1203. https://doi.org/10.1021/ja01197a061.

(52) Legrand, L.; Tranchant, A.; Messina, R. Behaviour of Aluminium as Anode in Dimethylsulfone-Based Electrolytes. Electrochimica Acta 1994, 39 (10), 1427–1431. https://doi.org/10.1016/0013-4686(94)85054-2.
(53) Legrand, L.; Tranchant, A.; Messina, R. Electrodeposition Studies of Aluminum on Tungsten Electrode from DMSO 2 Electrolytes: Determination of AlIII Species Diffusion Coefficients. J. Electrochem. Soc. 1994, 141 (2), 378. https://doi.org/10.1149/1.2054735.
(54) Legrand, L.; Heintz, M.; Tranchant, A.; Messina, R. Sulfone-Based Electrolytes for Aluminum Electrodeposition. Electrochimica Acta 1995, 40 (11), 1711–1716. https://doi.org/10.1016/0013-4686(95)00019-B.
(55) Legrand, L.; Tranchant, A.; Messina, R. Aluminium Behaviour and Stability in AlCl3DMSO2 Electrolyte. Electrochimica Acta 1996, 41 (17), 2715–2720. https://doi.org/10.1016/0013-4686(96)00126-0.
(56) Miyake, M.; Fujii, H.; Hirato, T. Electroplating of Al on Mg Alloy in a Dimethyl Sulfone–Aluminum Chloride Bath. Surf. Coat. Technol. 2015, 277, 160–164. https://doi.org/10.1016/j.surfcoat.2015.07.047.
(57) Nakayama, Y.; Senda, Y.; Kawasaki, H.; Koshitani, N.; Hosoi, S.; Kudo, Y.; Morioka, H.; Nagamine, M. Sulfone-Based Electrolytes for Aluminium Rechargeable Batteries. Phys. Chem. Chem. Phys. 2015, 17 (8), 5758–5766. https://doi.org/10.1039/C4CP02183E.
(58) Kitada, A.; Nakamura, K.; Fukami, K.; Murase, K. Electrochemically Active Species in Aluminum Electrodeposition Baths of AlCl3/Glyme Solutions. Electrochimica Acta 2016, 211, 561.
(59) Zhang, Z.; Kitada, A.; Gao, S.; Fukami, K.; Tsuji, N.; Yao, Z.; Murase, K. A Concentrated AlCl3–Diglyme Electrolyte for Hard and Corrosion-Resistant Aluminum Electrodeposits. ACS Appl. Mater. Interfaces 2020, 12 (38), 43289–43298. https://doi.org/10.1021/acsami.0c12602.
(60) Kitada, A.; KATO, Y.; Fukami, K.; Murase, K. Room Temperature Electrodeposition of Flat and Smooth Aluminum Layers from An AlCl3/Diglyme Bath. J. Surf. Finish. Soc. Jpn. 2018, 69, 310–311. https://doi.org/10.4139/sfj.69.310.
(61) Howells, R. D.; Mc Cown, J. D. Trifluoromethanesulfonic Acid and Derivatives. Chem. Rev. 1977, 77 (1), 69–92. https://doi.org/10.1021/cr60305a005.
(62) Slim, Z.; Menke, E. J. Comparing Computational Predictions and Experimental Results for Aluminum Triflate in Tetrahydrofuran. J. Phys. Chem. B 2020, 124 (24), 5002–5008. https://doi.org/10.1021/acs.jpcb.0c02570.
(63) Hu, J. J.; Long, G. K.; Liu, S.; Li, G. R.; Gao, X. P. A LiFSI–LiTFSI Binary-Salt Electrolyte to Achieve High Capacity and Cycle Stability for a Li–S Battery. Chem. Commun. 2014, 50 (93), 14647–14650. https://doi.org/10.1039/C4CC06666A.
(64) Yang, H.; Zhuang, G.; Ross, P. Thermal Stability of LiPF 6 Salt and Li-Ion Battery Electrolytes Containing LiPF 6. J. Power Sources - J POWER SOURCES 2006, 161, 573–579. https://doi.org/10.1016/j.jpowsour.2006.03.058.
(65) Younesi, R.; Veith, G. M.; Johansson, P.; Edström, K.; Vegge, T. Lithium Salts for Advanced Lithium Batteries: Li–Metal, Li–O2, and Li–S. Energy Environ. Sci. 2015, 8 (7), 1905–1922. https://doi.org/10.1039/C5EE01215E.

(66) Ha, S.-Y.; Lee, Y.-W.; Woo, S. W.; Koo, B.; Kim, J.-S.; Cho, J.; Lee, K. T.; Choi, N.-S. Magnesium(II) Bis(Trifluoromethane Sulfonyl) Imide-Based Electrolytes with Wide Electrochemical Windows for Rechargeable Magnesium Batteries. ACS Appl. Mater. Interfaces 2014, 6 (6), 4063–4073. https://doi.org/10.1021/am405619v.
(67) Keyzer, E. N.; Glass, H. F. J.; Liu, Z.; Bayley, P. M.; Dutton, S. E.; Grey, C. P.; Wright, D. S. Mg(PF6)2-Based Electrolyte Systems: Understanding Electrolyte-Electrode Interactions for the Development of Mg-Ion Batteries. J. Am. Chem. Soc. 2016, 138 (28), 8682–8685. https://doi.org/10.1021/jacs.6b04319.
(68) Wang, Y.; Xing, L.; Li, W.; Bedrov, D. Why Do Sulfone-Based Electrolytes Show Stability at High Voltages? Insight from Density Functional Theory. J. Phys. Chem. Lett. 2013, 4 (22), 3992–3999. https://doi.org/10.1021/jz401726p.
(69) Xing, L.; Wang, C.; Li, W.; Xu, M.; Meng, X.; Zhao, S. Theoretical Insight into Oxidative Decomposition of Propylene Carbonate in the Lithium Ion Battery. J. Phys. Chem. B 2009, 113 (15), 5181–5187. https://doi.org/10.1021/jp810279h.
(70) Dunn, B.; Kamath, H.; Tarascon, J.-M. Electrical Energy Storage for the Grid: A Battery of Choices. Science 2011, 334 (6058), 928–935. https://doi.org/10.1126/science.1212741.
(71) Manthiram, A. A Reflection on Lithium-Ion Battery Cathode Chemistry. Nat. Commun. 2020, 11 (1), 1550. https://doi.org/10.1038/s41467-020-15355-0.
(72) Wu, F.; Yang, H.; Bai, Y.; Wu, C. Paving the Path toward Reliable Cathode Materials for Aluminum-Ion Batteries. Adv. Mater. Deerfield Beach Fla 2019, 31 (16), e1806510. https://doi.org/10.1002/adma.201806510.
(73) Lin, M.-C.; Gong, M.; Lu, B.; Wu, Y.; Wang, D.-Y.; Guan, M.; Angell, M.; Chen, C.; Yang, J.; Hwang, B.-J.; Dai, H. An Ultrafast Rechargeable Aluminium-Ion Battery. Nature 2015, 520 (7547), 324–328. https://doi.org/10.1038/nature14340.
(74) Kravchyk, K. V.; Wang, S.; Piveteau, L.; Kovalenko, M. V. Efficient Aluminum Chloride–Natural Graphite Battery. Chem. Mater. 2017, 29 (10), 4484–4492. https://doi.org/10.1021/acs.chemmater.7b01060.
(75) Greco, G.; Tatchev, D.; Hoell, A.; Krumrey, M.; Raoux, S.; Hahn, R.; Elia, G. A. Influence of the Electrode Nano/Microstructure on the Electrochemical Properties of Graphite in Aluminum Batteries. J. Mater. Chem. A 2018, 6 (45), 22673–22680. https://doi.org/10.1039/C8TA08319C.
(76) Geng, L.; Lv, G.; Xing, X.; Guo, J. Reversible Electrochemical Intercalation of Aluminum in Mo6S8. Chem. Mater. 2015, 27 (14), 4926–4929. https://doi.org/10.1021/acs.chemmater.5b01918.
(77) Lee, B.; Lee, H. R.; Yim, T.; Kim, J. H.; Lee, J. G.; Chung, K. Y.; Cho, B. W.; Oh, S. H. Investigation on the Structural Evolutions during the Insertion of Aluminum Ions into Mo6S8 Chevrel Phase. J. Electrochem. Soc. 2016, 163 (6), A1070. https://doi.org/10.1149/2.0011607jes.
(78) X-MOL. x-mol.net. https://www.x-mol.net/paper/article/1356342681998311424 (accessed 2023-05-09).
(79) Wang, H.; Bai, Y.; Chen, S.; Luo, X.; Wu, C.; Wu, F.; Lu, J.; Amine, K. Binder-Free V2O5 Cathode for Greener Rechargeable Aluminum Battery. ACS Appl. Mater. Interfaces 2015, 7 (1), 80–84. https://doi.org/10.1021/am508001h.

(80) Wang, S.; Jiao, S.; Wang, J.; Chen, H.-S.; Tian, D.; Lei, H.; Fang, D.-N. High-Performance Aluminum-Ion Battery with CuS@C Microsphere Composite Cathode. ACS Nano 2017, 11 (1), 469–477. https://doi.org/10.1021/acsnano.6b06446.
(81) Mori, T.; Orikasa, Y.; Nakanishi, K.; Kezheng, C.; Hattori, M.; Ohta, T.; Uchimoto, Y. Discharge/Charge Reaction Mechanisms of FeS2 Cathode Material for Aluminum Rechargeable Batteries at 55°C. J. Power Sources 2016, 313, 9–14. https://doi.org/10.1016/j.jpowsour.2016.02.062.
(82) Wang, S.; Yu, Z.; Tu, J.; Wang, J.; Tian, D.; Liu, Y.; Jiao, S. A Novel Aluminum-Ion Battery: Al/AlCl $_3$ -[EMIm]Cl/Ni $_3$ S $_2$ @Graphene. Adv. Energy Mater. 2016, 6 (13), 1600137. https://doi.org/10.1002/aenm.201600137.
(83) Donahue, F. M.; Mancini, S. E.; Simonsen, L. Secondary Aluminium-Iron (III) Chloride Batteries with a Low Temperature Molten Salt Electrolyte. J. Appl. Electrochem. 1992, 22 (3), 230–234. https://doi.org/10.1007/BF01030182.
(84) Suto, K.; Nakata, A.; Murayama, H.; Hirai, T.; Yamaki, J.; Ogumi, Z. Electrochemical Properties of Al/Vanadium Chloride Batteries with AlCl3-1-Ethyl-3-Methylimidazolium Chloride Electrolyte. J. Electrochem. Soc. 2016, 163 (5), A742. https://doi.org/10.1149/2.0991605jes.
(85) Nakaya, K.; Nakata, A.; Hirai, T.; Ogumi, Z. Oxidation of Nickel in AlCl3-1-Butylpyridinium Chloride at Ambient Temperature. J. Electrochem. Soc. 2014, 162 (1), D42. https://doi.org/10.1149/2.0401501jes.
(86) Tian, H.; Zhang, S.; Meng, Z.; He, W.; Han, W.-Q. Rechargeable Aluminum/Iodine Battery Redox Chemistry in Ionic Liquid Electrolyte. ACS Energy Lett. 2017, 2 (5), 1170–1176. https://doi.org/10.1021/acsenergylett.7b00160.
(87) Armand, M.; Tarascon, J.-M. Building Better Batteries. Nature 2008, 451 (7179), 652–657. https://doi.org/10.1038/451652a.
(88) Gao, X.-P.; Yang, H.-X. Multi-Electron Reaction Materials for High Energy Density Batteries. Energy Environ. Sci. 2010, 3 (2), 174–189. https://doi.org/10.1039/B916098A.
(89) 2 – Past, Present and Future of Lithium-Ion Batteries: Can New Technologies Open up New Horizons? | Elsevier Enhanced Reader. https://doi.org/10.1016/B978-0-444-59513-3.00002-9.
(90) Hu, Y.; Sun, D.; Luo, B.; Wang, L. Recent Progress and Future Trends of Aluminum Batteries. Energy Technol. 2019, 7 (1), 86–106. https://doi.org/10.1002/ente.201800550.
(91) Shkrob, I. A.; Wishart, J. F.; Abraham, D. P. What Makes Fluoroethylene Carbonate Different? J. Phys. Chem. C 2015, 119 (27), 14954–14964. https://doi.org/10.1021/acs.jpcc.5b03591.
(92) Tseng, C.-H.; Chang, J.-K.; Chen, J.-R.; Tsai, W. T.; Deng, M.-J.; Sun, I.-W. Corrosion Behaviors of Materials in Aluminum Chloride–1-Ethyl-3-Methylimidazolium Chloride Ionic Liquid. Electrochem. Commun. 2010, 12 (8), 1091–1094. https://doi.org/10.1016/j.elecom.2010.05.036.
(93) Gaussian 09 Citation | Gaussian.com. https://gaussian.com/g09citation/ (accessed 2022-12-06).

(94) Becke, A. D. Density-functional Thermochemistry. III. The Role of Exact Exchange. J. Chem. Phys. 1993, 98 (7), 5648–5652. https://doi.org/10.1063/1.464913.
(95) Krishnan, R.; Binkley, J. S.; Seeger, R.; Pople, J. A. Self-consistent Molecular Orbital Methods. XX. A Basis Set for Correlated Wave Functions. J. Chem. Phys. 1980, 72 (1), 650–654. https://doi.org/10.1063/1.438955.
(96) Marenich, A. V.; Cramer, C. J.; Truhlar, D. G. Universal Solvation Model Based on Solute Electron Density and on a Continuum Model of the Solvent Defined by the Bulk Dielectric Constant and Atomic Surface Tensions. J. Phys. Chem. B 2009, 113 (18), 6378–6396. https://doi.org/10.1021/jp810292n.
(97) Roy, L. E.; Jakubikova, E.; Guthrie, M. G.; Batista, E. R. Calculation of One-Electron Redox Potentials Revisited. Is It Possible to Calculate Accurate Potentials with Density Functional Methods? J. Phys. Chem. A 2009, 113 (24), 6745–6750. https://doi.org/10.1021/jp811388w.
(98) Jafari, S.; Tavares Santos, Y. A.; Bergmann, J.; Irani, M.; Ryde, U. Benchmark Study of Redox Potential Calculations for Iron–Sulfur Clusters in Proteins. Inorg. Chem. 2022, 61 (16), 5991–6007. https://doi.org/10.1021/acs.inorgchem.1c03422.
(99) Shao, N.; Sun, X.-G.; Dai, S.; Jiang, D. Electrochemical Windows of Sulfone-Based Electrolytes for High-Voltage Li-Ion Batteries. J. Phys. Chem. B 2011, 115 (42), 12120–12125. https://doi.org/10.1021/jp204401t.
(100) Yan, C.; Lv, C.; Wang, L.; Cui, W.; Zhang, L.; Dinh, K. N.; Tan, H.; Wu, C.; Wu, T.; Ren, Y.; Chen, J.; Liu, Z.; Srinivasan, M.; Rui, X.; Yan, Q.; Yu, G. Architecting a Stable High-Energy Aqueous Al-Ion Battery. J. Am. Chem. Soc. 2020, 142 (36), 15295–15304. https://doi.org/10.1021/jacs.0c05054.
(101) Lithium-Ion Batteries. https://shop.elsevier.com/books/lithium-ion-batteries/pistoia/978-0-444-59513-3 (accessed 2022-12-20).
(102) Zu, C.-X.; Li, H. Thermodynamic Analysis on Energy Densities of Batteries. Energy Environ. Sci. 2011, 4 (8), 2614–2624. https://doi.org/10.1039/C0EE00777C.
(103) Leisegang, T.; Meutzner, F.; Zschornak, M.; Münchgesang, W.; Schmid, R.; Nestler, T.; Eremin, R. A.; Kabanov, A. A.; Blatov, V. A.; Meyer, D. C. The Aluminum-Ion Battery: A Sustainable and Seminal Concept? Front. Chem. 2019, 7.
(104) Fan, H.; Liu, X.; Luo, L.; Zhong, F.; Cao, Y. All-Climate High-Voltage Commercial Lithium-Ion Batteries Based on Propylene Carbonate Electrolytes. ACS Appl. Mater. Interfaces 2022, 14 (1), 574–580. https://doi.org/10.1021/acsami.1c16767.
(105) Hu, C.-C.; Chiu, P.-H.; Wang, S.-J.; Cheng, S.-H. Isobaric Vapor–Liquid Equilibria for Binary Systems of Diethyl Carbonate + Propylene Carbonate, Diethyl Carbonate + Propylene Glycol, and Ethanol + Propylene Carbonate at 101.3 KPa. J. Chem. Eng. Data 2015, 60 (5), 1487–1494. https://doi.org/10.1021/acs.jced.5b00064.
(106) Xing, L.; Zheng, X.; Schroeder, M.; Alvarado, J.; von Wald Cresce, A.; Xu, K.; Li, Q.; Li, W. Deciphering the Ethylene Carbonate–Propylene Carbonate Mystery in Li-Ion Batteries. Acc. Chem. Res. 2018, 51 (2), 282–289. https://doi.org/10.1021/acs.accounts.7b00474.
(107) Becke, A. D. Density-Functional Thermochemistry. III. The Role of Exact Exchange. J. Chem. Phys. 1993, 98, 5648–5652. https://doi.org/10.1063/1.464913.

(108) Jay, A.; Huet, C.; Salles, N.; Gunde, M.; Martin-Samos, L.; Richard, N.; Landa, G.; Goiffon, V.; De Gironcoli, S.; Hémeryck, A.; Mousseau, N. Finding Reaction Pathways and Transition States: R-ARTn and d-ARTn as an Efficient and Versatile Alternative to String Approaches. J. Chem. Theory Comput. 2020, 16 (10), 6726–6734. https://doi.org/10.1021/acs.jctc.0c00541.
(109) Bauernschmitt, R.; Ahlrichs, R. Stability Analysis for Solutions of the Closed Shell Kohn-Sham Equation. J. Chem. Phys. 1996, 104, 9047–9052. https://doi.org/10.1063/1.471637.
(110) Menges, F. Spectragryph - optical spectroscopy software. Spectroscopy. http://spectragryph.com/ (accessed 2022-12-08).
(111) Konezny, S. J.; Doherty, M. D.; Luca, O. R.; Crabtree, R. H.; Soloveichik, G. L.; Batista, V. S. Reduction of Systematic Uncertainty in DFT Redox Potentials of Transition-Metal Complexes. J. Phys. Chem. C 2012, 116 (10), 6349–6356. https://doi.org/10.1021/jp300485t.
(112) Huang, W.; Frech, R.; Wheeler, R. A. Molecular Structures and Normal Vibrations of Trifluoromethane Sulfonate (CF3SO3-) and Its Lithium Ion Pairs and Aggregates. J. Phys. Chem. 1994, 98 (1), 100–110. https://doi.org/10.1021/j100052a018.
(113) Frech, R.; Huang, W. Anion-Solvent and Anion-Cation Interactions in Lithium and Tetrabutylammonium Trifluoromethanesulfonate Solutions. J. Solut. Chem. 1994, 23 (4), 469–481. https://doi.org/10.1007/BF00972613.
(114) Frech, R.; Huang, W. Ionic Association in Poly (Propylene Oxide) Complexed with Divalent Metal Trifluoromethanesulfonate Salts. Solid State Ion. 1993, 66 (1), 183–188. https://doi.org/10.1016/0167-2738(93)90042-2.
(115) Huang, W.; Frech, R. Dependence of Ionic Association on Polymer Chain Length in Poly(Ethylene Oxide)-Lithium Triflate Complexes. Polymer 1994, 35 (2), 235–242. https://doi.org/10.1016/0032-3861(94)90684-X.
(116) Bernson, A.; Lindgren, J.; Huang, W.; Frech, R. Coordination and Conformation in PEO, PEGM and PEG Systems Containing Lithium or Lanthanum Triflate. Polymer 1995, 36 (23), 4471–4478. https://doi.org/10.1016/0032-3861(95)96855-3.
(117) Wendsjö, Å.; Lindgren, J.; Thomas, J. O.; Farrington, G. C. The Effect of Temperature and Concentration on the Local Environment in the System M(CF3SO3)2PEOn for M=Ni, Zn and Pb. Solid State Ion. 1992, 53–56, 1077–1082. https://doi.org/10.1016/0167-2738(92)90293-X.

Chapter 4: Outlook and Future Work

4.1 Introduction

The previous chapters are the results of one pathway to study electrolytes for the purpose of improving rechargeable-ion batteries to meet future energy storage needs. Both the PC and EMS-based electrolytes proved to be capable of great stability and electrochemical activity shown in the cyclic voltammogram. The propylene carbonate-based electrolyte was shown to have the ability to plate aluminum in a non-corrosive electrochemical environment, however, there is a lack of reversibility that is present. Various additives have been proposed for the purpose of improving the reversibility of an aluminum-based electrolyte as well as increased coating. A few examples of these additives will be mentioned here to illustrate the direction of future work.

4.2 Incorporating Chloride-Rich Electrolytes

The work presented in the previous chapters is an analysis of aluminum triflate-based electrolytes in two different organic solvents known as ethyl methyl sulfone and propylene carbonate. This work was conducted to improve the design of previous halogen-free electrolytes studies in recent history. [1,2] The need for this improvement is motivated by the lack of electronegativity altogether in the case of Reed's investigation into diglyme revealing the lack of reversibility shown in Slim's study with THF being the chosen solvent. Aluminum triflate in THF was shown to be an improvement on the design that Reed left, evidence being the presence of the onset of the reduction of the aluminum peak near 0V. Recently in 2022, Slim published a paper to evaluate the potential of adding chlorine in solution with hopes of aluminum deposition and reversibility. Various mixtures of the aforementioned $Al(OTF)_3$/THF electrolyte were prepared for the purpose of first studying the ionic association when chlorine is present through the addition of $AlCl_3$ and LiCl.[3]

While investigating the $Al(OTF)_3$/THF electrolyte, a deeper look into various ways contact ion pairing presents itself in solution such as solvent-separated ion pairing and aggregates which lead to the following dissociation reaction for $Al(OTF)_3$ in THF.

$$Al(OTF) + 4THF \rightarrow Al(THF)_4^{3+} + 3OTF^- \quad (1)$$

$$Al(OTF)_3 + 4THF \rightarrow [Al(THF)_4(OTF)][OTF]^+ + OTF^- \quad (2)$$

$$Al(OTF)_3 + 2THF \rightarrow [Al(THF)_2(OTF)_2]^+ + OTF^- \quad (3)$$

When Li cations have OTF^- in their vicinity, the formation of Li-OTF ionic aggregates can be excluded from the 1:3 electrolyte due to the absence of the peak at 1047 cm^{-1},

which is typically attributed to LiOTF aggregates. [4] The spectroscopic analysis of the ionic association of the $AlCl_3$/THF solutions was compared to Raman spectroscopy gathered by Alves et al. which suggested $AlCl_4^-$ to dominate in the dilute electrolyte, while $AlCl_3(THF)_3$ are more favorable in a viscous environment. [5] The region including 800-1800 cm-1 confirms the presence of $AlCl_4^-$ which reveals a peak at 1640 cm^{-1} at a 1:3 mole ratio. Slim proposed a disassociation mechanism for the reaction between $Al(OTF)_3$ and LiCl in THF at a 1:3 mole ratio.

$$Al(OTF)_3 + 3LiCl + 2THF \rightarrow AlCl_3(THF)_2 + 3LiOTF \quad (4)$$

$$AlCl_3(THF)_2 + Cl^- \rightleftharpoons AlCl_4^- + 2THF \quad (5)$$

DFT calculations were conducted to evaluate the vibrational frequencies of $AlCl_4^-$, which suggest the presence of bands in the region on 200-600 cm^{-1}. There were peaks observed but they could not be linked to $AlCl_4^-$ by previous studies. This finding leads to the conclusion that polymerization of $AlCl_4^-$ in THF is possible yet unlikely in dilute solutions.

The electrochemical behavior of these electrolytes was studied through cyclic voltammetry (CV) experiments on 0.1M $Al(OTF)_3$/THF, 1:3 $Al(OTF)_3$ + LiCl/THF, and 0.1M $AlCl_3$/THF using a cell set up comprised of a gold working electrode in a standard three-electrode setup. Adding LiCl in solution resulted in a shift reduction potential coupled with a drastic increase in current which suggested greater aluminum electrodeposition in Cl^--rich environments. This observation is like the shift observed in magnesium aluminum chloride electrolyte. [6]

Scanning electron microscopy (SEM) was utilized to confirm the reductive properties shown through cyclic voltammetry and chronoamperometry plots, which would correspond to aluminum ions being reduced to aluminum metal on the copper substrate. The 1:3 electrolyte showed high corrosivity which appears as dark pits in the surface morphology. The chloride-free $Al(OTF)_3$/THF electrolyte show surface structural rearrangement at high magnification, revealing streaks of nanoparticles. This non-homogeneity is expected when depositing aluminum on a copper substrate as mentioned in the previous chapter.

The effectiveness of chlorine's ability to shift the FTIR peaks altered the ionic association which allowed the chlorine-rich electrolyte to show increased deposition on the copper substrate in comparison to the halogen-free electrolytes studies previously. Implementing $AlCl_3$ and LiCl as an additive with the Al-PC complex can be a focus of future work, however, the addition of chlorine even at low ratios appears to show corrosion through SEM analysis of the surface morphology.

4.3 Hydride-enhanced plating and stripping

Another method that has been extensively studied is the impact of adding hydride enhancement to an aluminum-based electrolyte. The addition of a halogen to the aluminum triflate-based electrolyte in an organic solvent proved to agree with the behavior of chlorine in other electrolytes which is causing severe corrosion to the contracted materials.

In a report by Slim, the role of hydrides was studied for its ability to enhance aluminum plating and stripping in a room-temperature active-halide-free electrolyte. The electrolyte is based on $Al(OTF)_3$/THF coupled with lithium aluminum hydride designated as an additive. This electrolyte is nearly identical to the electrolyte studies in the previous chapter where the solvent is exchanged, which motivates potentially utilizing hydride with the Al-PC, and Al-EMS complex to a lesser degree. [7]

To compare the ionic association of (OTF^-)-based electrolytes to chloride (Cl^-)-based system, the spectroscopic and electrochemical aspects were studied. [7–16] This study revealed that H-species catalyzes the Al plating/stripping process in Cl^- electrolytes aa mentioned previously by Daenen[11] and Graef, [12] while removing the necessity of a haloaluminate species present. The addition of hydride in solution shows a drastic change in the DFT calculations as well as the FTIR spectra. The increased plating would show unambiguous evidence of aluminum deposition through surface morphology analysis by means of a scanning electron microscope (SEM), and X-ray diffraction (XRD) spectroscopy.

Similarly to the study of ionic association studies in the previous chapters the foundation of understanding spectroscopic attributes of triflate ions was established by Frech et al. [4,17–19] This study also introduces a new way to evaluate the Al-OTF^- electrolyte using NMR studies by Lefebyre and Conway. [20] Vibrational and spectroscopic evaluation of Cl^- and triflate-based electrolytes reveal unique interaction which is suggested to be due to the distinct bond length each has. This study suggested the behavior of aluminum species in Cl^- based electrolyte behaves according to the Schlesinger reaction. [20–22]

$$AlCl_3 + AlH_4^- + 2THF \rightleftharpoons AlH_xCl_{(3-x)}(2THF) + [AlH_{(4-x)}Cl_x]^- \quad (1)$$

Aluminum electrochemical behavior relating to plating and stripping was evaluated through cyclic voltammetry on a gold working electrode which is consistent with the previous work conducted. The CV presented in this study shows an expected reversible process in the presence of hydride between -1 and 0 V (vs Al/Al^{3+}), which is likely associated with the deposition of lithium and aluminum.

In the triflate and Cl- based electrolytes there is evidence of stripping of aluminum when sweeping positively which is an improvement on the behavior in the chloride-rich

environment free of hydride, while noting that this reaction is often paired with H_2 evolution as can be seen in the attempts I have made when incorporating hydride in solution. When LiH or $LiAlH_4$ are slowly added to the triflate-based electrolyte, the temperature is elevated from the exothermic reaction that occurs. These findings lead to the proposed electrochemical reaction mechanism at a 1:3 mole ratio of $Al(OTF)_3$ to $LiAlH_4$ in THF:

$$4AlH_3 + 3e^- \rightleftharpoons Al + 3AlH_4^- \qquad (4)$$

$$2H^- \rightarrow H_2 + 2e^- \qquad (5)$$

Chronoamperometry measurements suggest that Cl^- -based electrolytes present an increased current in comparison to the OTF^- based electrolyte, which reinforces what was mentioned previously that Cl^- exceedingly facilitates plating. [3] The optical microscope reveals clear evidence of aluminum deposition increase in the presence of Cl^-, evidence being the grain-like deposit shown on the copper substrate. The SEM images show a distinct increase in the grain size of deposited particles on the copper substrate. Scanning electron microscope images show clear agreement with the optical microscope and the increased current shown through chronoamperometry.

The chemical morphology of the surface of the Cu substrate was evaluated through XPS to uncover insight into the depth profile of the deposit. The OTF-based electrolyte shows a much more pronounced Al peak in comparison to the previous research investigating electrolytes in an environment free of hydrides. This Al metal peak shows the advantageous attributes of hydride to not only plate aluminum complexes but Al metal itself in a pronounced fashion. After etching for 5 minutes, no peaks related to the Cu substrate were observed in the Cu2p region, which agrees with the various spectroscopic ways the surface was evaluated and confirms that Al deposits from the Cl^- electrolyte are thicker than the OTF^--based electrolyte. This study is encouraging in providing a pathway to move forwards in enhancing aluminum-triflate-based electrolytes in organic solvents while recognizing that there are some roadblocks such as hydrogen evolution regarding implementing hydrides and the corrosion that chlorides cause.

4.4 Borohydrides reversibility assistance

Lithium aluminum hydride in the presence of $Al(OTF)_3$ proved to be less prone to hydride reactivity. Cyclic voltammetry in the studies that were discussed in the previous sections suggests the possibility of reversible electrochemical stripping and plating of aluminum when partnered with $LiAlH_4$. There has been consideration into the potential of borohydrides (BH_4^-) similarly plating and stripping aluminum ions. Borohydrides have been known to play a. vital role in magnesium and calcium electrolyte synthesis. [23–25]

A previous study by Mohtadi et al. on the potential of borohydrides improving magnesium ion batteries that have advantageous attributes such as a high volumetric

capacity and abundance. [26] However, there are some key challenges such as the organomagnesium salts are the only complexes compatible with magnesium anodes that allow for reversible electrochemical magnesium plating and stripping. [27, 28] This study makes a proposition of electrolytes that are $Mg(BH_4)_2$ for Mg batteries. Substantial enhancement in the coulombic efficiency was established in the presence of $LiBH_4$. Although reversibility was achieved along with improved current density there is still a need to understand the exact nature of (BH_4^-) in rechargeable ion batteries and specifically how its attributes can be utilized for the purpose of improving aluminum-ion batteries.

Significant interest in multivalent cation batteries is not designated to aluminum and magnesium, calcium has also garnered considerable interest. Wang et al. published a paper on plating and stripping calcium in organic electrolytes in which there is an effort to reversibly deposit and strip calcium at room temperature. Up until 2017, elevated temperatures of 75 to 100°C were necessary for this reversibility. In this study, when mixing $Ca(BH_4)_2$ in an organic solvent tetrahydrofuran (THF), the dominant product is calcium metal. This work was not able to prove it can solve the problems of calcium as an anode for room-temperature calcium-ion batteries, there is an exponential increase in quantities of calcium plated and stripped at room temperature. [24]

4.5 Conclusion

The addition of $LiAlH_4$ in the aluminum-propylene carbonate electrolyte has been measured using cyclic voltammetry to examine the electrochemical activity shown in Figures 4.1 and 4.2. These voltammograms show what appears to be hydrogen gas evolution when combining Al-PC and $LiAlH_4$ in a 1:3 ratio in Figure 4.1. Establishing the appropriate ratio of hydride to Al-PC is the primary direction of future work.

4.5 supporting information

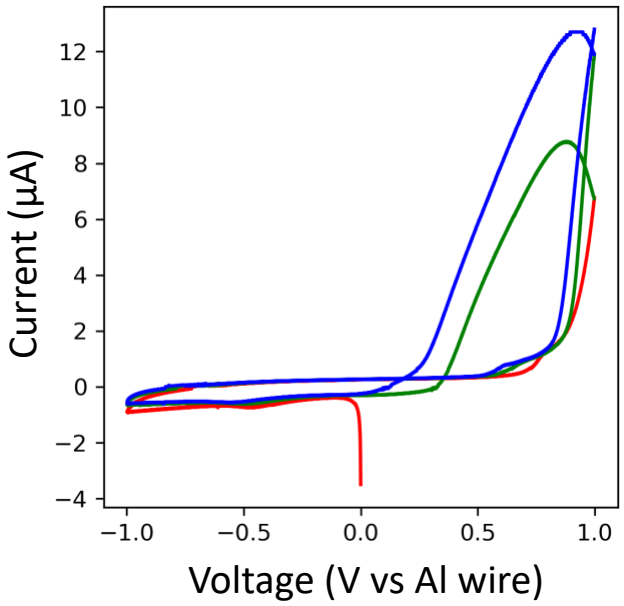

Figure 4.1 Cyclic voltammogram on a golf working electrode for 1:3 $Al(OTF)_3$:$LiAlH_4$/PC (first scan is red, second is green, and third is blue).

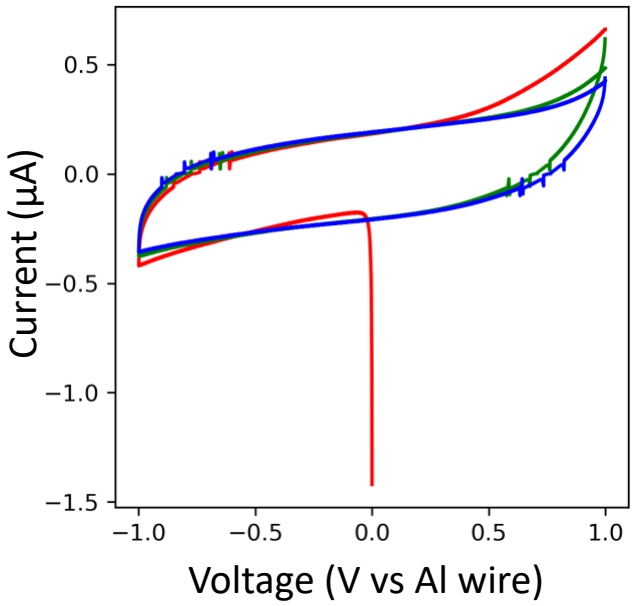

Figure 4.2 Cyclic voltammogram on gold working electrode fork $LiAlH_4$/PC (first scan is red, second is green, and third is blue)

4.6 References

(1) Reed, L. D.; Arteaga, A.; Menke, E. J. A Combined Experimental and Computational Study of an Aluminum Triflate/Diglyme Electrolyte. *J. Phys. Chem. B* **2015**, *119* (39), 12677–12681. https://doi.org/10.1021/acs.jpcb.5b08501.

(2) Slim, Z.; Menke, E. J. Comparing Computational Predictions and Experimental Results for Aluminum Triflate in Tetrahydrofuran. *J. Phys. Chem. B* **2020**, *124* (24), 5002–5008. https://doi.org/10.1021/acs.jpcb.0c02570.

(3) Slim, Z.; Menke, E. J. Aluminum Electrodeposition from Chloride-Rich and Chloride-Free Organic Electrolytes. *J. Phys. Chem. C* **2022**, *126* (5), 2365–2373. https://doi.org/10.1021/acs.jpcc.1c09126.

(4) Huang, W.; Frech, R.; Wheeler, R. A. Molecular Structures and Normal Vibrations of Trifluoromethane Sulfonate (CF3SO3-) and Its Lithium Ion Pairs and Aggregates. *J. Phys. Chem.* **1994**, *98* (1), 100–110. https://doi.org/10.1021/j100052a018.

(5) Alves, C. C.; Campos, T. B. C.; Alves, W. A. FT-Raman Spectroscopic Analysis of the Most Probable Structures in Aluminum Chloride and Tetrahydrofuran Solutions. *Spectrochim. Acta. A. Mol. Biomol. Spectrosc.* **2012**, *97*, 1085–1088. https://doi.org/10.1016/j.saa.2012.07.009.

(6) See, K. A.; Liu, Y.-M.; Ha, Y.; Barile, C. J.; Gewirth, A. A. Effect of Concentration on the Electrochemistry and Speciation of the Magnesium Aluminum Chloride Complex Electrolyte Solution. *ACS Appl. Mater. Interfaces* **2017**, *9* (41), 35729–35739. https://doi.org/10.1021/acsami.7b08088.

(7) Slim, Z.; Menke, E. Hydride-Enhanced Plating and Stripping of Aluminum from Triflate-Based Organic Electrolytes. **2022**.

(8) Couch, D. E.; Brenner, A. A Hydride Bath for the Electrodeposition of Aluminum. *J. Electrochem. Soc.* **1952**, *99* (6), 234. https://doi.org/10.1149/1.2779711.

(9) Ishibashi, N.; Yoshio, M. Electrodeposition of Aluminium from the NBS Type Bath Using Tetrahydrofuran—Benzene Mixed Solvent. *Electrochimica Acta* **1972**, *17* (8), 1343–1352. https://doi.org/10.1016/0013-4686(72)80080-X.

(10) Yoshio, M.; Ishibashi, N. High-Rate Plating of Aluminium from the Bath Containing Aluminium Chloride and Lithium Aluminium Hydride in Tetrahydrofuran. *J. Appl. Electrochem.* **1973**, *3* (4), 321–325. https://doi.org/10.1007/BF00613040.

(11) Daenen, T. E. G. Cyclic Reaction Mechanism in the Electrodeposition of Aluminium. *Nature* **1979**, *280*, 378–380. https://doi.org/10.1038/280378a0.

(12) Graef, M. W. M. The Mechanism of Aluminum Electrodeposition from Solutions of AlCl3 and LiAlH4 in THF. *J. Electrochem. Soc.* **1985**, *132* (5), 1038. https://doi.org/10.1149/1.2114011.

(13) Badawy, W. A.; Sabrah, B. A.; Hilal, N. H. Y. A New Bath for the Electrodeposition of Aluminium. II. Kinetics and Mechanism of the Deposition and Dissolution Processes. *J. Appl. Electrochem.* **1987**, *17* (2), 357–369. https://doi.org/10.1007/BF01023302.

(14) *Speciation Analyses|PerkinElmer*. https://www.perkinelmer.com/category/speciation-analyses (accessed 2023-07-18).

(15) Kan, H.; Zhu, S.; Zhang, N.; Wang, X. Electrodeposition of Aluminum and Aluminum—Magnesium Alloys at Room Temperature. *J. Cent. South Univ.* **2015**, *22* (10), 3689–3697. https://doi.org/10.1007/s11771-015-2911-1.
(16) Lefebvre, M.; Conway, B. Nucleation and Morphologies in the Process of Electrocrystallization of Aluminium on Smooth Gold and Glassy-Carbon Substrates. *J. Electroanal. Chem. - J ELECTROANAL CHEM* **2000**, *480*, 46–58. https://doi.org/10.1016/S0022-0728(99)00444-1.
(17) Frech, R.; Huang, W. Ionic Association in Poly (Propylene Oxide) Complexed with Divalent Metal Trifluoromethanesulfonate Salts. *Solid State Ion.* **1993**, *66* (1), 183–188. https://doi.org/10.1016/0167-2738(93)90042-2.
(18) Frech, R.; Huang, W. Anion-Solvent and Anion-Cation Interactions in Lithium and Tetrabutylammonium Trifluoromethanesulfonate Solutions. *J. Solut. Chem.* **1994**, *23* (4), 469–481. https://doi.org/10.1007/BF00972613.
(19) Huang, W.; Frech, R. Dependence of Ionic Association on Polymer Chain Length in Poly(Ethylene Oxide)-Lithium Triflate Complexes. *Polymer* **1994**, *35* (2), 235–242. https://doi.org/10.1016/0032-3861(94)90684-X.
(20) Lefebvre, M. C.; Conway, B. E. NMR Spectroscopy Studies on Speciation of Al Complex Ions in AlCl3+LiAlH4 Solutions in Tetrahydrofuran for Electroplating of Al. *J. Electroanal. Chem.* **1998**, *448* (2), 217–227. https://doi.org/10.1016/S0022-0728(97)00073-9.
(21) Lefebvre, M.; Conway, B. Elementary Steps and Mechanism of Electrodeposition of Al from Complex Hydride Ions in Tetrahydrofuran Baths. *J. Electroanal. Chem. - J ELECTROANAL CHEM* **2000**, *480*, 34–45. https://doi.org/10.1016/S0022-0728(99)00443-X.
(22) Finholt, A. E.; Bond, A. C. Jr.; Schlesinger, H. I. Lithium Aluminum Hydride, Aluminum Hydride and Lithium Gallium Hydride, and Some of Their Applications in Organic and Inorganic Chemistry1. *J. Am. Chem. Soc.* **1947**, *69* (5), 1199–1203. https://doi.org/10.1021/ja01197a061.
(23) Mohtadi, R.; Matsui, M.; Arthur, T. S.; Hwang, S.-J. Magnesium Borohydride: From Hydrogen Storage to Magnesium Battery. *Angew. Chem. Int. Ed Engl.* **2012**, *51* (39), 9780–9783. https://doi.org/10.1002/anie.201204913.
(24) Wang, D.; Gao, X.; Chen, Y.; Jin, L.; Kuss, C.; Bruce, P. G. Plating and Stripping Calcium in an Organic Electrolyte. *Nat. Mater.* **2018**, *17* (1), 16–20. https://doi.org/10.1038/nmat5036.
(25) Melemed, A. M.; Skiba, D. A.; Gallant, B. M. Toggling Calcium Plating Activity and Reversibility through Modulation of Ca2+ Speciation in Borohydride-Based Electrolytes. *J. Phys. Chem. C Nanomater. Interfaces* **2022**, *126* (2), 892–902. https://doi.org/10.1021/acs.jpcc.1c09400.
(26) Aurbach, D.; Lu, Z.; Schechter, A.; Gofer, Y.; Gizbar, H.; Turgeman, R.; Cohen, Y.; Moshkovich, M.; Levi, E. Prototype Systems for Rechargeable Magnesium Batteries. *Nature* **2000**, *407* (6805), 724–727. https://doi.org/10.1038/35037553.
(27) *Progress in electrolytes for rechargeable Li-based batteries and beyond - ScienceDirect*. https://www.sciencedirect.com/science/article/pii/S2468025716300218 (accessed 2023-07-20).

(28) Muldoon, J.; Bucur, C. B.; Oliver, A. G.; Sugimoto, T.; Matsui, M.; Kim, H. S.; Allred, G. D.; Zajicek, J.; Kotani, Y. Electrolyte Roadblocks to a Magnesium Rechargeable Battery. *Energy Environ. Sci.* **2012**, *5* (3), 5941–5950. https://doi.org/10.1039/C2EE03029B.